A molecular simulation study of commensurate – incommensurate adsorption of n-alkanes in cobalt formate frameworks

Rajamani Krishna, Jasper Martijn van Baten

Molecular Simulation
Journal of
Experimental Nanoscience

Taylor & Francis
Taylor & Francis Group

A molecular simulation study of commensurate □ incommensurate adsorption of n-alkanes in cobalt formate frameworks

Journal:	*Molecular Simulation/Journal of Experimental Nanoscience*
Manuscript ID:	GMOS-2008-0241.R1
Journal:	Molecular Simulation
Date Submitted by the Author:	31-Dec-2008
Complete List of Authors:	Krishna, Rajamani; University of Amsterdam, Van 't Hoff Institute for Molecular Sciences van Baten, Jasper; University of Amsterdam, Van 't Hoff Institute for Molecular Sciences
Keywords:	linear alkanes, metal organic frameworks, cobalt formate, non-monotonous, adsorption

A molecular simulation study of commensurate – incommensurate adsorption of n-alkanes in cobalt formate frameworks

R. Krishna*, J.M. van Baten

Van 't Hoff Institute for Molecular Sciences, University of Amsterdam, Nieuwe Achtergracht 166,

1018 WV Amsterdam, The Netherlands

*CORRESPONDING AUTHOR: Tel + 31 20 5257007; Fax: + 31 20 5255604; email: r.krishna@uva.nl

ABSTRACT

The channels of the cobalt formate frameworks consist of one-dimensional channels that have a zig-zag configuration. Propane (C3) has a length that is commensurate with the channel segment length; longer n-alkanes such as n-butane (nC4), n-pentane (nC5) and n-hexane (nC6) have conformations that straddle two channels segments. Configurational-bias Monte Carlo (CBMC) simulations show that the adsorption strength of C3 is higher than that of n-butane (nC4), and n-pentane (nC5); this unusual hierarchy is a direct consequence of commensurate – incommensurate adsorption. CBMC simulations also reveal the possibility of separating C3-nC6,C3-nC4, nC4-nC6, nC4-nC5 *liquid* mixtures for which the adsorbed phase contains predominantly the *shorter* alkane. Molecular dynamics (MD) simulations show that the hierarchy of self-diffusivities is non-monotonic and is the mirror image of the hierarchy of adsorption strengths.

Keywords: diffusivity; adsorption; Molecular Dynamics; Configurational-Bias Monte Carlo; linear alkanes; metal organic frameworks; cobalt formate; manganese formate; commensurate; non-monotonous

1. Introduction

In recent years there has been a remarkable upsurge in research activity on metal-organic frameworks (MOFs), in view of several potential applications in the field of storage [1-4], and also separation of a variety of mixtures [5-21]. Due to the wide variety of pore sizes, and pore geometries a number of interesting separation possibilities are possible with MOFs. For example, Finsy et al.[11] have reported a significantly higher adsorption capacity for xylene isomers in MIL-47, than for its isomers, n-octane (nC8) and ethyl benzene (EtBz). The higher capacity for xylene isomers is due to their improved "stacking efficiency" within the channels of MIL-47, as illustrated in the snapshots in Figures 1a, and 1b for *p*-xylene and nC8 respectively; see also the pure component isotherms in Figure 2. Bárcia et al.[7] report the results of an experimental study to show the feasibility of separating alkane isomers by adsorption within the framework of Zn(bdc)dabco (see structure in Figure 3). In a subsequent study, Dubbeldam et al. [21] have used molecular simulations have shown that the principle behind alkane isomers separation using Zn(bdc)dabco framework is based on the differences in "efficiency" with which the isomer molecules can interact with the dabco linker atoms.

The current investigation focuses on another unusual separation potential of MOFs and has its genesis in the recent work by Li et al.[22], that reported adsorption isotherms for n-alcohols in cobalt formate (Co-FA) framework structure. The metal network exhibits diamondoid connectivity and the overall framework gives rise to zig-zag channels along the *b* axis where guest dimethylformamide molecules reside. The effective pore size of these one-dimensional channels is 5 – 6 Å. The unit cell and pore landscape of Co-FA is depicted in Figure 4; one unit cell of Co-FA comprises a total of four distinct channel "segments"; each channel segment forms part of the repeat zig-zag structure. The experimental adsorption data of Li et al.[22] for propanol and n-butanol in Co-FA, are particularly intriguing; see Figure 5. We note that the adsorption strength of propanol is higher than that of n-butanol over the entire range of experimental pressures. The first major objective of the present communication is to show,

with the help of molecular simulations, that this unusual hierarchy in adsorption strengths is caused by commensurate-incommensurate molecular lengths of linear molecules within the one-dimensional channels of Co-FA. For this purpose we have carried out a set of Configurational-bias Monte Carlo (CBMC) simulations to determine the adsorption isotherms of linear alkanes: methane (C1), ethane (C2), propane (C3), n-butane (nC4), n-pentane (nC5), n-hexane (nC6), and n-heptane (nC7) in Co-FA. The second objective is to demonstrate the exploitation of commensurate-incommensurate molecular lengths to adsorb a *shorter* linear alkane preferentially from a liquid mixture with a longer linear alkane. The third objective, using Molecular Dynamics (MD) diffusion of n-alkanes in Co-FA, is to show that the non-monotonous hierarchy of adsorption strengths is accompanied by a non-monotonous hierarchy in diffusivities.

2. Simulation details

The structural information for Co-FA is from Li et al. [22]. The adsorption isotherms were computed using Configurational-bias Monte Carlo (CBMC) simulations in the grand canonical (GC) ensemble. The united atom force field for alkanes, developed by Dubbeldam et al. [23], is used to describe alkane-alkane, Lennard-Jones, interactions. For alkane-alkane interactions the tabulated force fields are available in Dubbeldam et al. [23]; the potential for the n-alkanes includes bond stretching, bending, and torsion. The framework was assumed to be rigid in the simulations.

For the atoms in the guest metal organic framework, the generic UFF [24] was used. The DREIDING [25] force fields was used for the organic linker atoms. The Lorentz-Berthelot mixing rules were applied for calculating σ and ε/k_B for guest-host interactions.

Furtther simulation details, including structural information, CBMC and MD simulation methodologies, tabulated force fields, pore landscapes, snapshots showing the location and conformation of n-alkanes within the pores, and simulation data are available in the Supplementary material accompanying this publication.

3. Adsorption of linear alkanes in Co-FA

Consider the CBMC simulations of the adsorption isotherms of linear alkanes in Co-FA at 300 K; see Figure 6a. The hierarchy of adsorption strengths for C1, C2 and C3 is as expected; increasing chain length results in a higher adsorption strength; see Henry coefficient data in Figure 6b. However, with increasing chain lengths beyond C3 we note an unusual adsorption hierarchy: C3 > nC4 > nC5. Further increase in chain length, results in the expected hierarchy, i.e. nC7>nC6>nC5. The saturation capacity for C1, C2, and C3 is found to be 4 molecules per unit cell, corresponding to one molecule per channel segment. Snapshots of the location of molecules along the 1D zig-zag channels of Co-FA confirm that each channel segment contains no more than one molecule each of C1, C2 and C3; see Figure 7. nC5, nC6 and nC7 have conformations that make these molecules straddle two channel segments, and this is also reflected in the saturation capacities of these molecules of 2 molecules per unit cell, i.e. corresponding to 1 molecule in two channel segments. nC4 has an intermediate character; at low pressures the nC4 has a conformation with a tendency to occupy a small portion of the adjoining segment. At very high pressures, nC4 adopts a more "cramped" configuration, with each molecule occupying one channel segment and yielding a saturation capacity of 4 molecules per unit cell. When a molecule has a tendency to straddle two channel segments (nC4 at low pressures, nC5, nC6, and nC7) not all of the C atoms can effectively interact with the atoms of the framework; this leads to a lower adsorption strength and a non-monotonous adsorption hierarchy witnessed in the Henry coefficient data in Figure 6b. It is interesting to note that non-monotonous behaviour of the Henry coefficient for n-alkanes has also been observed for cage-type zeolites such as CHA, ERI and LTA, caused by commensurate – incommensurate adsorption within cages [26-28].

The non-monotonous adsorption characteristics, along with differences in saturation capacities can be exploited to achieve unusual separation possibilities. Consider a mixture of C3 and nC6. From the pure component adsorption isotherms in Figure 6 we note that at low pressures the adsorption strengths of C3 is nearly the same as that of nC6. However the saturation capacity of C3 is twice that of nC6. We can device a strategy for separating C3 from nC6 by exploiting the differences in the saturation capacities.

CBMC simulations of the component loadings for a mixture with equal partial fluid phase fugacities, $f_1 = f_2$, are shown in Figure 8a. When operating at partial fugacities in excess of 1 MPa, with a bulk *liquid* phase, we note that the adsorbed phase contains practically no nC6 and is predominantly C3.

Analogously for nC4-nC5 liquid mixtures, the adsorbed phase contains the shorter alkane, almost exclusively; see Figure 8b. For C3-nC4, and nC4-nC6 mixtures the separation is somewhat less selective. The CBMC simulations results in Figure 9 show that at high loadings, the adsorbed phase is not exclusively the shorter alkane but also contains a small proportion of the longer alkane. The separations indicated in Figures 8 and 9 have possible industrial potential, and needs to be experimentally confirmed. It is perhaps relevant to point out here that we had earlier used molecular simulations to demonstrate the feasibility of separating n-alkane mixtures by exploiting differences in the saturation capacity in cage-type zeolites such as CHA, ERI, and AFX zeolites [29]. More recently the experimental work of Denayer et al.[30] has provided experimental confirmation of the separation potential anticipated by the molecular simulations.

4. Diffusion of linear alkanes in Co-FA

MD simulations of self-diffusivities of C1, C2, C3, nC4, nC5, nC6 and nC7 in Co-FA are shown in Figure 10a for a variety of loadings. At a loading of 1 molecule per unit cell, the values of the selfdiffusivities are plotted in Figure 10b as a function of C number. The hierarchy of diffusivities of C1, C2, and C3 is as expected; the molecule with the longer chain length has the lower diffusivity. With increasing chain length we observe a non-monotonous behavior with the hierarchy: nC5>nC4>C3 ≈nC6. The hierarchy of diffusivities is an exact mirror image of the hierarchy of Henry coefficients; compare Figures 6b and 10b. Put another way, if the molecular length is incommensurate with the channel segment length, the adsorption strength is low, but its diffusivity is high.

In the context of separation process development, it must be emphasized that since adsorption and diffusion run counter to each other, we should aim for either an equilibrium based separation or a

diffusional (i.e. kinetic) based separation. A combination of the two, for example, in a MOF membrane separation will not work, as the two effects may cancel each other out.

5. Conclusions

CBMC and MD simulations of adsorption and diffusion of linear alkanes within the one-dimensional channels of cobalt formate frameworks have revealed a non-monotonic behavior in Henry coefficients and diffusivities as a function of the n-alkane chain length. The non-monotonicity is caused due to commensurate – incommensurate effects in adsorption; C3 has a molecular length that is commensurate with the channel segment length. nC4, nC5, nC6 and nC7 have conformations that make these molecules straddle two channel segments; this leads to a lower adsorption strength due to inefficient interaction with the framework atoms. The hierarchy of diffusivities is inverse of the hierarchy of adsorption strengths.

CBMC simulations also reveal the possibility of separating C3-nC6, C3-nC4, nC4-nC6, nC4-nC5 *liquid* mixtures for which the adsorbed phase contains predominantly the *shorter* alkane.

Manganese formate frameworks are iso-structural to Co-FA, and a similar non-monotonicity in adsorption and diffusion behaviour is observed from molecular simulations; details are available in the supplementary material.

Our study underlines the ability of molecular simulations to provide a molecular level understanding of observed experimental phenomena, and also to unravel novel separations with structured nanoprous materials such as MOFs.

6. Acknowledgements

RK acknowledges the grant of a TOP subsidy from the Netherlands Foundation for Fundamental Research (NWO-CW) for intensification of reactors.

Supplementary Material associated with this article can be found, in the online version, at doi:yyy/xxx.xx.xxx.

7. Literature cited

[1] O.M. Yaghi, M. O'Keeffe, N.W. Ockwig, H.K. Chae, M. Eddaoudi, J. Kim, Reticular synthesis and the design of new materials, Nature 423 (2003) 705-714.

[2] J.L.C. Rowsell, O.M. Yaghi, Metal–organic frameworks: a new class of porous materials, Microporous Mesoporous Mater. 73 (2004) 3-14.

[3] O.M. Yaghi, Metal-organic Frameworks: A tale of two entanglements, Nature Materials 6 (2007) 92-93.

[4] R.Q. Snurr, J.T. Hupp, S.T. Nguyen, Prospects for nanoporous metal-organic materials in advanced separations processes, A.I.Ch.E.J. 50 (2004) 1090-1095.

[5] L. Bastin, P.S. Bárcia, E.J. Hurtado, J.A.C. Silva, A.E. Rodrigues, B. Chen, A Microporous Metal-Organic Framework for Separation of CO_2/N_2 and CO_2/CH_4 by Fixed-Bed Adsorption, J. Phys. Chem. C 112 (2008) 1575-1581.

[6] L. Pan, D.H. Olson, L.R. Ciemnolonski, R. Heddy, J. Li, Separation of Hydrocarbons with a Microporous Metal–Organic Framework, Angew. Chem. Int. Ed. 45 (2006) 616-619.

[7] P.S. Bárcia, F. Zapata, J.A.C. Silva, A.E. Rodrigues, B. Chen, Kinetic Separation of Hexane Isomers by Fixed-Bed Adsorption with a Microporous Metal-Organic Framework, J. Phys. Chem. B 111 (2008) 6101-6103.

[8] B. Chen, C. Liang, J. Yang, D.S. Contreras, Y.L. Clancy, E.B. Lobkovsky, O.M. Yaghi, S. Dai, A Microporous Metal–Organic Framework for Gas-Chromatographic Separation of Alkanes, Angew. Chem. Int. Ed. 45 (2006) 1590-1595.

[9] L. Pan, B. Parker, X. Huang, D.H. Olson, J.Y. Lee, J. Li, Zn(tbip) (H_2 tbip)=5-*tert*-Butyl Isophthalic Acid): A Highly Stable Guest-Free Microporous Metal Organic Framework with Unique Gas Separation Capability, J. Am. Chem. Soc. 128 (2006) 4180-4181.

[10] D.N. Dybtsev, H. Chun, S.H. Yoon, D. Kim, K. Kim, Microporous Manganese Formate: A Simple Metal-Organic Porous Material with High Framework Stability and Highly Selective Gas Sorption Properties, J. Am. Chem. Soc. 126 (2004) 32-33.

[11] V. Finsy, H. Verelst, L. Alaerts, D. De Vos, P.A. Jacobs, G.V. Baron, J.F.M. Denayer, Pore-Filling-Dependent Selectivity Effects in the Vapor-Phase Separation of Xylene Isomers on the Metal-Organic Framework MIL-47, J. Am. Chem. Soc. 130 (2008) 7110-7118.

[12] L. Alaerts, C.E.A. Kirschhock, M. Maes, M. van der Veen, V. Finsy, A. Depla, J.A. Martens, G.V. Baron, P.A. Jacobs, J.F.M. Denayer, D. De Vos, Selective Adsorption and Separation of Xylene Isomers and Ethylbenzene with the Microporous Vanadium(IV) Terephthalate MIL-47, Angew. Chem. Int. Ed. 46 (2007) 4293-4297.

[13] Q.M. Wang, D. Shen, M. Bülow, M.L. Lau, S. Deng, F.R. Fitch, N.O. Lemcoff, J. Semanscin, Metallo-organic molecular sieve for gas separation and purification, Microporous Mesoporous Mater. 55 (2002) 217-230.

[14] L. Zhang, Q. Wang, T. Wu, Y.C. Liu, Understanding Adsorption and Interactions of Alkane Isomer Mixtures in Isoreticular Metal–Organic Frameworks, Chem. Eur. J. 13 (2007) 6387-6396.

[15] S. Wang, Q. Yang, C. Zhong, Adsorption and separation of binary mixtures in a metal-organic framework Cu-BTC: A computational study, Sep. Purif. Technol. 60 (2008) 30-35.

[16] Q. Yang, C. Xue, C. Zhong, J.F. Chen, Molecular Simulation of Separation of CO_2 from Flue Gases in Cu-BTC Metal-Organic Framework, A.I.Ch.E.J. 53 (2007) 2832-2840.

[17] Q. Yang, C. Zhong, Molecular Simulation of Carbon Dioxide/Methane/Hydrogen Mixture Adsorption in Metal-Organic Frameworks, J. Phys. Chem. B 110 (2006) 17776-17783.

[18] S. Keskin, D.S. Sholl, Screening Metal-Organic Framework materials for membrane-based methane/carbon dioxide separations, J. Phys. Chem. C 111 (2007) 14055-14059.
[19] J. Jiang, S.I. Sandler, Monte Carlo Simulation for the Adsorption and Separation of Linear and Branched Alkanes in IRMOF-1, Langmuir 22 (2006) 5702-5707.
[20] R. Babarao, Z. Hu, J. Jiang, S. Chempath, S.I. Sandler, Storage and separation of CO_2 and CH_4 in silicalite, C_{168} schwarzite, and IRMOF-1: A comparative study from Monte Carlo simulation, Langmuir 23 (2007) 659-666.
[21] D. Dubbeldam, C.J. Galvin, K.S. Walton, D.E. Ellis, R.Q. Snurr, Separation and Molecular-Level Segregation of Complex Alkane Mixtures in Metal-Organic Frameworks, J. Am. Chem. Soc. 130 (2008) 10884-10885.
[22] K. Li, D.H. Olson, J.Y. Lee, W. Bi, K. Wu, T. Yuen, Q. Xu, J. Li, Multifunctional Microporous MOFs Exhibiting Gas/Hydrocarbon Adsorption Selectivity, Separation Capability and Three-Dimensional Magnetic Ordering, Adv. Funct. Mater. 18 (2008) 2205-2214.
[23] D. Dubbeldam, S. Calero, T.J.H. Vlugt, R. Krishna, T.L.M. Maesen, B. Smit, United Atom Forcefield for Alkanes in Nanoporous Materials, J. Phys. Chem. B 108 (2004) 12301-12313.
[24] A.K. Rappé, C.J. Casewit, K.S. Colwel, W.A. Goddard, W.M. Skiff, UFF, a Full Periodic Table Force Field for Molecular Mechanics and Molecular Dynamics Simulations, J. Am. Chem. Soc. 114 (1992) 10024-10035.
[25] S.L. Mayo, B.D. Olafson, W.A. Goddard, DREIDING: A Generic Force Field for Molecular Simulations, J. Phys. Chem. 94 (1990) 8897-8909.
[26] D. Dubbeldam, S. Calero, T.L.M. Maesen, B. Smit, Understanding the window effect in zeolite catalysis, Angew. Chem. Int. Ed. 42 (2003) 3624-3626.
[27] D. Dubbeldam, S. Calero, T.L.M. Maesen, B. Smit, Incommensurate diffusion in confined systems, Phys. Rev. Lett. 90 (24) Art. No. 245901 (2003)
[28] D. Dubbeldam, B. Smit, Computer simulation of incommensurate diffusion in zeolites: Understanding window effects, J. Phys. Chem. B 107 (2003) 12138-12152.
[29] R. Krishna, J.M. van Baten, Separating n-alkane mixtures by exploiting differences in the adsorption capacity within cages of CHA, AFX and ERI zeolites, Sep. Purif. Technol. 60 (2008) 315-320.
[30] J.F.M. Denayer, L.I. Devriese, S. Couck, J.A. Martens, R. Singh, P.A. Webley, G.V. Baron, Cage and Window Effects in the Adsorption of n-Alkanes on Chabazite and SAPO-34, J. Phys. Chem. C 112 (2007) 16593-16599.

8. Captions for Figures

Figure 1. Snapshots showing the location and conformations of (a) p-xylene, and (b) nC8 within the pores of MIL-47. The structural and simulation details are available in the Supplementary material accompanying this publication.

Figure 2. CBMC simulations of pure component isotherms for n-octane (nC8), ethyl-benzene (EtBz), o-, m-, and p- xylenes (oX, mX, pX) in MIL-47 at 343 K.

Figure 3. Pore landscape and structure of Zn(bdc)dabco. The structural and simulation details are available in the Supplementary material accompanying this publication.

Figure 4. Pore landscapes and structure of Co-FA.

Figure 5. Adsorption isotherms for propanol and n-butanol in Co-FA. Experimental data of Li et al.[22]. See Supplementary material for the unit cell dimensions and the conversion of loadings to units of molecules per unit cell.

Figure 6. (a) CBMC simulations of adsorption isotherms for C1, C2, C3, nC4, nC5, nC6 and nC7 in Co-FA at 300 K. (b) Henry coefficients as a function of C number.

.

Figure 7. Snapshots showing the location of C1, C2, C3, nC4, nC5, nC6 and nC7 molecules in Co-FA.

Figure 8. CBMC simulations of component loadings for (a) C3-nC6, and (b) nC4-nC5 mixtures in Co-FA at 300 K.

Figure 9. CBMC simulations of component loadings for (a) C3-nC4, and (c) nC4-nC6 mixtures in Co-FA at 300 K.

Figure 10. (a) MD simulations of self-diffusivities of C1, C2, C3, nC4, nC5, nC6 and nC7 in Co-FA at 300 K. (b) Diffusivities, at a loading of 1 molecule per unit cell, as a function of carbon number.

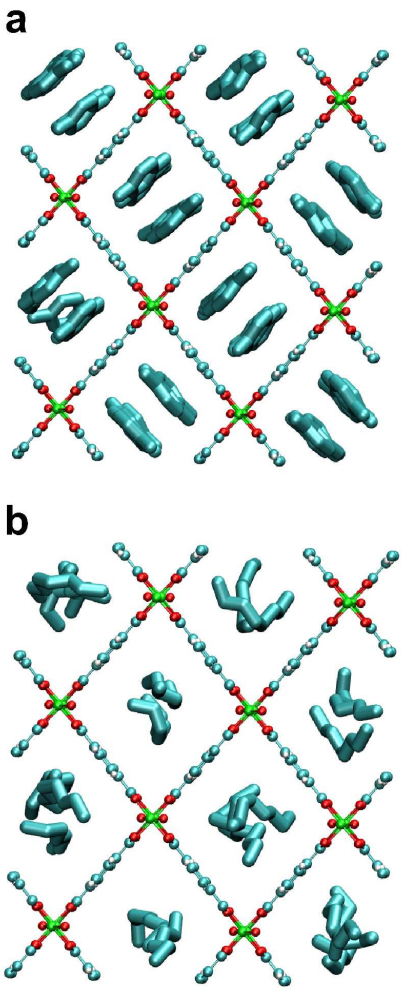

Figure 1. Snapshots showing the location and conformations of (a) p-xylene, and (b) nC8 within the pores of MIL-47. The structural and simulation details are available in the Supplementary material accompanying this publication.
209x297mm (600 x 600 DPI)

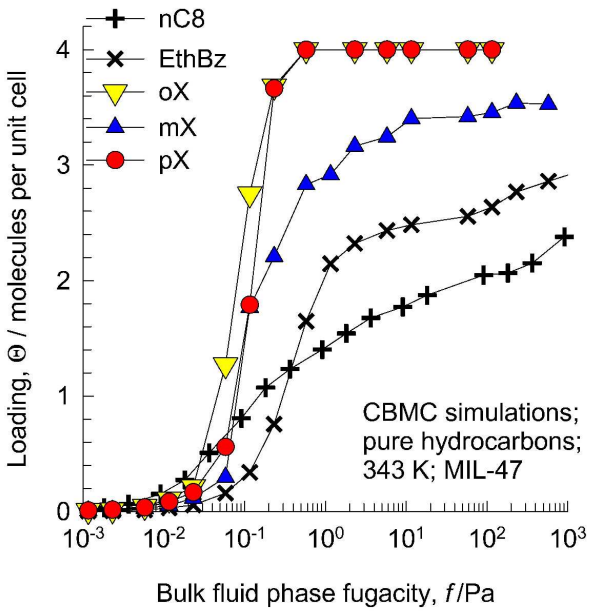

Figure 2. CBMC simulations of pure component isotherms for n-octane (nC8), ethyl-benzene (EtBz), o-, m-, and p- xylenes (oX, mX, pX) in MIL-47 at 343 K.
209x297mm (600 x 600 DPI)

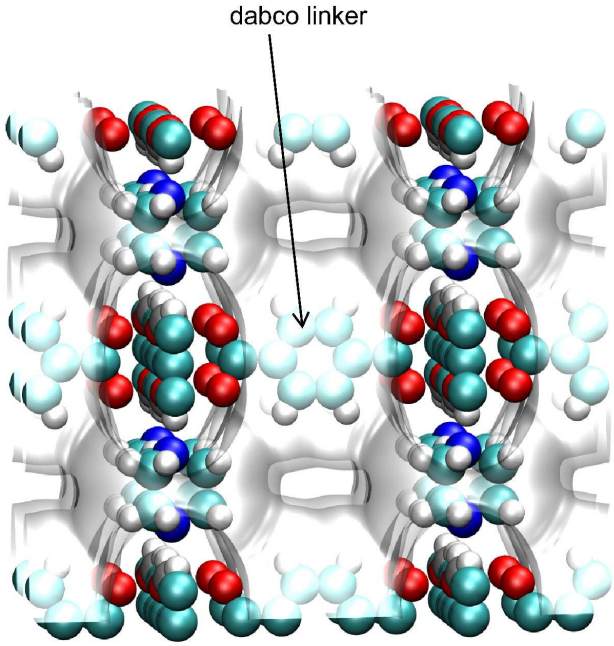

Figure 3. Pore landscape and structure of Zn(bdc)dabco. The structural and simulation details are available in the Supplementary material accompanying this publication.
209x297mm (600 x 600 DPI)

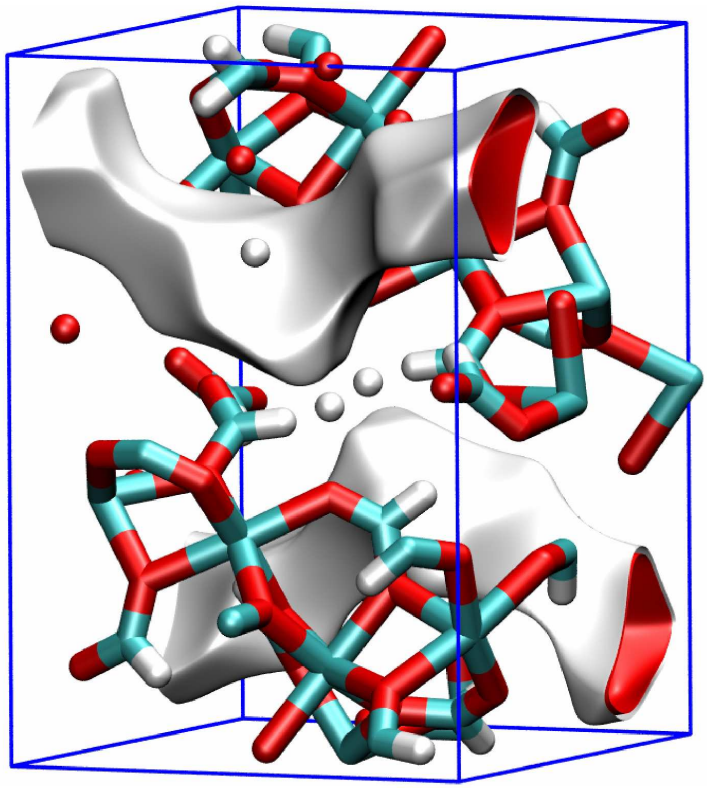

Figure 4. Pore landscapes and structure of Co-FA.
209x297mm (600 x 600 DPI)

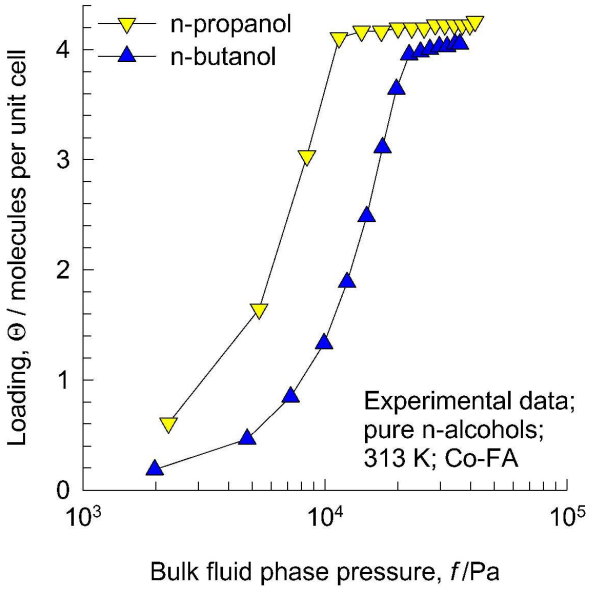

Figure 5. Adsorption isotherms for propanol and n-butanol in Co-FA. Experimental data of Li et al.[22]. See Supplementary material for the unit cell dimensions and the conversion of loadings to units of molecules per unit cell.
209x297mm (600 x 600 DPI)

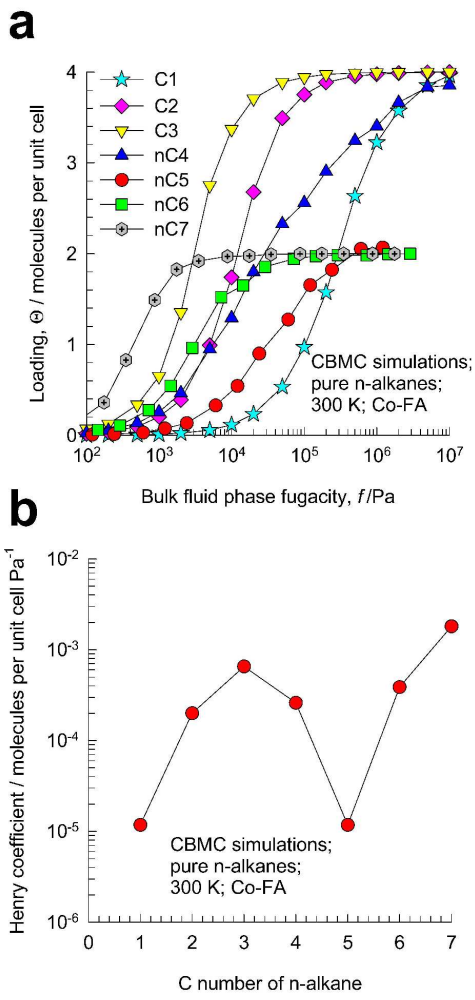

Figure 6. (a) CBMC simulations of adsorption isotherms for C1, C2, C3, nC4, nC5, nC6 and nC7 in Co-FA at 300 K. (b) Henry coefficients as a function of C number.
209x297mm (600 x 600 DPI)

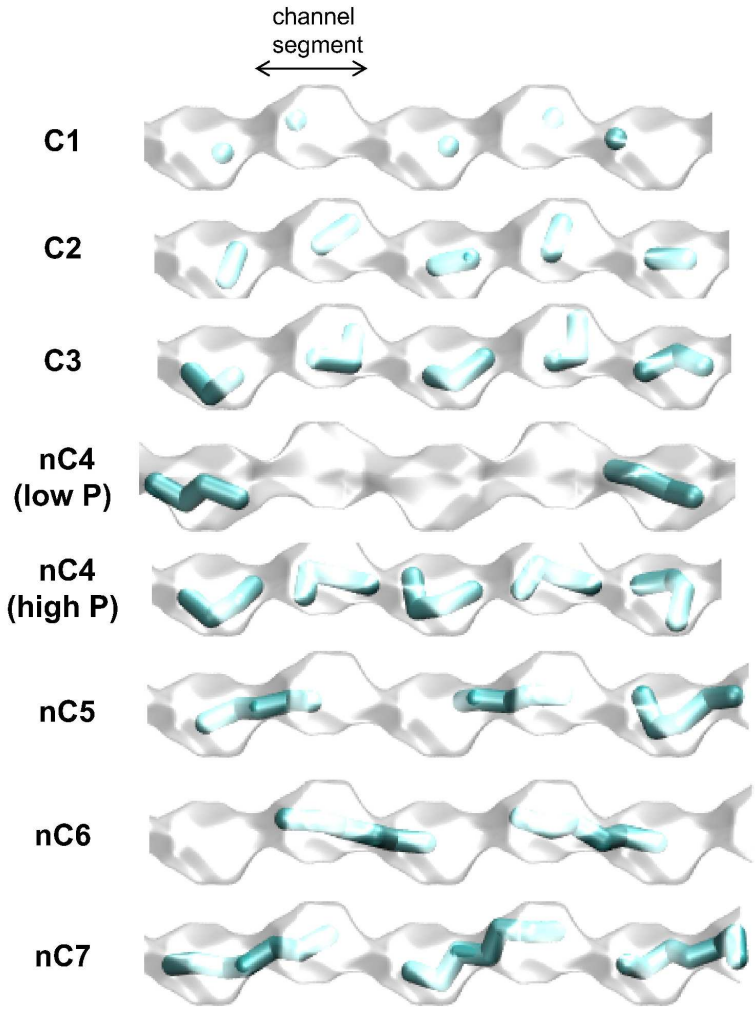

Figure 7. Snapshots showing the location of C1, C2, C3, nC4, nC5, nC6 and nC7 molecules in Co-FA.
209x297mm (600 x 600 DPI)

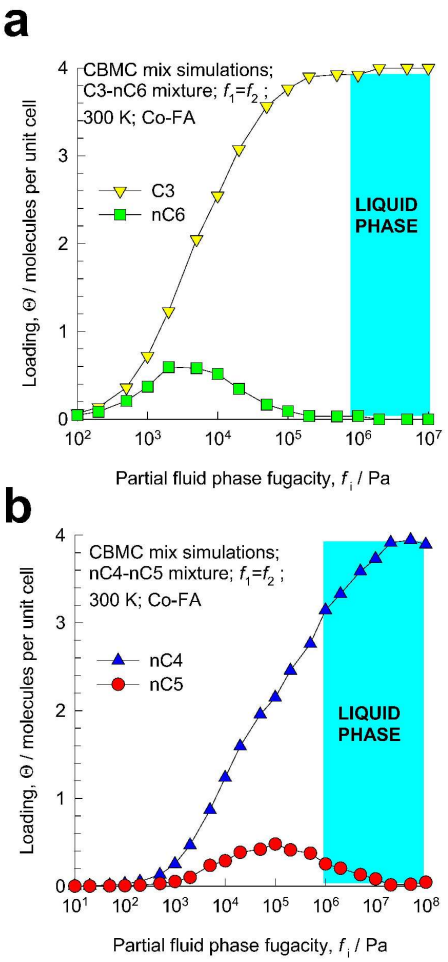

Figure 8. CBMC simulations of component loadings for (a) C3-nC6, and (b) nC4-nC5 mixtures in Co-FA at 300 K.
209x297mm (600 x 600 DPI)

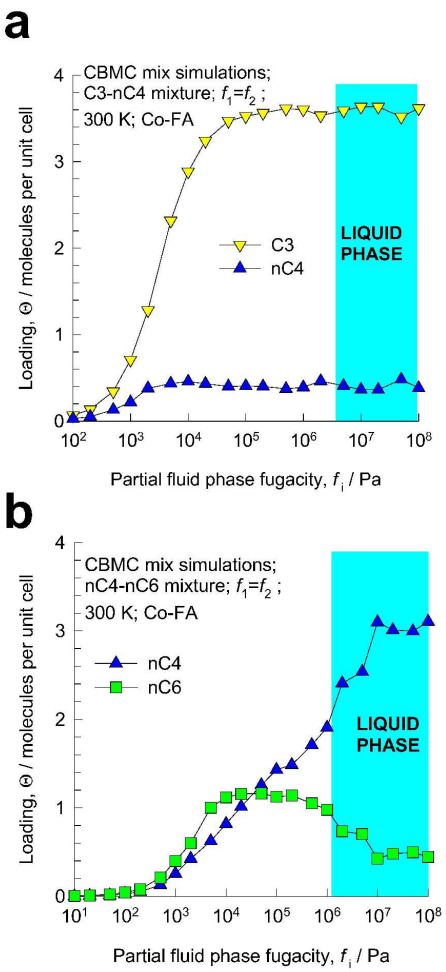

Figure 9. CBMC simulations of component loadings for (a) C3-nC4, and (c) nC4-nC6 mixtures in Co-FA at 300 K.
209x297mm (600 x 600 DPI)

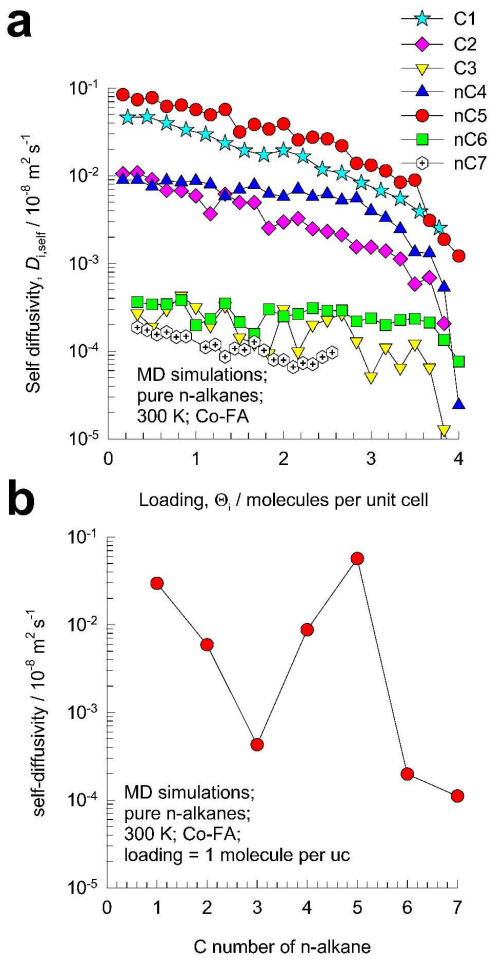

Figure 10. (a) MD simulations of self-diffusivities of C1, C2, C3, nC4, nC5, nC6 and nC7 in Co-FA at 300 K. (b) Diffusivities, at a loading of 1 molecule per unit cell, as a function of carbon number.
209x297mm (600 x 600 DPI)

Supplementary Material to accompany:

A molecular simulation study of commensurate – incommensurate adsorption of n-alkanes in cobalt formate frameworks

R. Krishna*, J.M. van Baten

Van 't Hoff Institute for Molecular Sciences, University of Amsterdam, Nieuwe Achtergracht 166,

1018 WV Amsterdam, The Netherlands

*CORRESPONDING AUTHOR: Tel + 31 20 5257007; Fax: + 31 20 5255604; email: r.krishna@uva.nl

Appendix A: Molecular Simulation methodology and simulation results

1. MOF structures

Besides Cobalt Formate frameworks, simulations were also carried out for Manganese Formate (Mn-FA), Zn(bdc)dabco, and MIL-47. The structural information for the metal organic frameworks have been taken from various publications on the respective frameworks: Cobalt Formate (Co-FA) from Li et al. [1]; Manganese Formate (Mn-FA) from Dybtsev et al. [2]; Zn(bdc)dabco from Bárcia et al.[3] and Lee et al. [4]; MIL-47 from Alaerts et al. [5], Finsy et al. [6] and Barthelet et al. [7]. The structure data files we used in our simulations are available on our website [8].

2. Monte Carlo simulation methodology

The adsorption isotherms were computed using Configurational-bias Monte Carlo (CBMC) simulations in the grand canonical (GC) ensemble. The united atom force field for alkanes, developed by Dubbeldam et al. [9], is used to describe alkane-alkane, Lennard-Jones, interactions. For alkane-alkane interactions the tabulated force fields are available in Dubbeldam et al. [9]; the potential for the n-alkanes includes bond stretching, bending, and torsion. Some simulation results have also been reported for aromatics and alkyl-aromatics in MIL-47. The force field for benzene follows the work of Ban et al.[10], and extended to alkyl aromatics by combining with the force field of Dubbeldam et al. [9].

The metal organic framework structures of Co-FA, Mn-FA, Zn(bdc)dabco, and MIL-47 were considered to be rigid in the simulations For the atoms in the guest metal organic framework, the generic UFF [11] was used. The DREIDING [12] force fields was used for the organic linker atoms. The Lennard-Jones parameters are summarized in Table 1. The Lorentz-Berthelot mixing rules were

applied for calculating σ and ε/k_B for guest-host interactions. For simulations with linear and branched alkanes with two or more C atoms, the Configurational-Bias Monte Carlo (CBMC) simulation technique [13, 14] was employed. The beads in the chain are connected by harmonic bonding potentials. A harmonic cosine bending potential models the bond bending between three neighboring beads, a Ryckaert-Bellemans potential controls the torsion angle. The beads in a chain separated by more than three bonds interact with each other through a Lennard-Jones potential. The Lennard-Jones potentials are shifted and cut at 12 Å. The CBMC simulation details have been given in detail elsewhere [9, 13-15]. The CBMC simulations were performed using the BIGMAC code developed by T.J.H. Vlugt[16] as basis.

3. MD simulation methodology

Diffusion of linear alkanes in Co-FA and Mn-FA were investigated and simulated using Newton's equations of motion until the system properties, on average, no longer change in time. The Verlet algorithm is used for time integration. A time step of 1 fs was used in all simulations. For each simulation, *initializing* CBMC moves are used to place the molecules in the domain, minimizing the energy. Next, follows an *equilibration* stage. These are essentially the same as the production cycles, only the statistics are not yet taken into account. This removes any initial large disturbances in the system that do not affect statistics on molecular displacements. After a fixed number of initialization and equilibrium steps, the MD simulation *production* cycles start. For every cycle, the statistics for determining the mean square displacements (MSDs) are updated. The MSDs are determined for time intervals ranging from 2 fs to 1 ns. In order to do this, an order-*N* algorithm, as detailed in Chapter 4 of Frenkel and Smit[13] is implemented. The Nosé-Hoover thermostat is applied to all the diffusing particles.

The DLPOLY code[17] was used along with the force field implementation as described in the previous section. DL_POLY is a molecular dynamics simulation package written by W. Smith, T.R. Forester and I.T. Todorov and has been obtained from CCLRCs Daresbury Laboratory via the website.[17]

The MD simulations were carried out for a variety of molecular loadings. All simulations were carried out on the LISA clusters of PCs equipped with Intel Xeon processors running at 3.4 GHz on the Linux operating system[18]. Each MD simulation, for a specified loading, was run for 120 h, determined to be long enough to obtain reliable statistics for determination of the diffusivities. In many cases, several independent MD simulations were run and the results averaged.

The self-diffusivities, $D_{\mathrm{i,self}}$, were computed by analyzing the mean square displacement of each species i for each of the coordinate directions:

$$D_{i,self} = \frac{1}{2n_i} \lim_{\Delta t \to \infty} \frac{1}{\Delta t} \left\langle \left(\sum_{l=1}^{n_i} \left(\mathbf{r}_{l,i}(t + \Delta t) - \mathbf{r}_{l,i}(t) \right)^2 \right) \right\rangle \qquad (1)$$

In this expression n_{i} represents the number of molecules of species i respectively, and $\mathbf{r}_{\mathrm{l,i}}(t)$ is the position of molecule l of species i at any time t. For one-dimensional pore structures of Mn-FA, and Co-FA, the diffusivities along the y-direction of diffusion are reported.

4. Animations

For visual appreciation of the diffusion phenomena in Co-FA, Mn-FA, Zn(bdc)dabco, and MIL-47, animations were created on the basis of the MD simulations; these can be viewed by downloading the movies from our website[8].

5. Simulation results for Co-FA

Figures 1 to 10 present the pore landscapes, and snapshots of n-alkanes in Co-FA. The simulation results, summarized in Figure 11, have been discussed in the main text of the paper.

6. Simulation results for Mn-FA

Figures 12 to 21 present the pore landscapes, and snapshots of n-alkanes in Mn-FA. The simulation results for adsorption of n-alkanes. As with Co-FA, the adsorbed phase is predominantly the shorter alkane. The near-complete separation of the nC4-nC5 mixture at high loadings is particularly

noteworthy. The diffusivity data for n-alkanes is summarized in Figure 22. Again we note the non-monotonicity as for Co-FA.

7. Simulation results for MIL-47

Figures 24 to 32 present the pore landscapes, and snapshots for xylenes, nC8, ethyl benzene and benzene within the channels of MIL-47. In Figure 33 the CBMC simulations of the pure component isotherms for C8 isomers are compared with the experimental results of Finsy et al. [6]. There is reasonably good agreement in the saturation capacities and the results indicate the possibility of separating C8 hydrocarbon isomers using differences in "stacking" efficiency within the channels of MIL-47.

8. Simulation results for Zn(bdc)dabco

Figures 34 to 45 present the pore landscapes, and snapshots of a variety of alkanes in Zn(bdc)dabco. Pure component, and ternary, CBMC simulations of the isotherms for nC6, 3MP, and 22DMB are present in Figure 46. The simulations at 300 K are in good agreement with the simulation results of Dubbeldam et al. [19]. Also shown in Figure 46 are the comparisons of the pure component isotherms for hexane isomers at 313 K obtained from CBMC simulations (top right) with the experimental data of Bárcia et al. [3] (bottom right). The agreement is very poor. We suspect that in the experiments the Zn(bdc) dabco structure must have undergone phase transition because the reported experimental loadings are about one order of magnitude lower than the usual loading values found for MOFs.

9. Acknowledgements

We are grateful to T.J.H. Vlugt, Delft, for providing the BIGMAC code. This code was modified to handle rigid molecular structures and charges, with generous assistance and technical inputs from S. Calero, Seville.

10. Notation

$D_{i,self}$	self-diffusivity, $m^2\ s^{-1}$
f_i	fugacity of species *i*, Pa
n_i	number of molecules of species *i* in simulation box, dimensionless
$\mathbf{r}_{l,i}(t)$	position of molecule *l* of species *i* at any time *t*, m
t	time, s
T	absolute temperature, K

Table 1. Lennard-Jones parameters for atoms in metal-organic host framework. For the atoms in the guest metal organic framework, the generic UFF [11] was used. The DREIDING [12] force fields was used for the organic linker atoms.

(pseudo-) atom	σ / Å	ε/k_B / K
Cu	3.114	2.518
Zn	2.69	0.41
Co	2.56	7.046
Mn	2.638	6.543
O	3.03	48.19
C	3.47	47.86
N	3.26	38.95
H	2.85	7.65

Table 2. Dimensions of unit cell, along with factor to convert loadings from molecules per unit cell to mol per kg of framework.

MOF	*a* / Å	*b* / Å	*c* / Å	Conversion factor
Co-FA	11.3834	9.9292	14.4324	0.56
Mn-FA	11.715	10.248	15.159	0.575
MIL-47	6.808	16.12	13.917	1.08
Zn(bdc)dabco	10.9288	10.9288	9.6084	1.75

11. References

[1] K. Li, D.H. Olson, J.Y. Lee, W. Bi, K. Wu, T. Yuen, Q. Xu, J. Li, Multifunctional Microporous MOFs Exhibiting Gas/Hydrocarbon Adsorption Selectivity, Separation Capability and Three-Dimensional Magnetic Ordering, Adv. Funct. Mater. 18 (2008) 2205-2214.

[2] D.N. Dybtsev, H. Chun, S.H. Yoon, D. Kim, K. Kim, Microporous Manganese Formate: A Simple Metal-Organic Porous Material with High Framework Stability and Highly Selective Gas Sorption Properties, J. Am. Chem. Soc. 126 (2004) 32-33.

[3] P.S. Bárcia, F. Zapata, J.A.C. Silva, A.E. Rodrigues, B. Chen, Kinetic Separation of Hexane Isomers by Fixed-Bed Adsorption with a Microporous Metal-Organic Framework, J. Phys. Chem. B 111 (2008) 6101-6103.

[4] J.Y. Lee, D.H. Olson, L. Pan, T.J. Emge, J. Li, Microporous Metal–Organic Frameworks with High Gas Sorption and Separation Capacity, Adv. Funct. Mater. 17 (2007) 1255-1262.

[5] L. Alaerts, C.E.A. Kirschhock, M. Maes, M. van der Veen, V. Finsy, A. Depla, J.A. Martens, G.V. Baron, P.A. Jacobs, J.F.M. Denayer, D. De Vos, Selective Adsorption and Separation of Xylene Isomers and Ethylbenzene with the Microporous Vanadium(IV) Terephthalate MIL-47, Angew. Chem. Int. Ed. 46 (2007) 4293-4297.

[6] V. Finsy, H. Verelst, L. Alaerts, D. De Vos, P.A. Jacobs, G.V. Baron, J.F.M. Denayer, Pore-Filling-Dependent Selectivity Effects in the Vapor-Phase Separation of Xylene Isomers on the Metal-Organic Framework MIL-47, J. Am. Chem. Soc. 130 (2008) 7110-7118.

[7] K. Barthelet, J. Marrot, D. Riou, G. Férey, A Breathing Hybrid Organic - Inorganic Solid with Very Large Pores and High Magnetic Characteristics, Angew. Chem. Int. Ed. 41 (2007) 281-284.

[8] J.M. van Baten, R. Krishna, MD animations of diffusion in nanoporous materials, University of Amsterdam, Amsterdam, http://www.science.uva.nl/research/cr/animateMD/, 4 November 2008.

[9] D. Dubbeldam, S. Calero, T.J.H. Vlugt, R. Krishna, T.L.M. Maesen, B. Smit, United Atom Forcefield for Alkanes in Nanoporous Materials, J. Phys. Chem. B 108 (2004) 12301-12313.

[10] S. Ban, A. van Laak, P.E. de Jongh, J.P.J.M. van der Eerden, T.J.H. Vlugt, Adsorption Selectivity of Benzene and Propene Mixtures for Various Zeolites, J. Phys. Chem. C 111 (2007) 17241-17248.

[11] A.K. Rappé, C.J. Casewit, K.S. Colwel, W.A. Goddard, W.M. Skiff, UFF, a Full Periodic Table Force Field for Molecular Mechanics and Molecular Dynamics Simulations, J. Am. Chem. Soc. 114 (1992) 10024-10035.

[12] S.L. Mayo, B.D. Olafson, W.A. Goddard, DREIDING: A Generic Force Field for Molecular Simulations, J. Phys. Chem. 94 (1990) 8897-8909.

[13] D. Frenkel, B. Smit, Understanding molecular simulations: from algorithms to applications, Academic Press, 2nd Edition, San Diego, 2002.

[14] T.J.H. Vlugt, R. Krishna, B. Smit, Molecular simulations of adsorption isotherms for linear and branched alkanes and their mixtures in silicalite, J. Phys. Chem. B 103 (1999) 1102-1118.

[15] D. Dubbeldam, S. Calero, T.J.H. Vlugt, R. Krishna, T.L.M. Maesen, E. Beerdsen, B. Smit, Force Field Parametrization through Fitting on Inflection Points in Isotherms, Phys. Rev. Lett. 93 (2004) 088302.

[16] T.J.H. Vlugt, BIGMAC, University of Amsterdam, http://molsim.chem.uva.nl/bigmac/, 1 November 2000.

[17] W. Smith, T.R. Forester, I.T. Todorov, The DL_POLY Molecular Simulation Package, Warrington, England, http://www.cse.clrc.ac.uk/msi/software/DL_POLY/index.shtml, March 2006.
[18] SARA, Computing & Networking Services, Amsterdam, https://subtrac.sara.nl/userdoc/wiki/lisa/description, 16 January 2008.
[19] D. Dubbeldam, C.J. Galvin, K.S. Walton, D.E. Ellis, R.Q. Snurr, Separation and Molecular-Level Segregation of Complex Alkane Mixtures in Metal-Organic Frameworks, J. Am. Chem. Soc. 130 (2008) 10884-10885.

12. Captions for Figures

Figures 1 to 11 present the pore landscapes, snapshots, and simulation results for Co-FA.

Figures 12 to 23 present the pore landscapes, snapshots, and simulation results for Mn-FA.

Figures 24 to 33 present the pore landscapes, snapshots, and simulation results for MIL-47.

Figures 34 to 46 present the pore landscapes, snapshots, and simulation results for Zn(bdc)dabco.

Figure 1

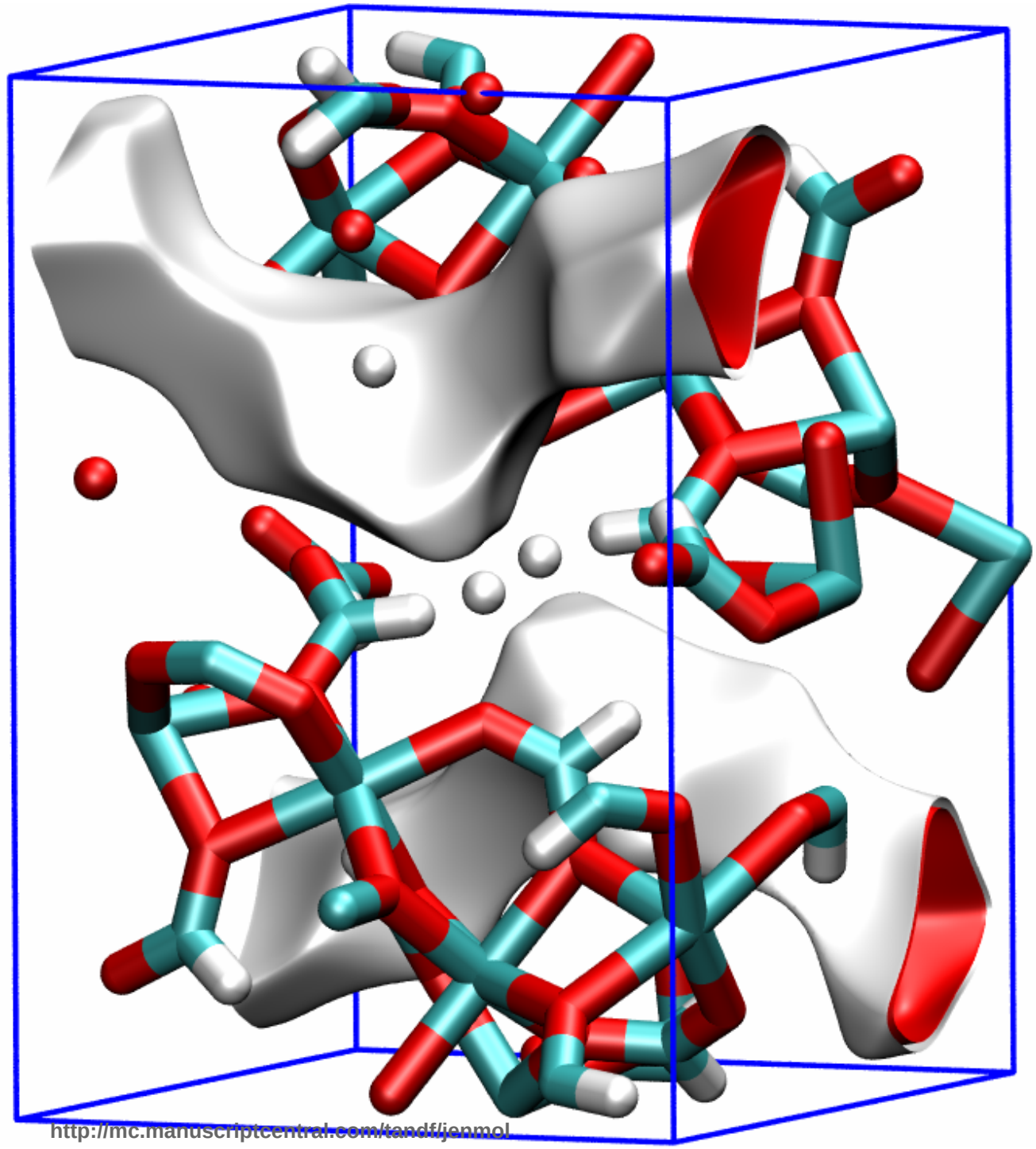

Unit cell for Co-FA

Figure 2

C1

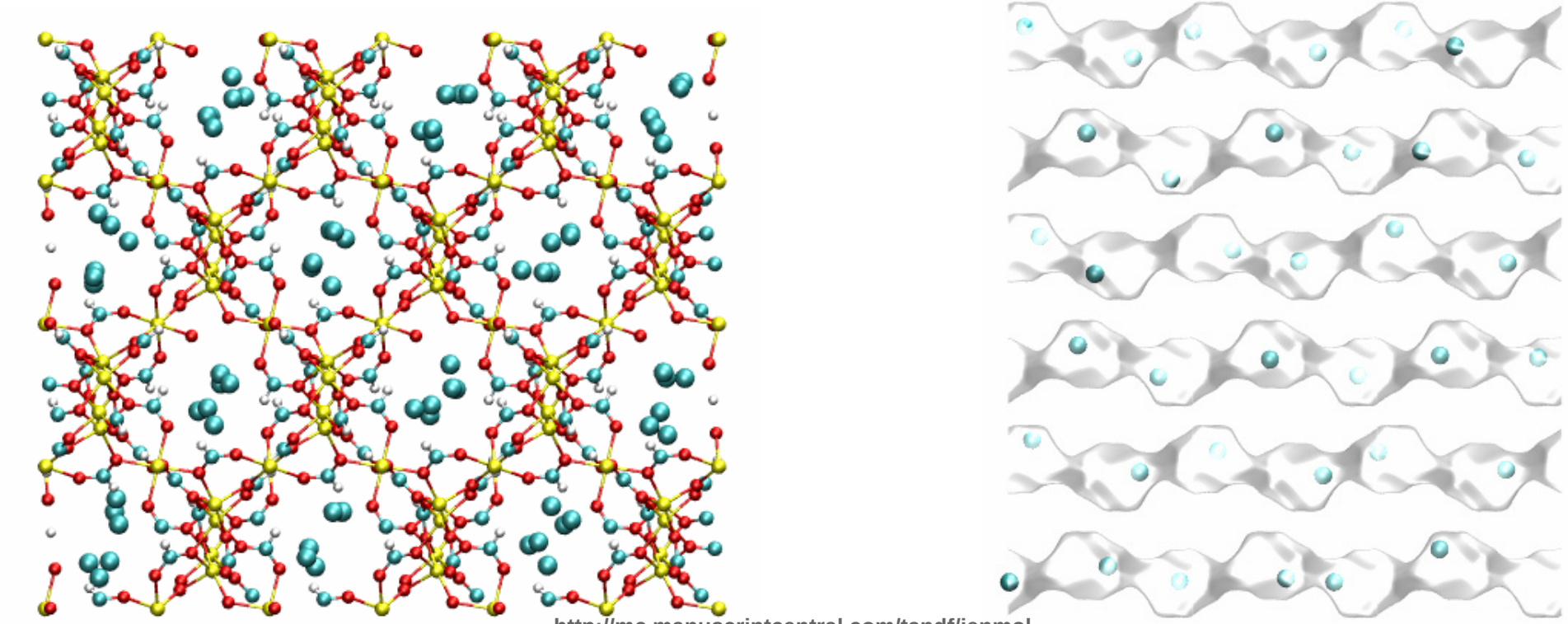

Figure 3

C2

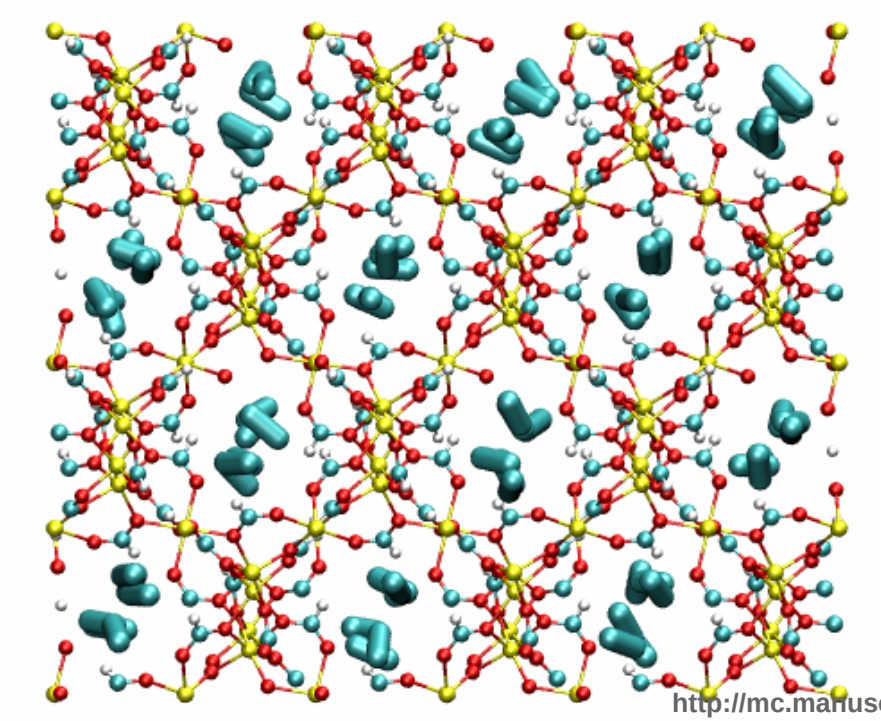

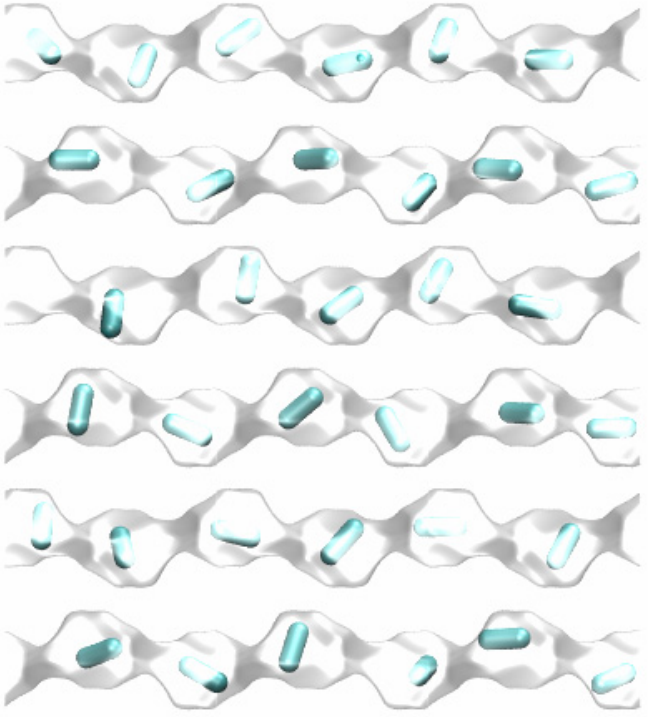

Figure 4

C3

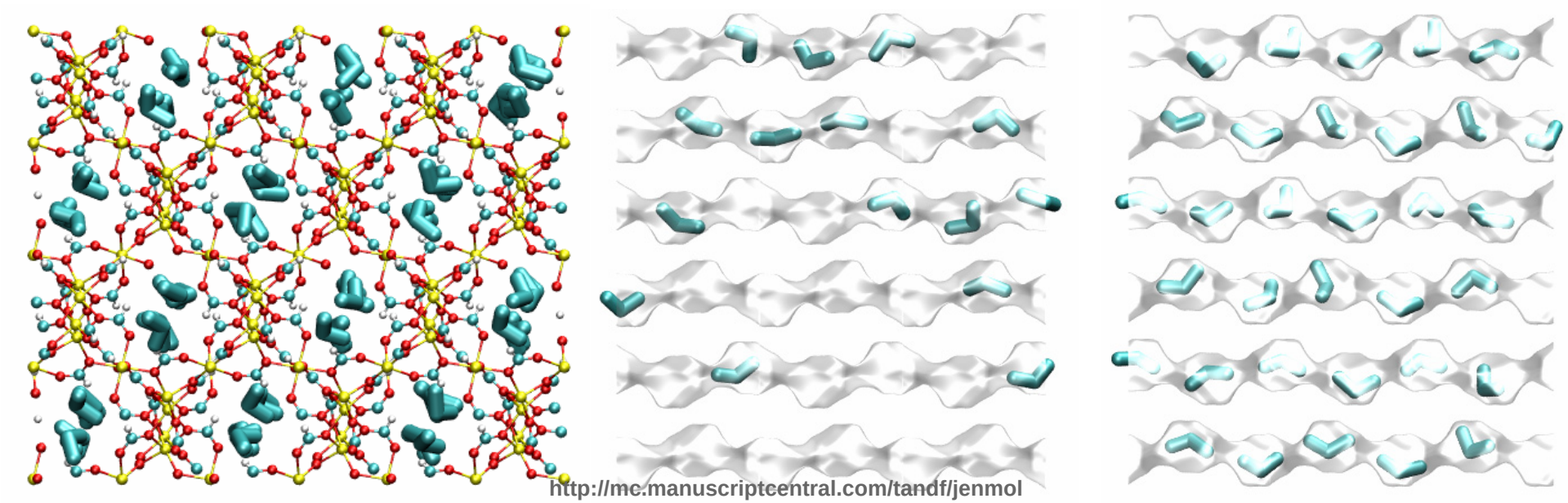

Figure 5

nC4

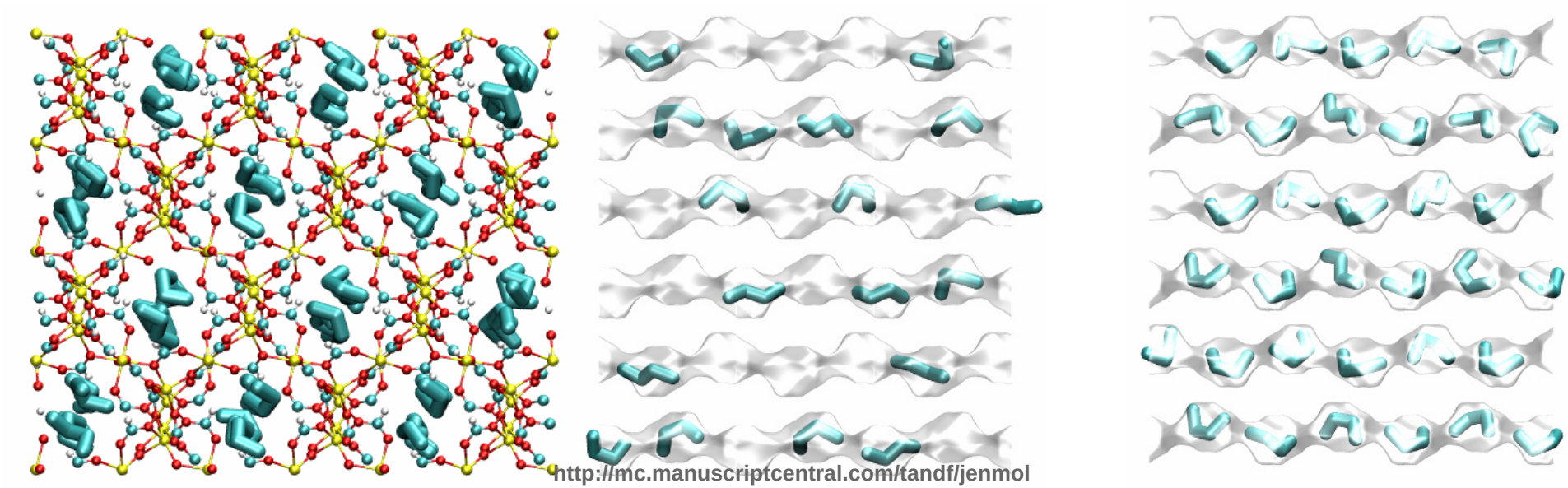

Figure 6

nC5

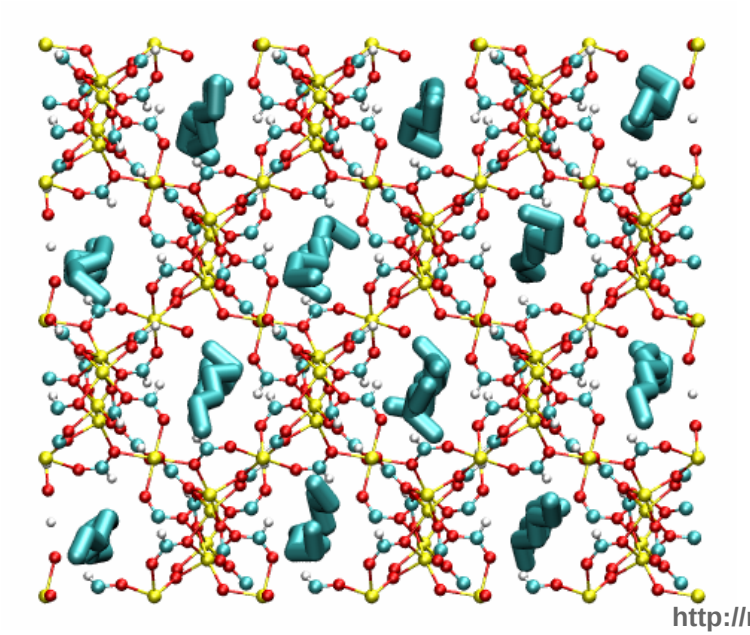

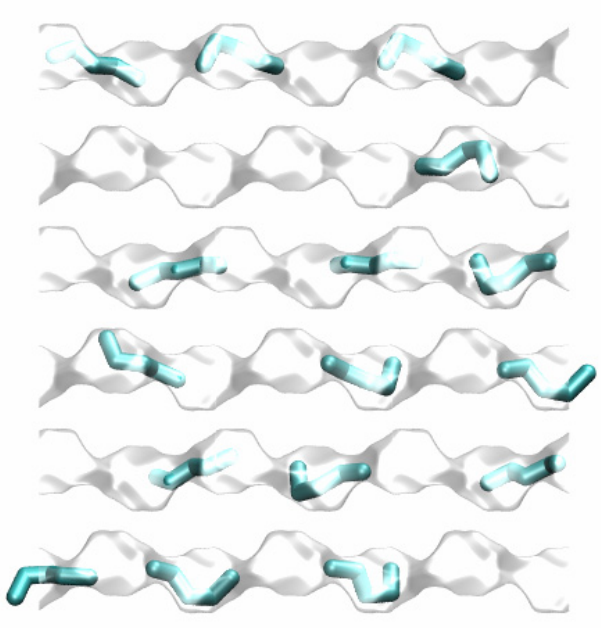

Figure 7

nC6

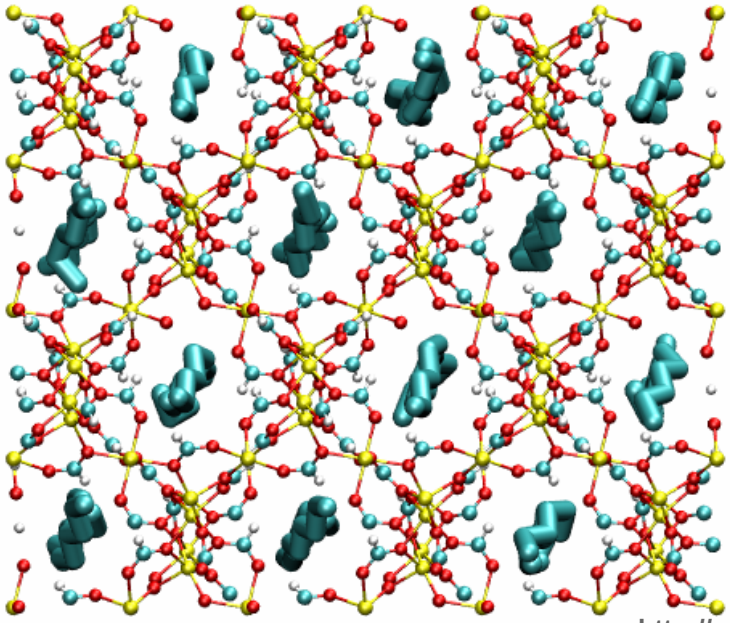

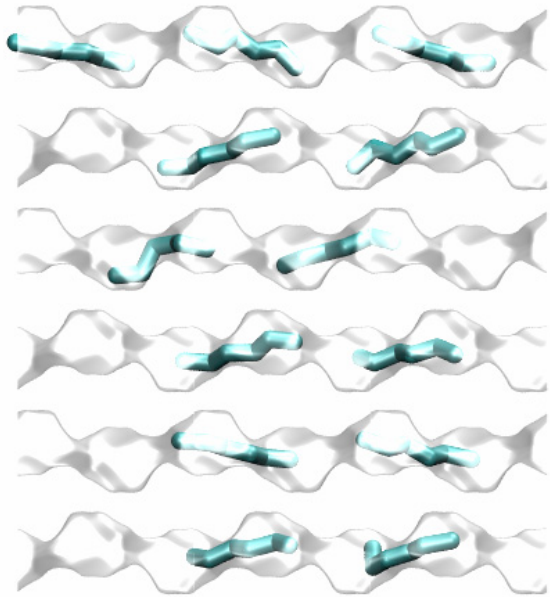

Figure 8

nC7

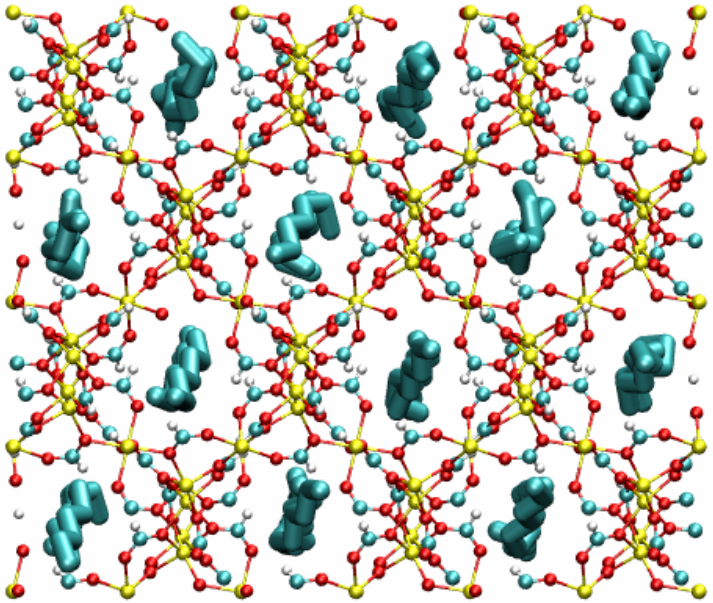

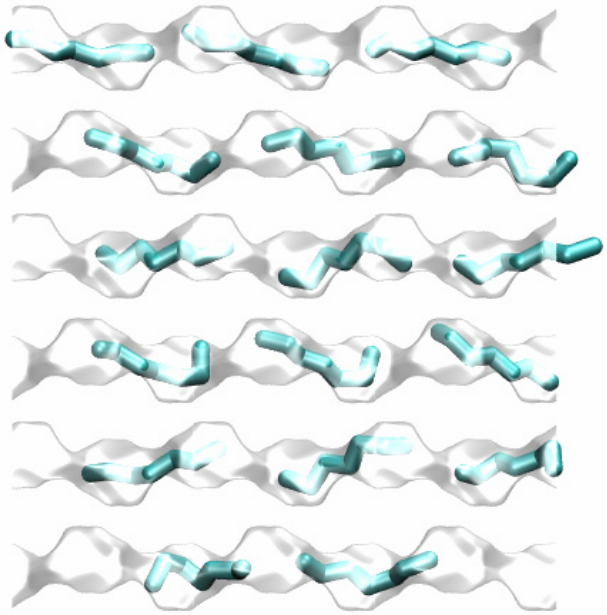

Figure 9

nC8

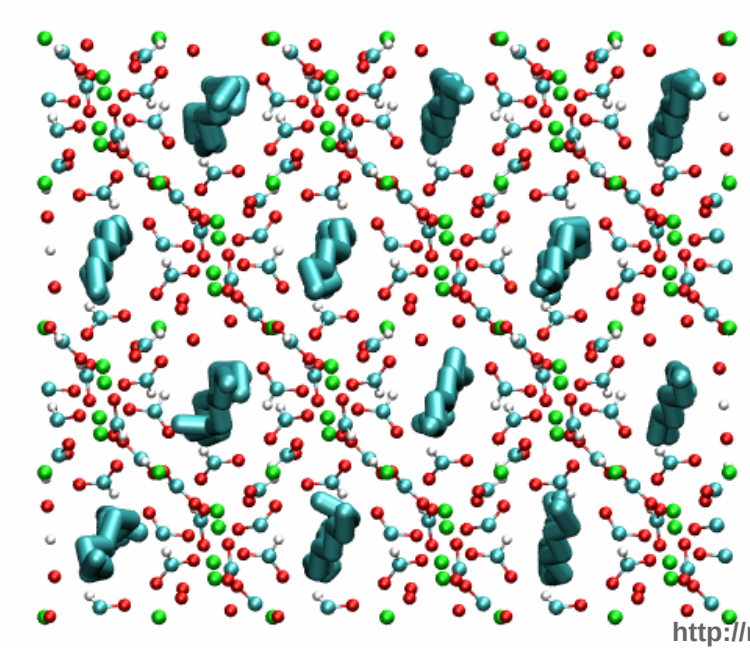

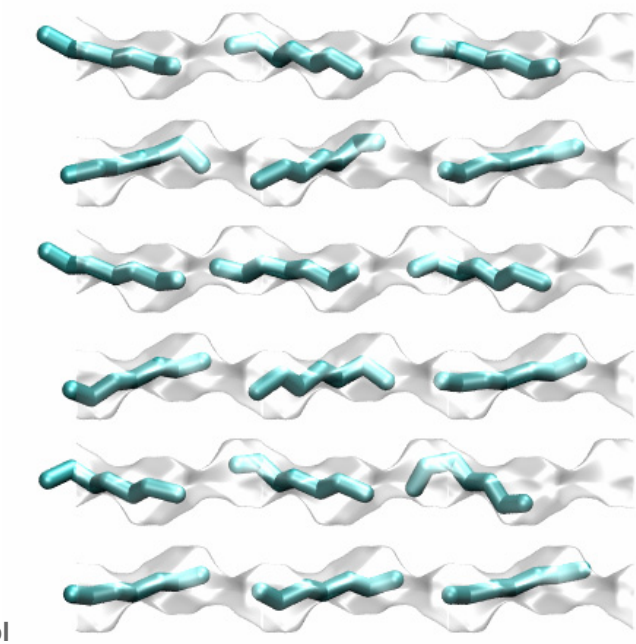

Figure 10

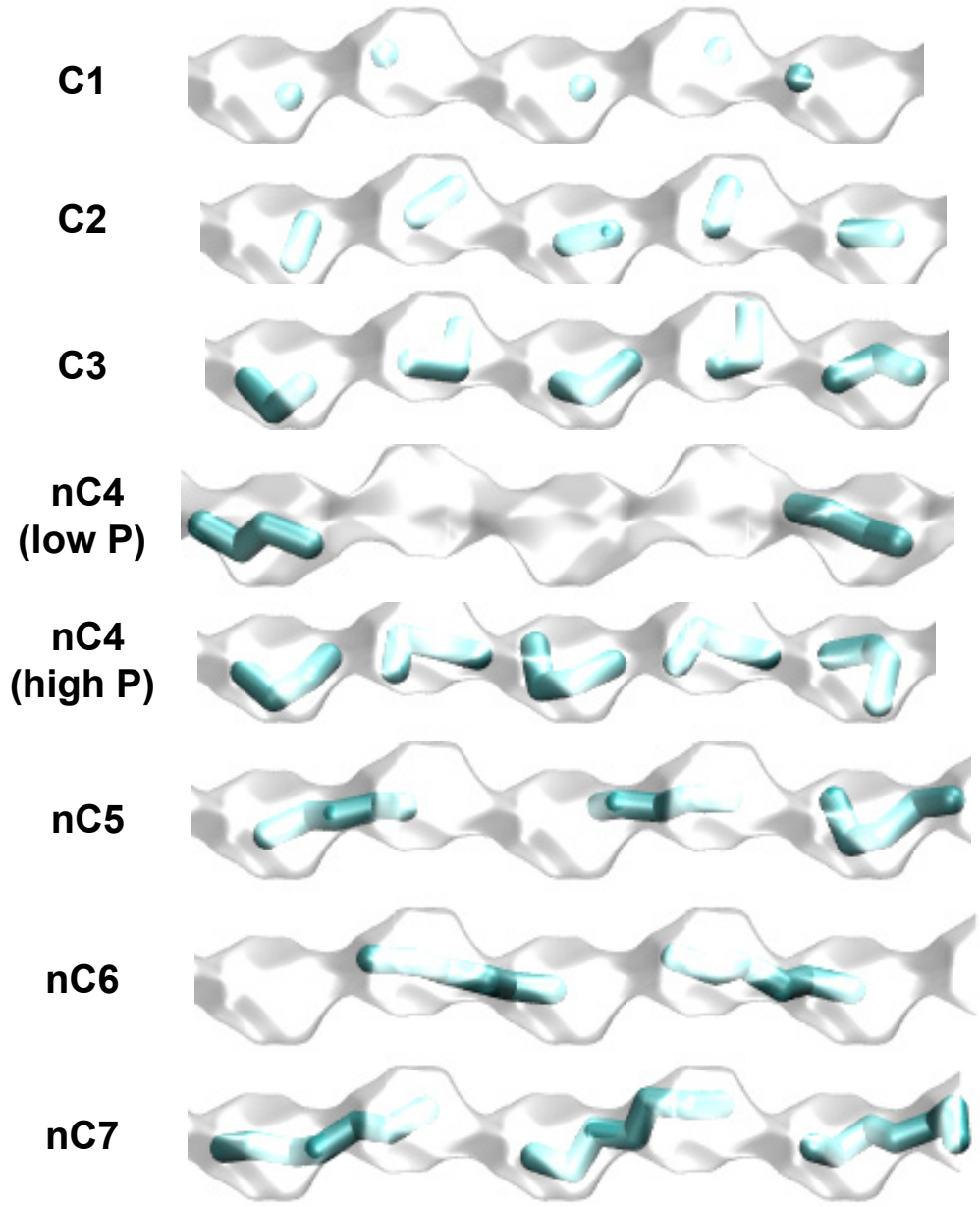

Figure 11

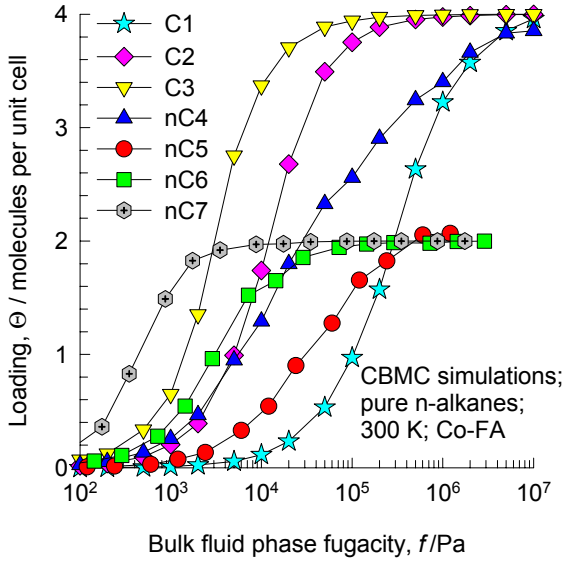

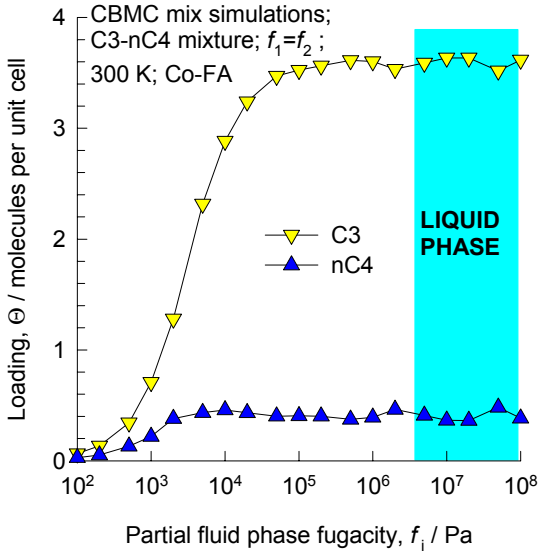

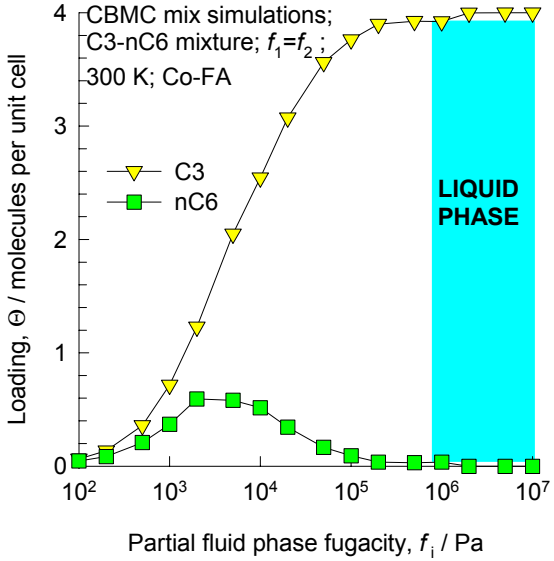

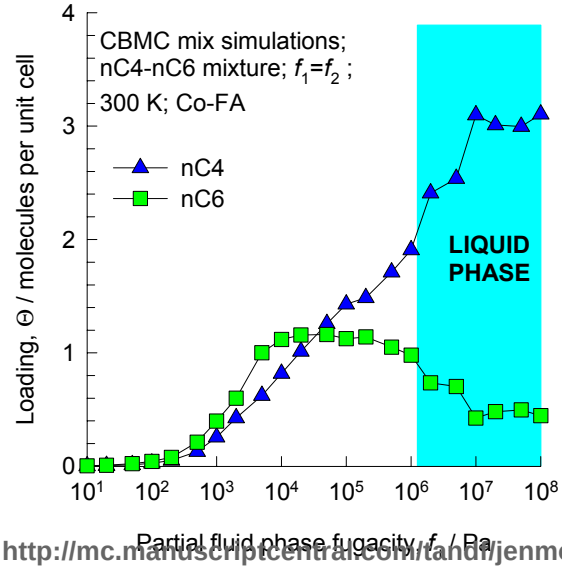

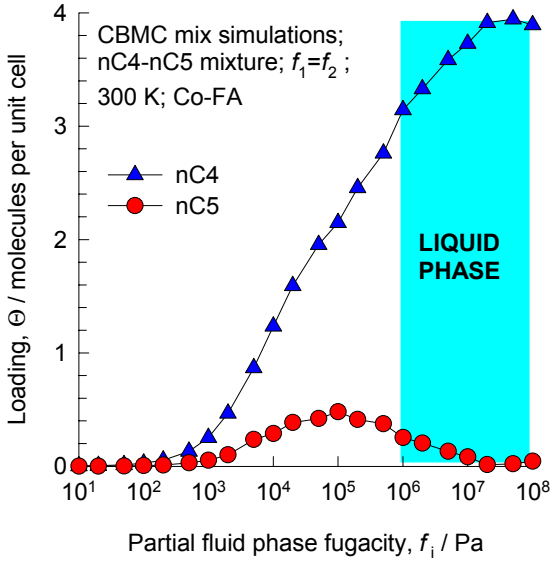

Figure 12

Unit cell for Mn-FA

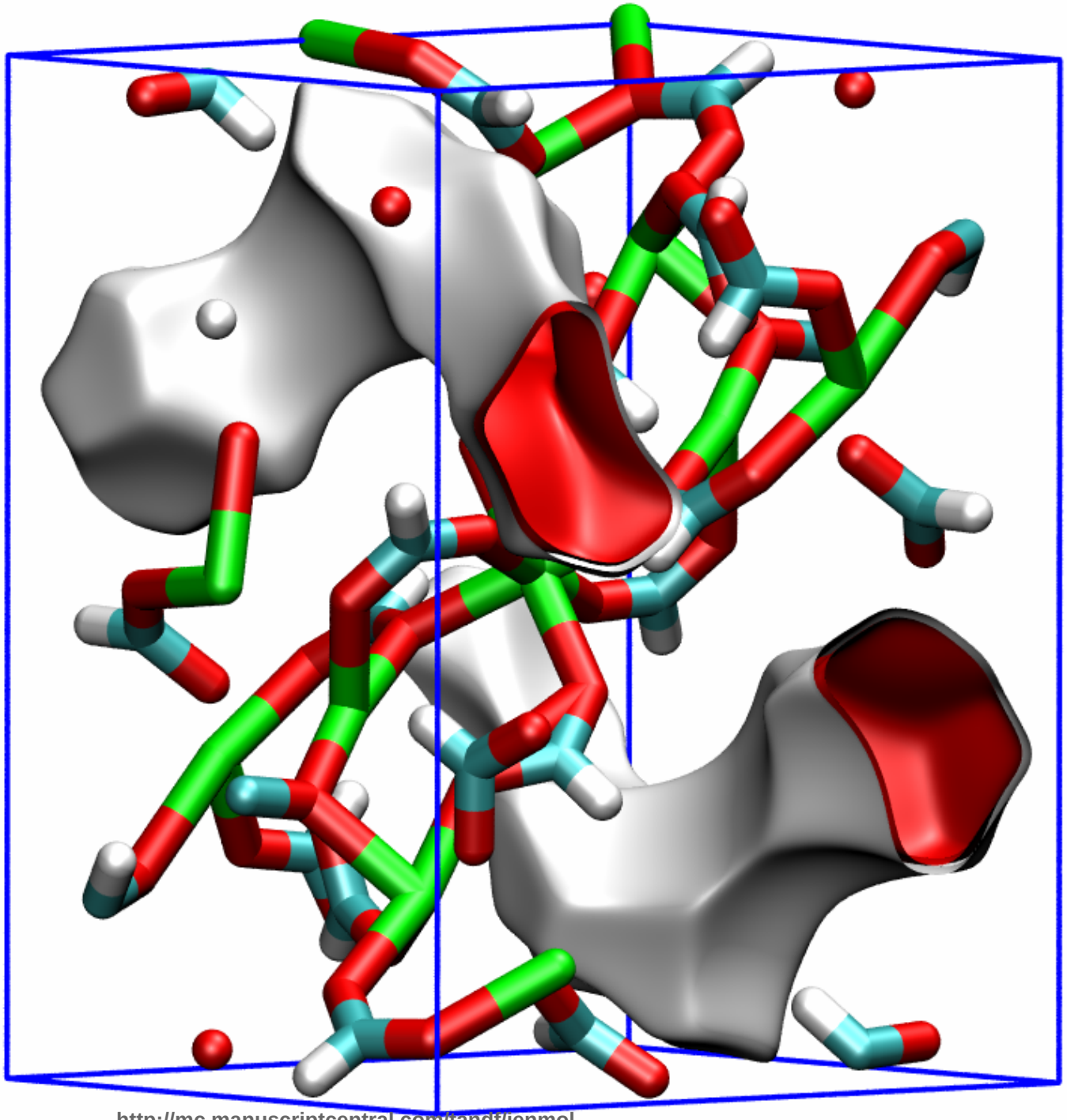

Figure 13

C1

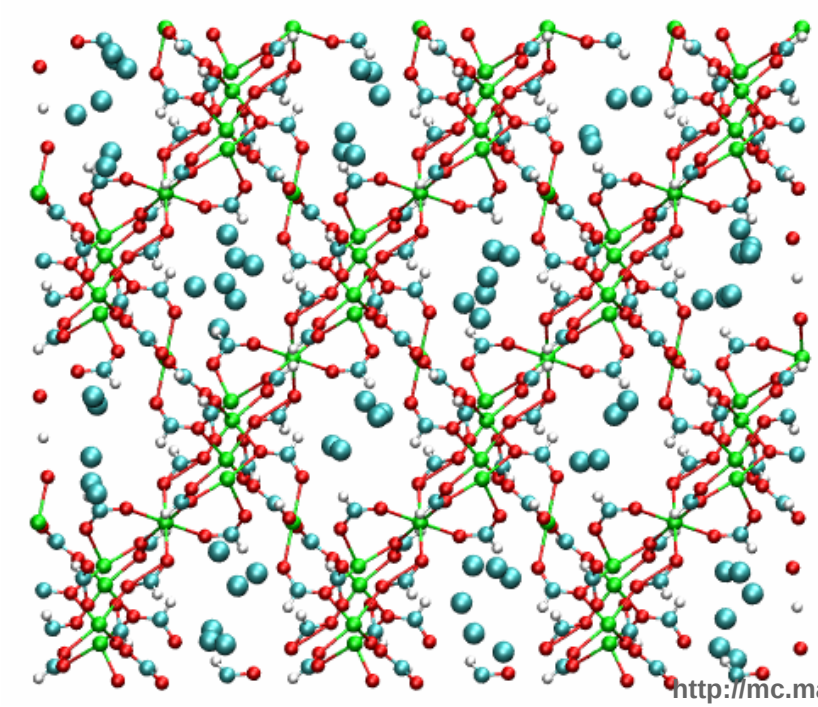

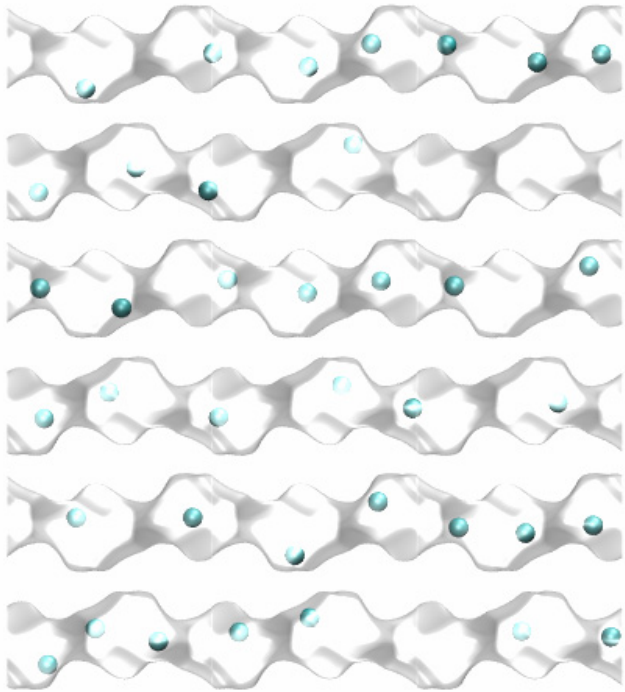

Figure 14

C2

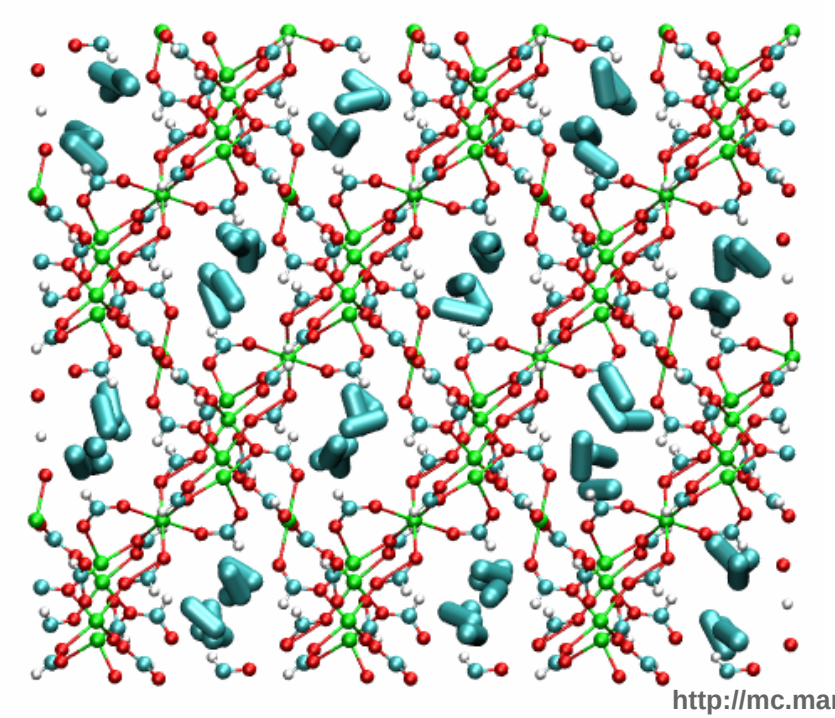

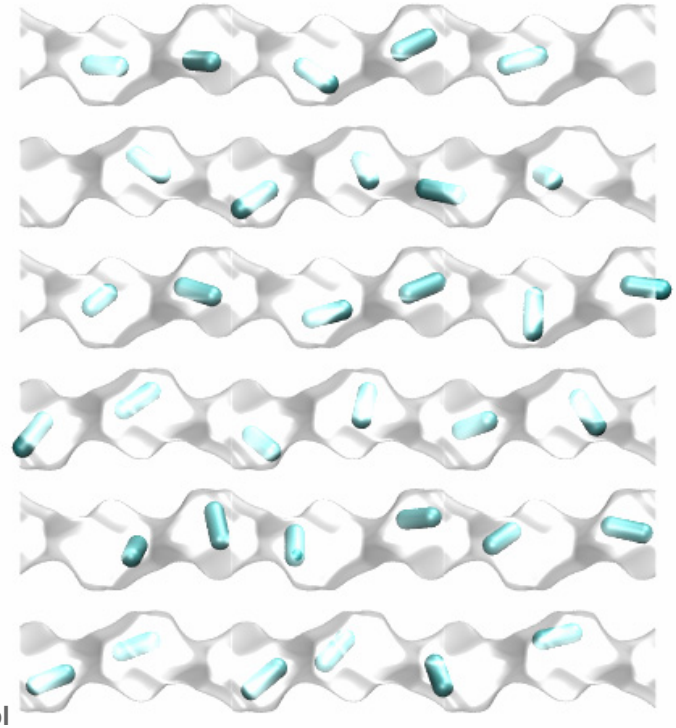

Figure 15

C3

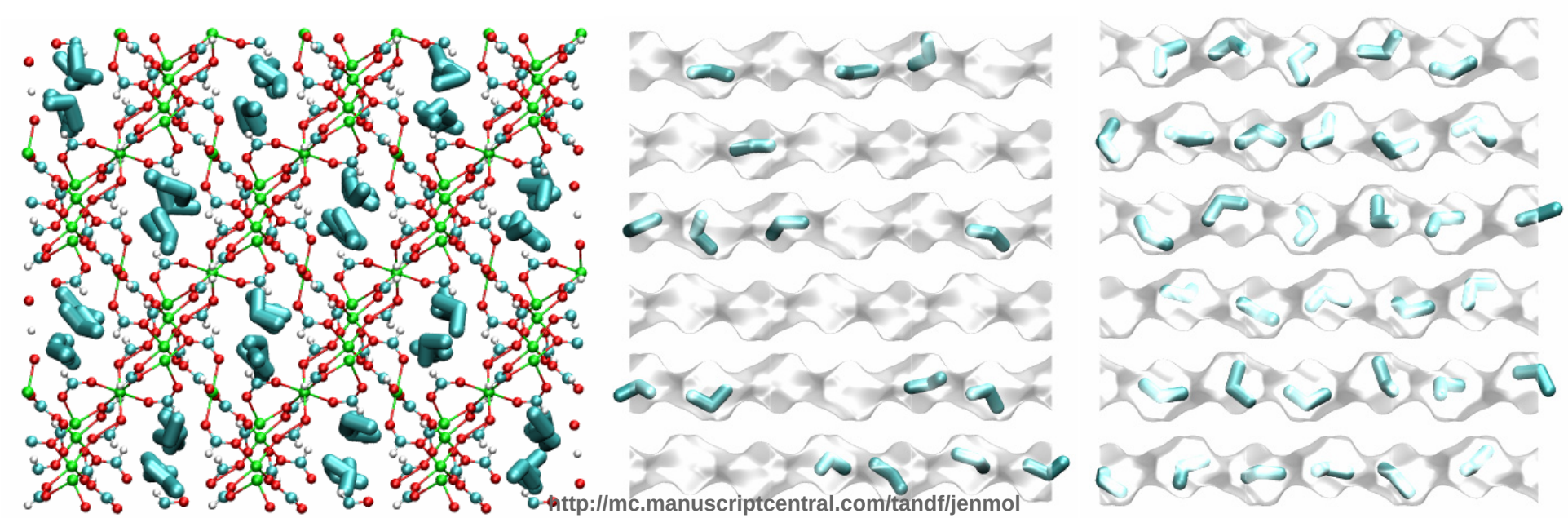

Figure 16

nC4

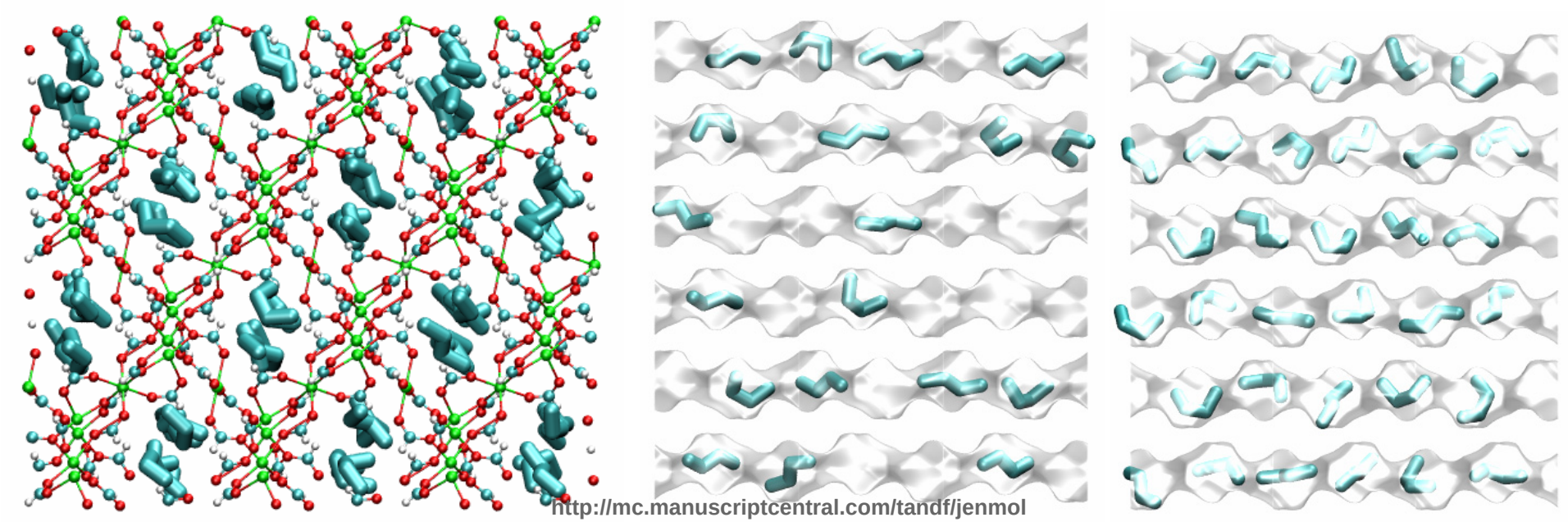

Figure 17

nC5

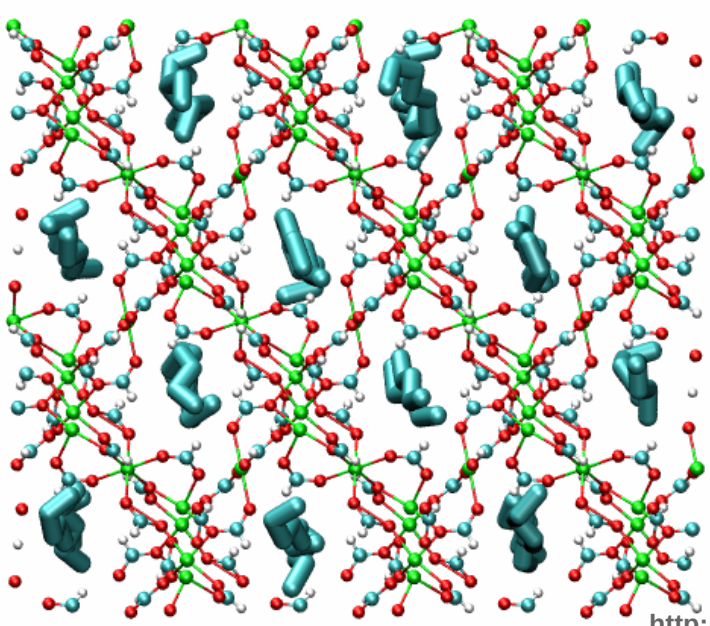

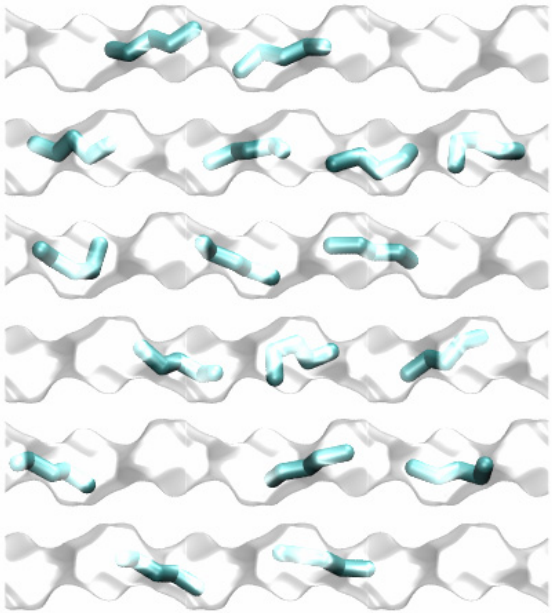

Figure 18

nC6

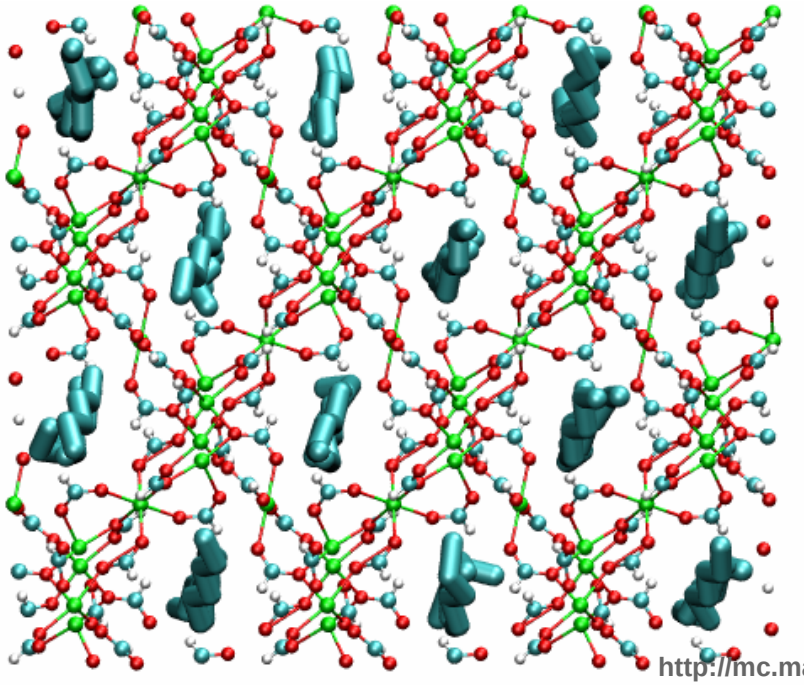

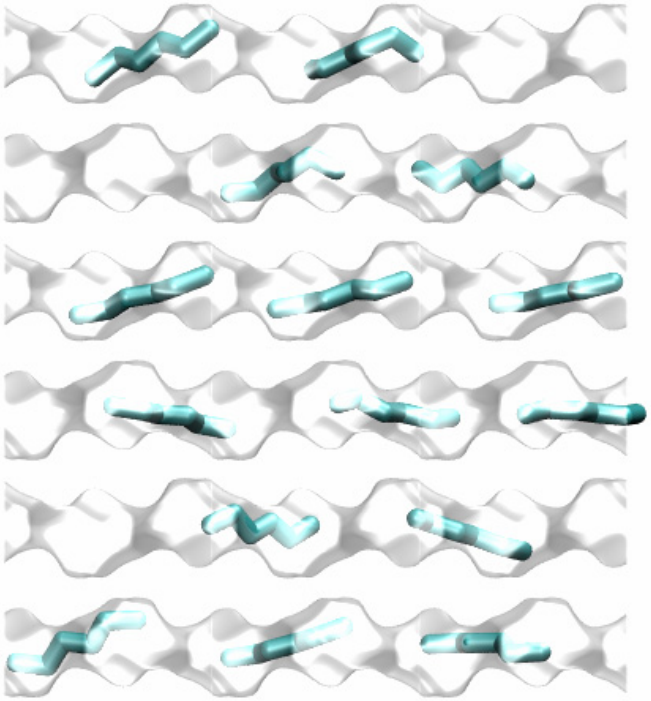

Figure 19

nC7

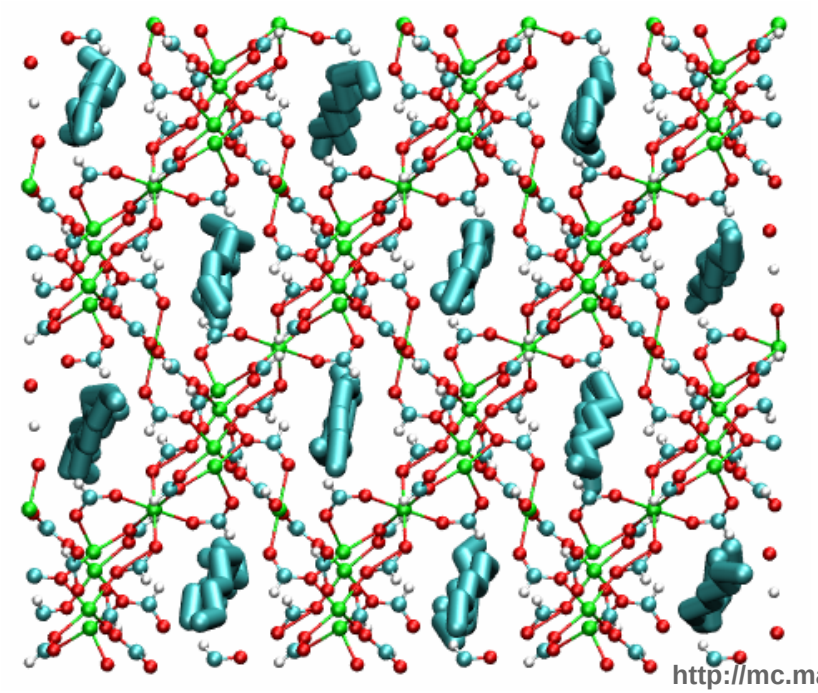

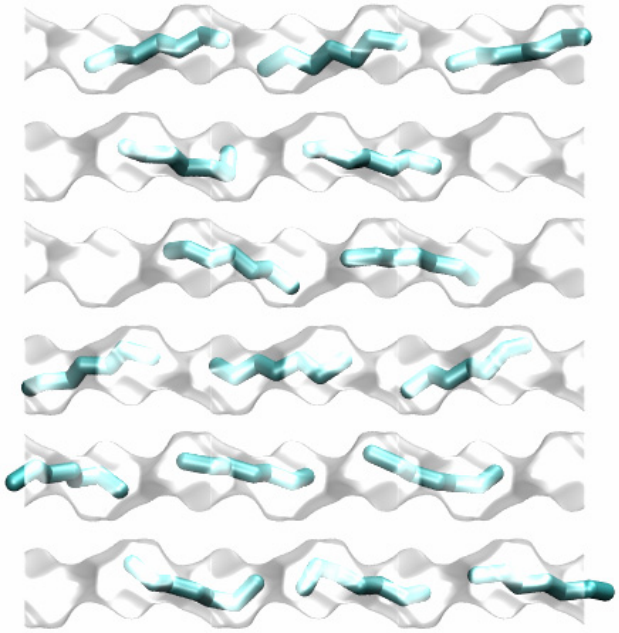

Figure 20

nC8

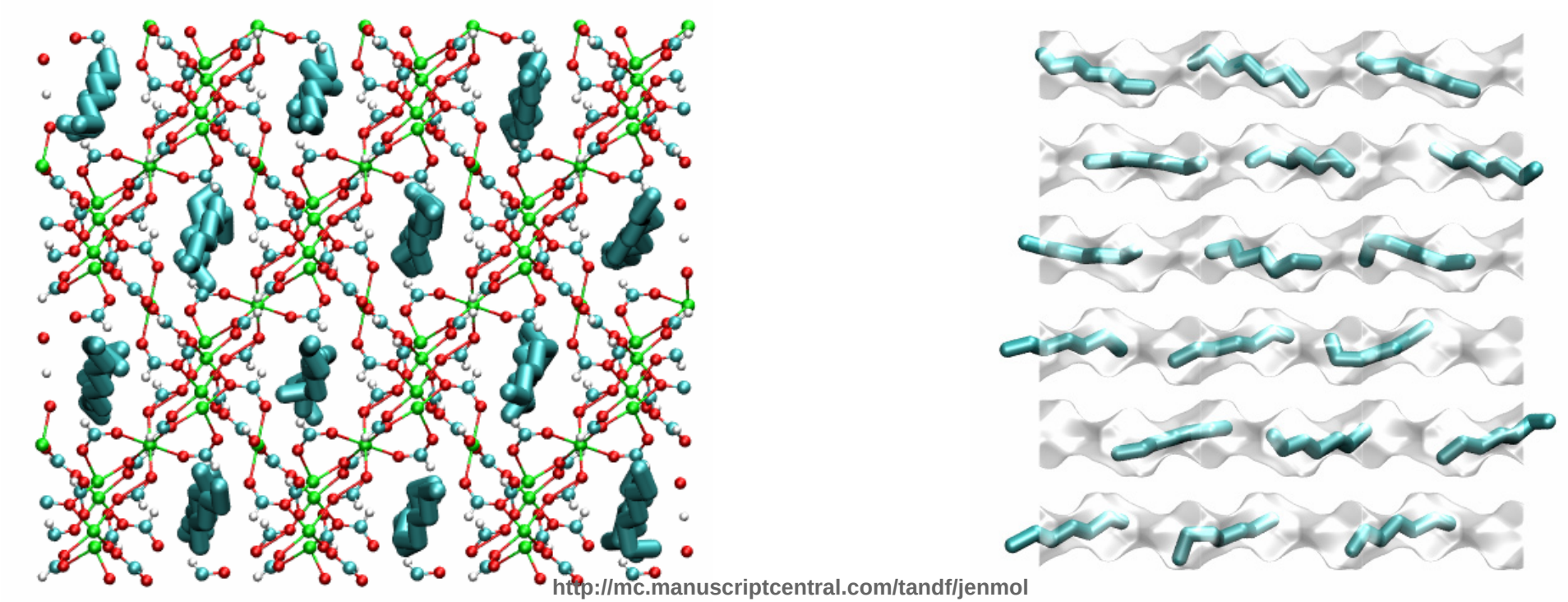

Figure 21

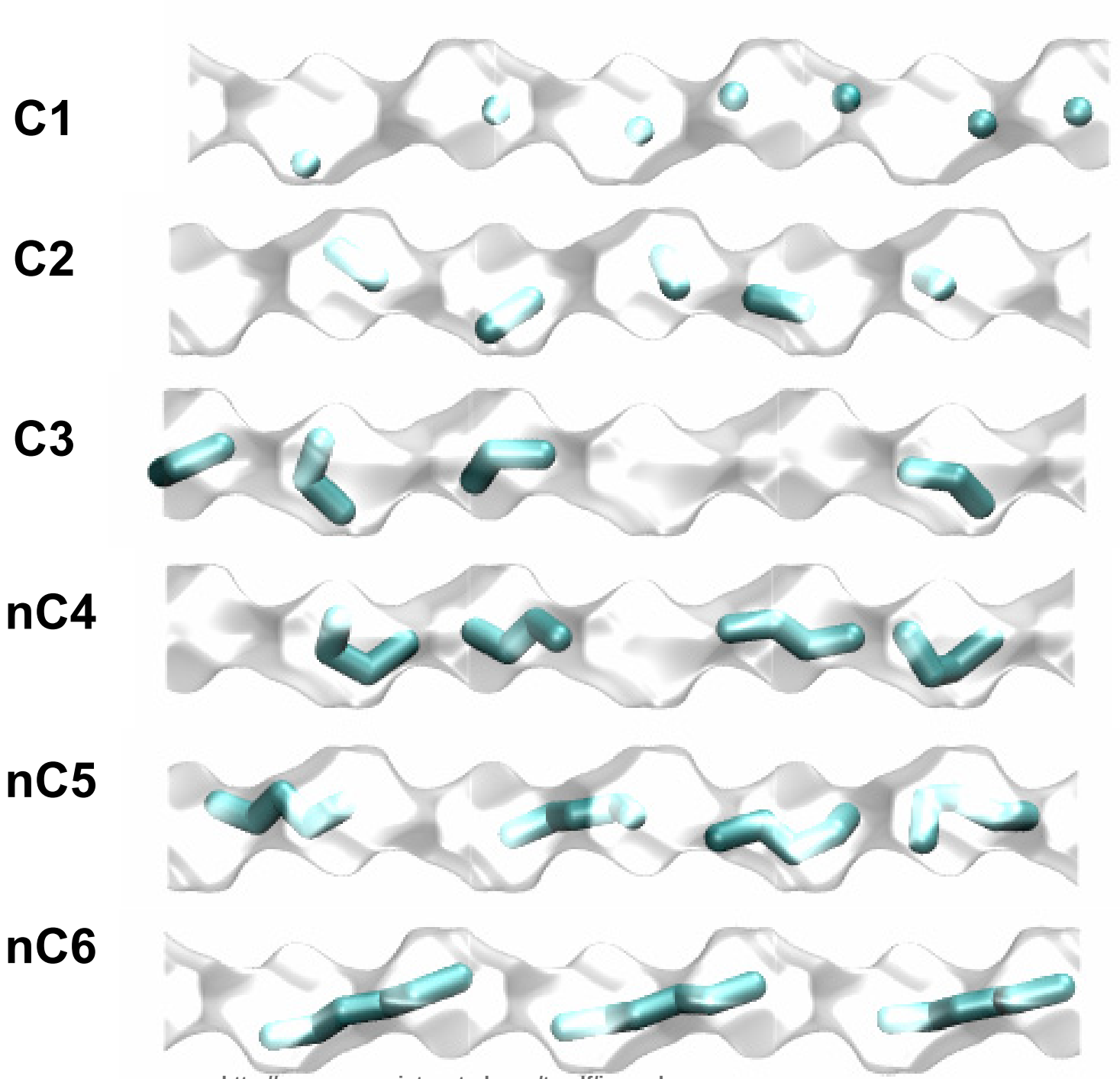

Figure 22

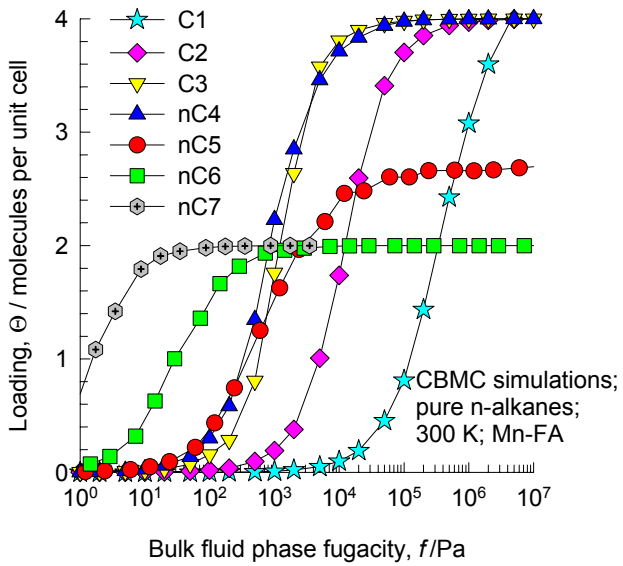

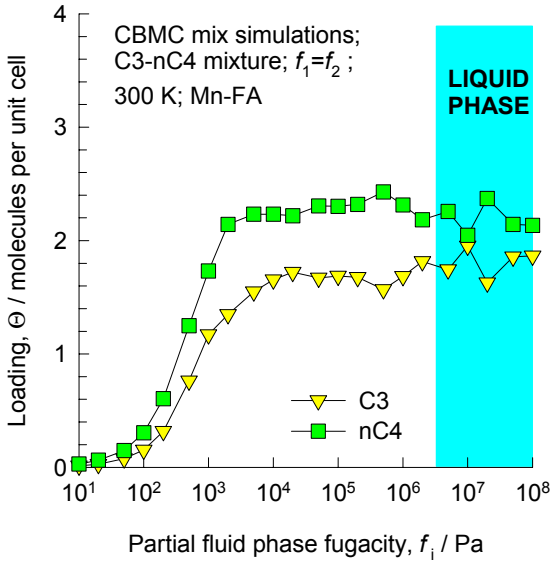

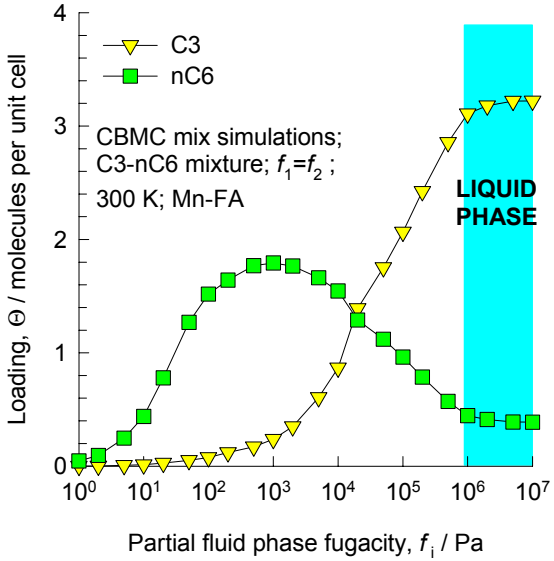

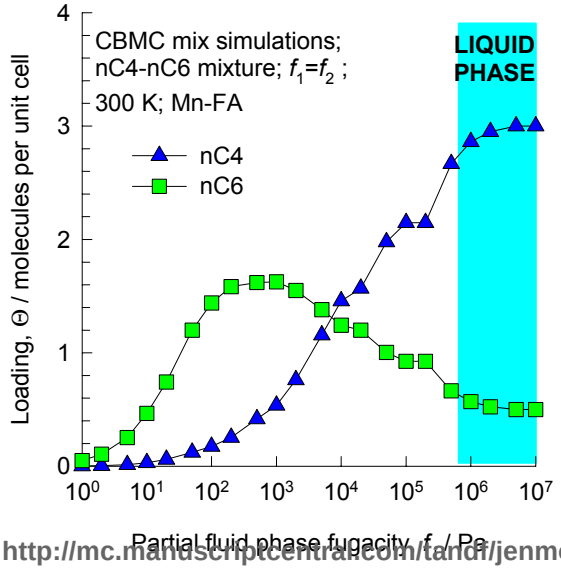

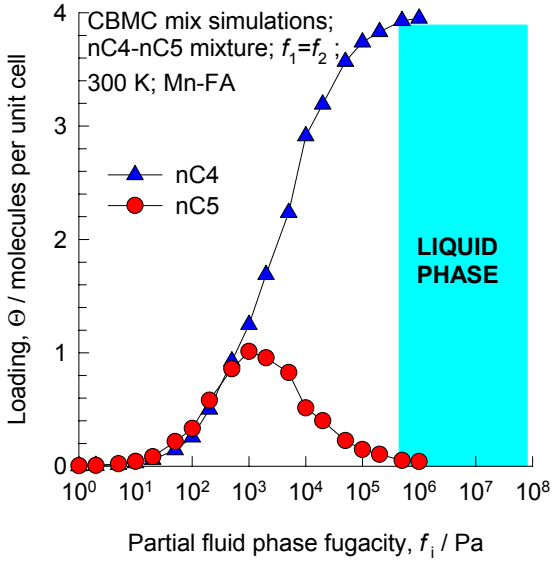

Figure 23

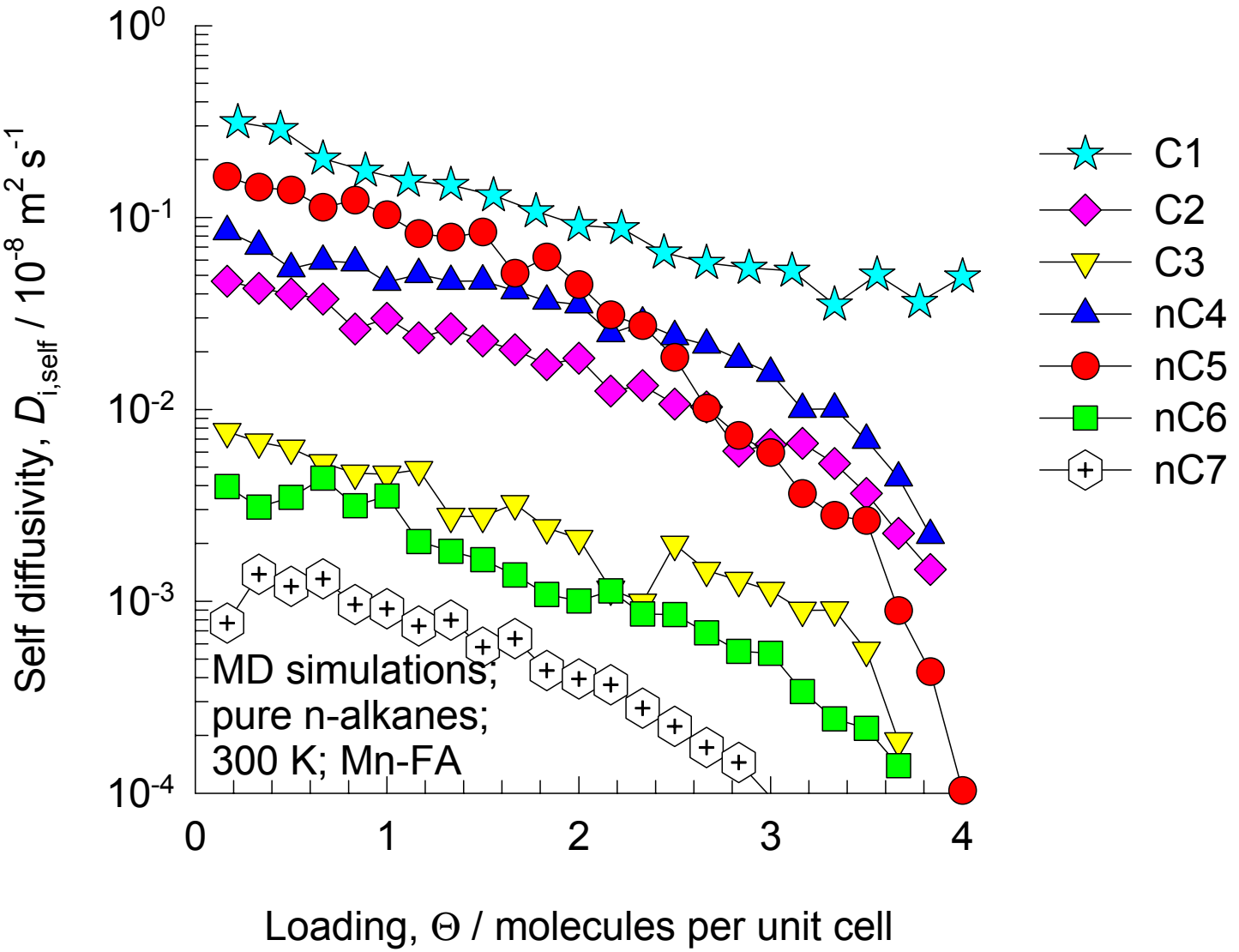
Self diffusivity, $D_{i,self}$ / 10^{-8} m^2 s^{-1}
10^0
10^{-1}
10^{-2}
10^{-3}
10^{-4}
0
1
2
3
4
Loading, Θ / molecules per unit cell
MD simulations;
pure n-alkanes;
300 K; Mn-FA
C1
C2
C3
nC4
nC5
nC6
nC7

Figure 24

MIL – 47 structure

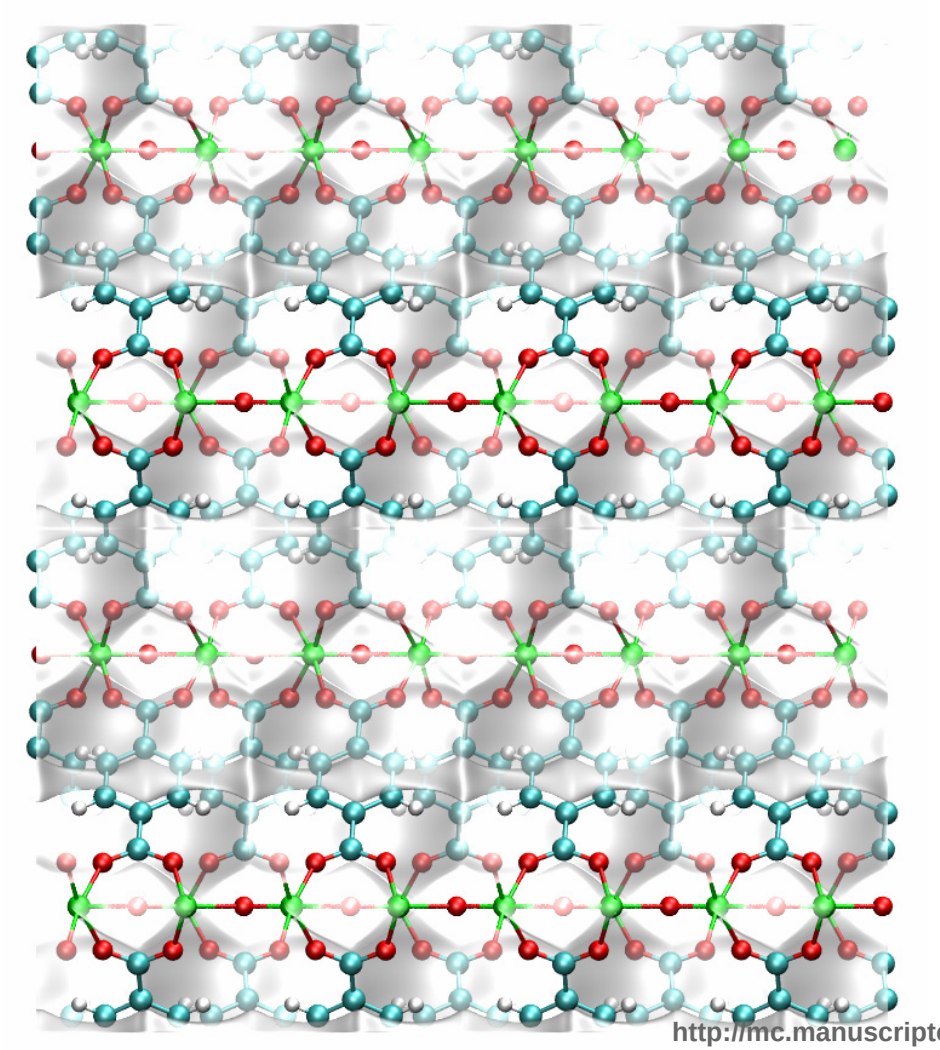

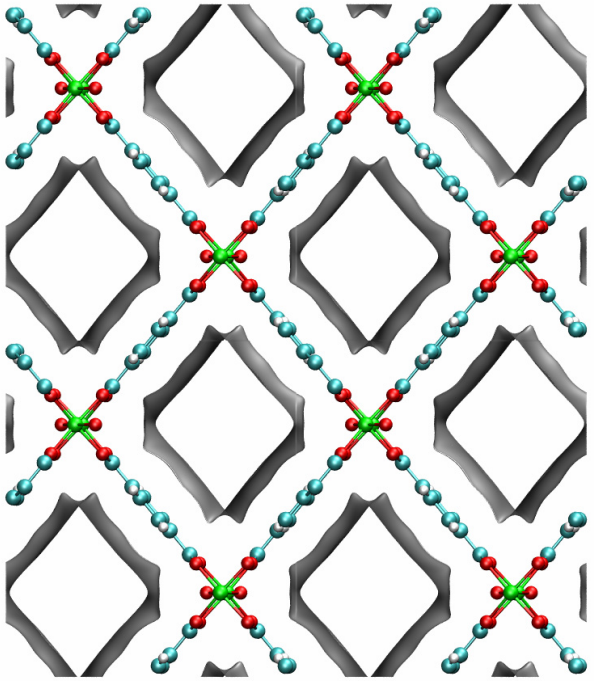

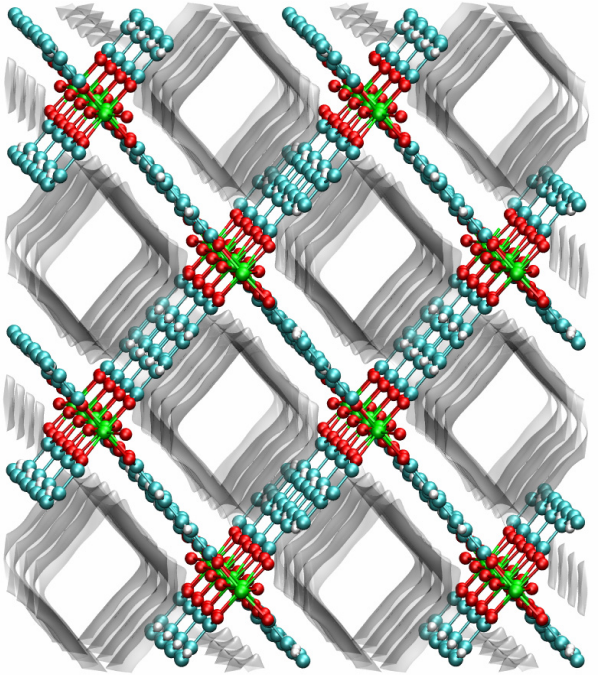

Figure 25

MIL – 47 unit cell, with pore landscape

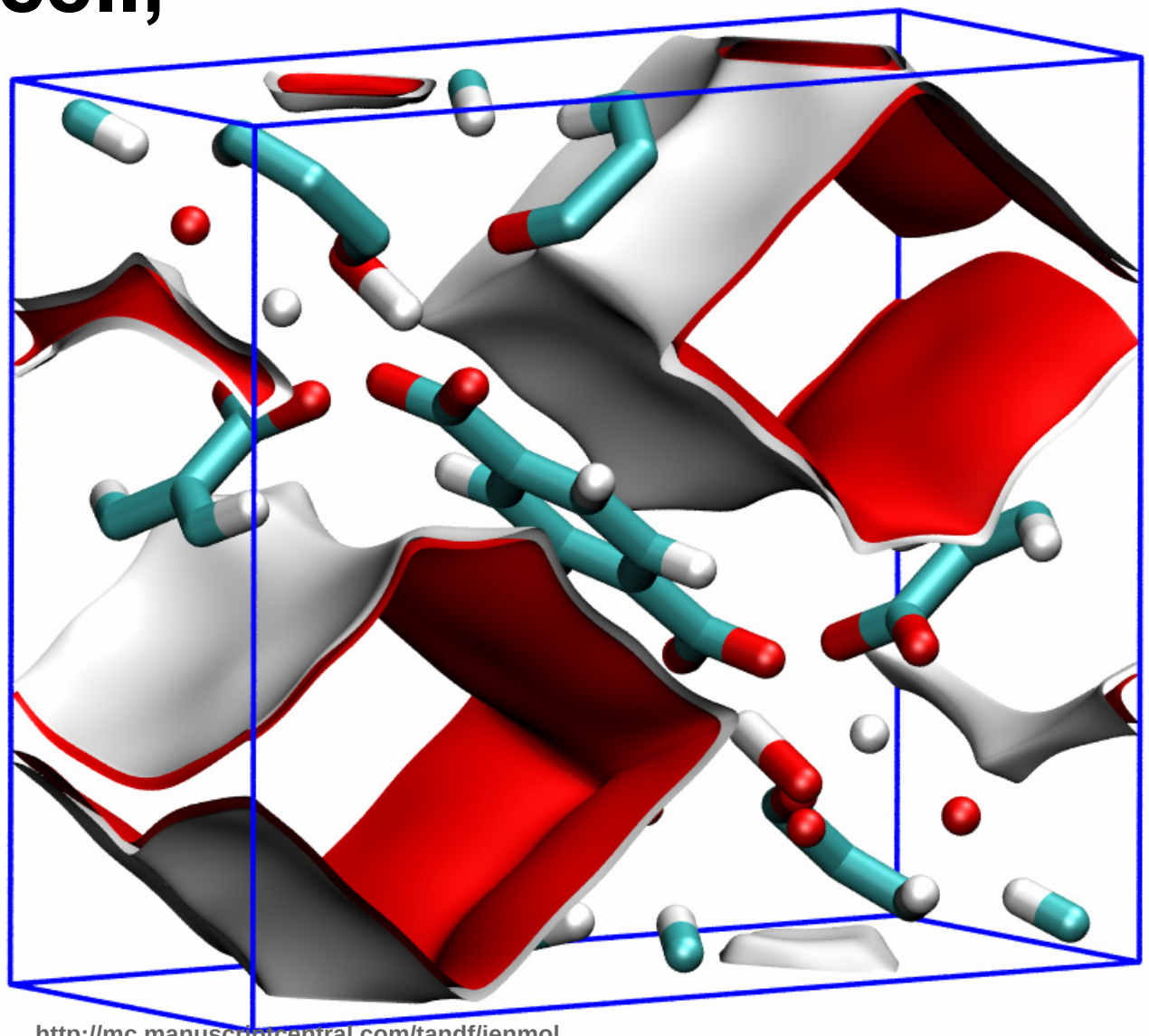

Figure 26

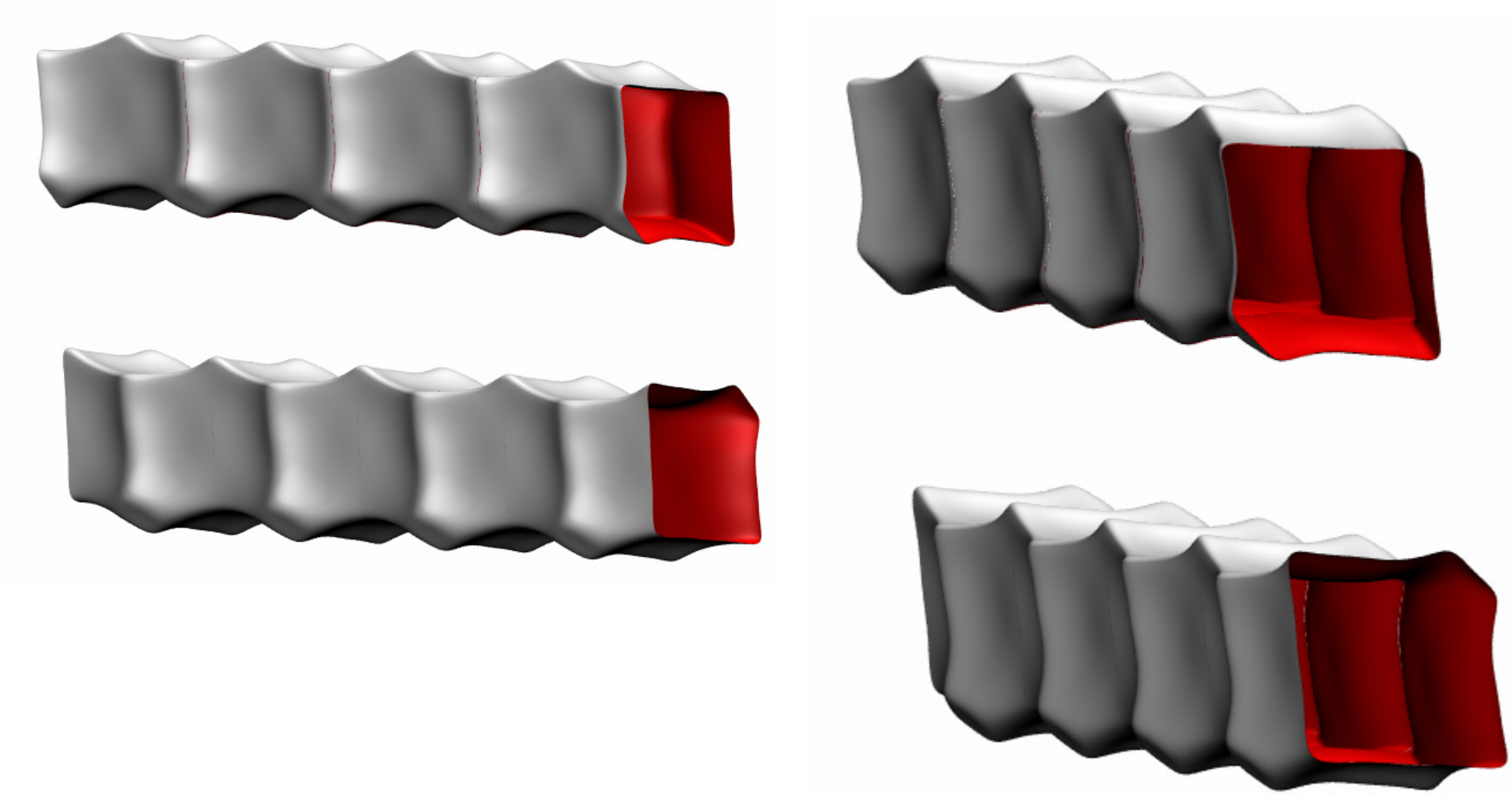

Figure 27

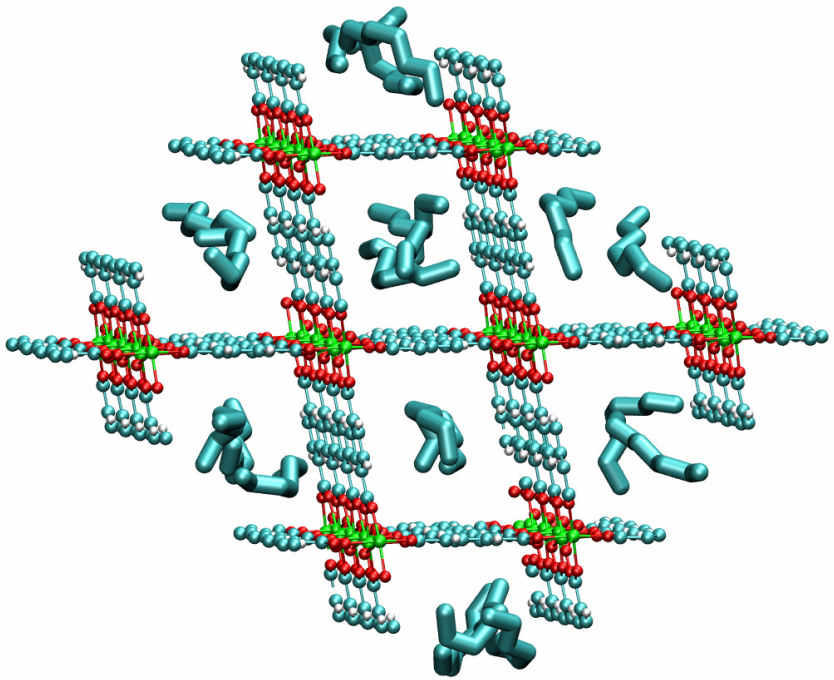

nC8

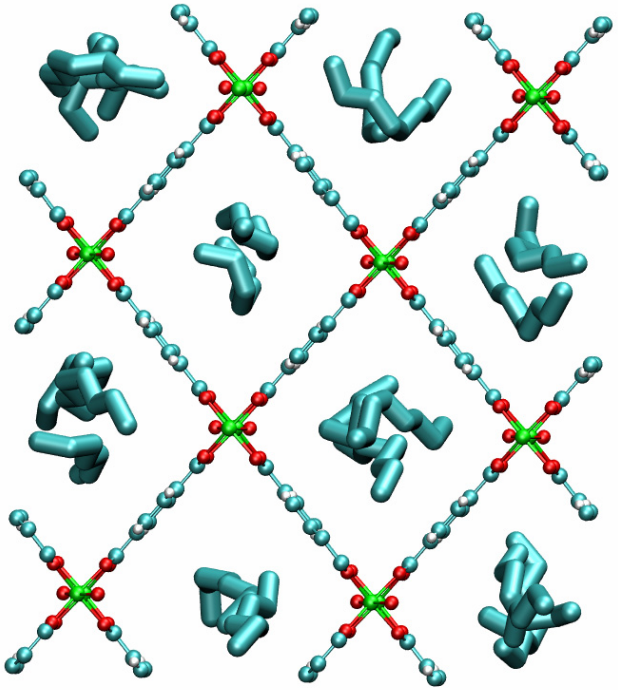

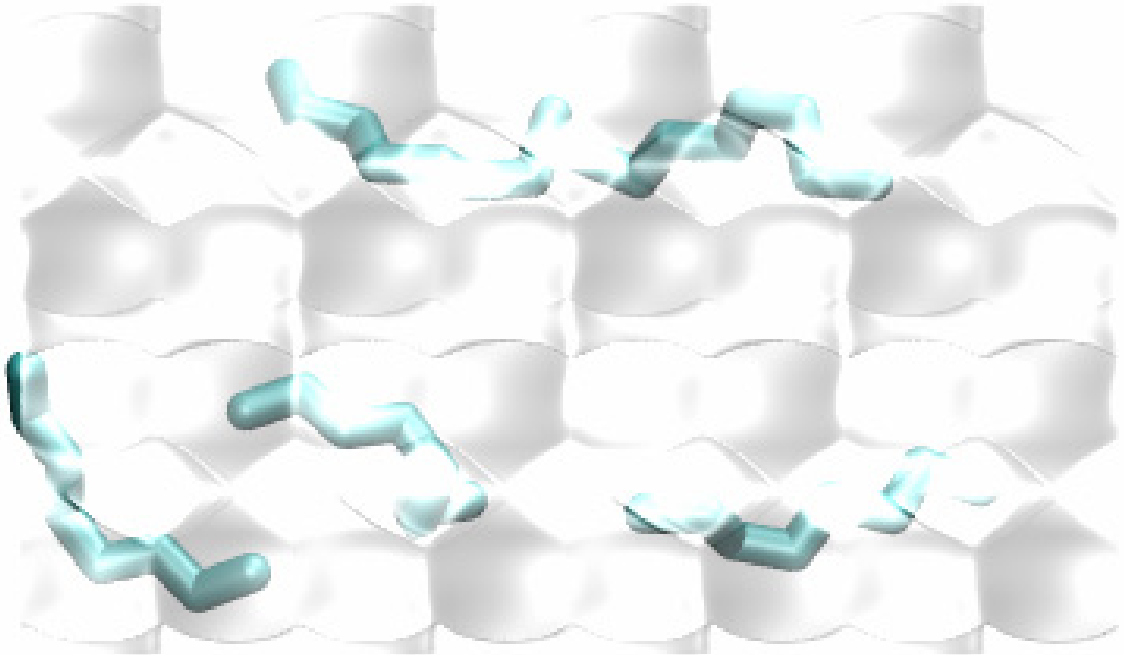

Figure 28

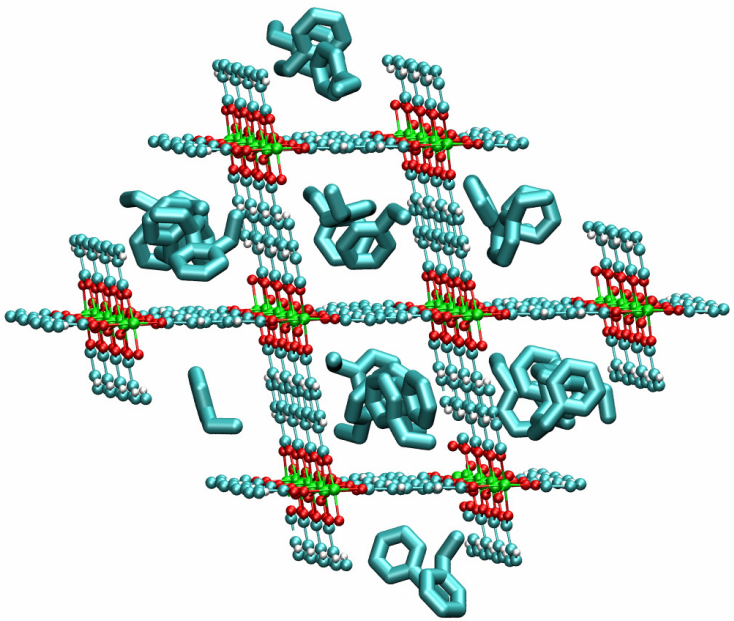

Ethyl benzene

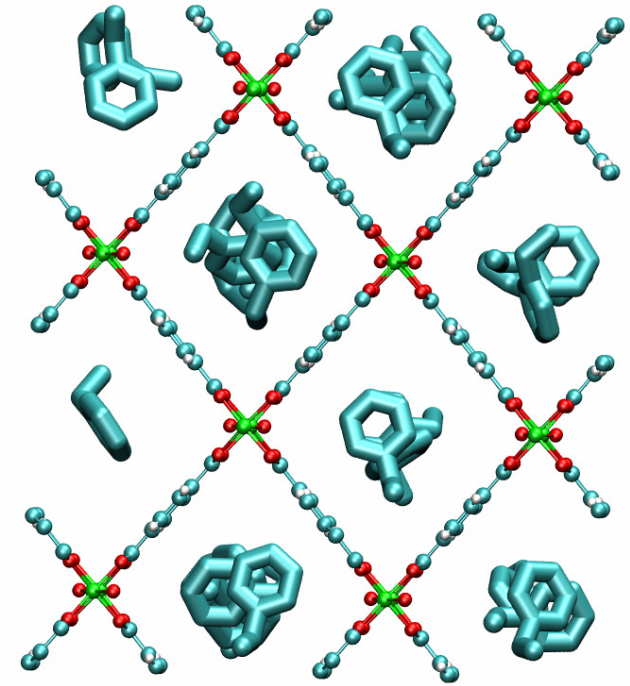

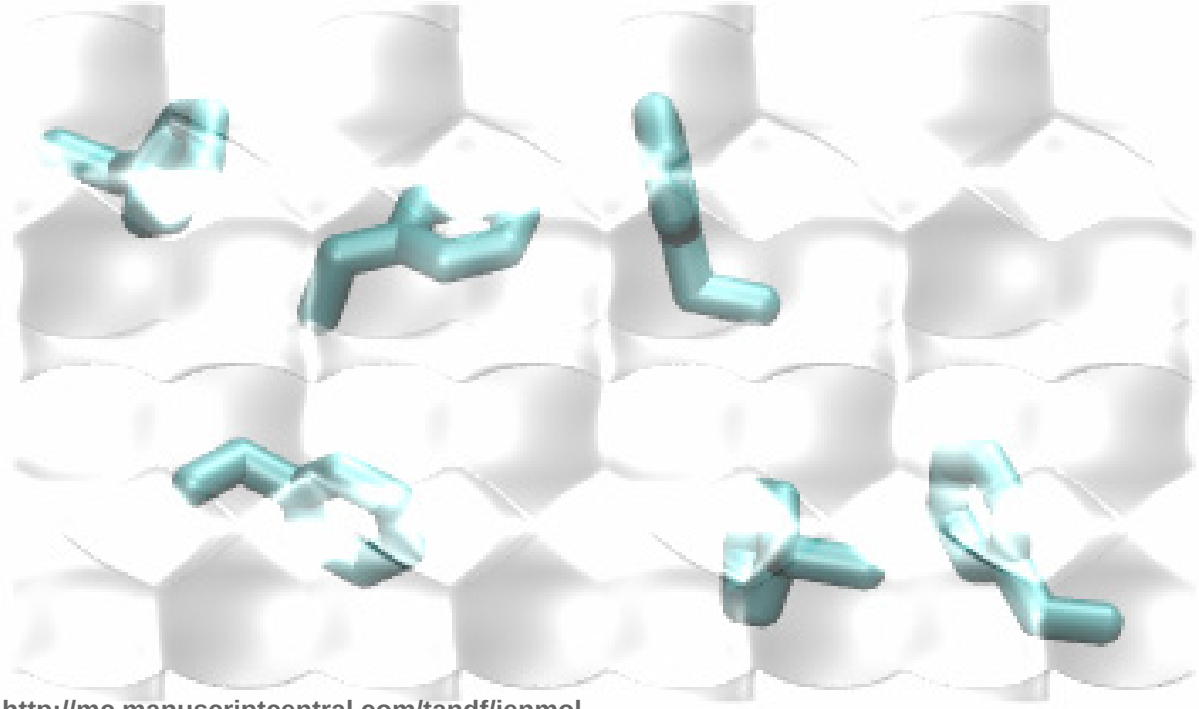

Figure 29

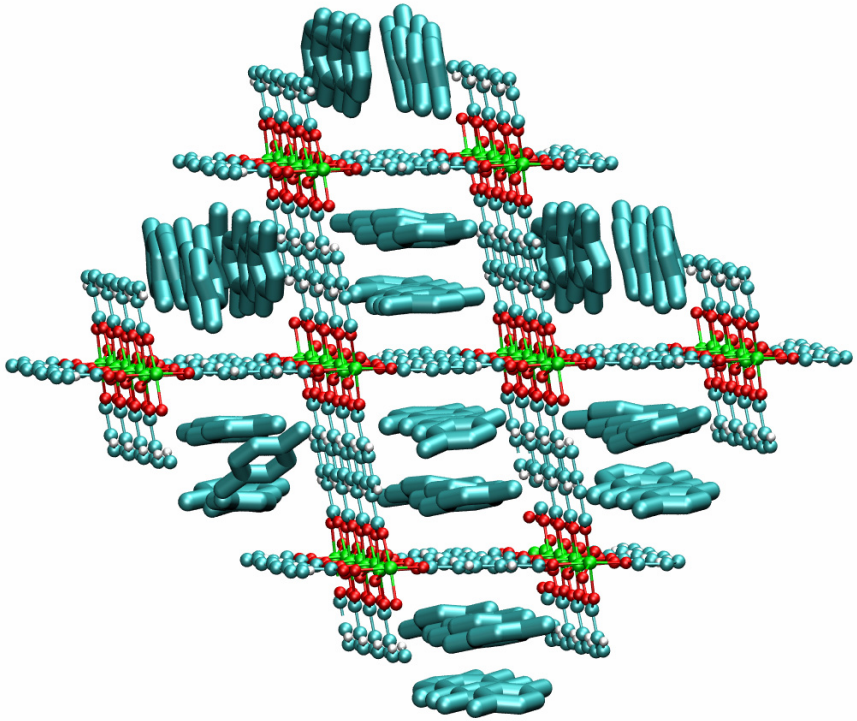

p-xylene

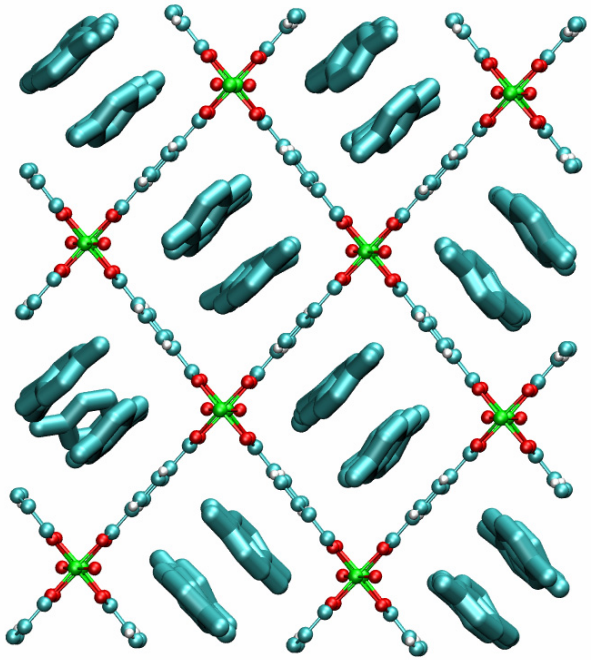

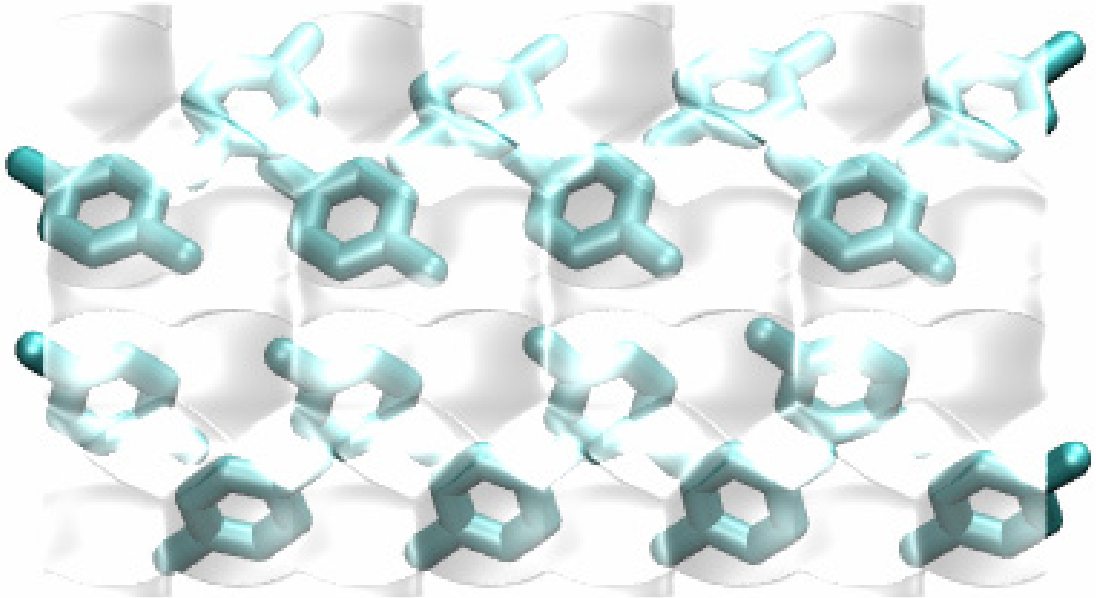

Figure 30

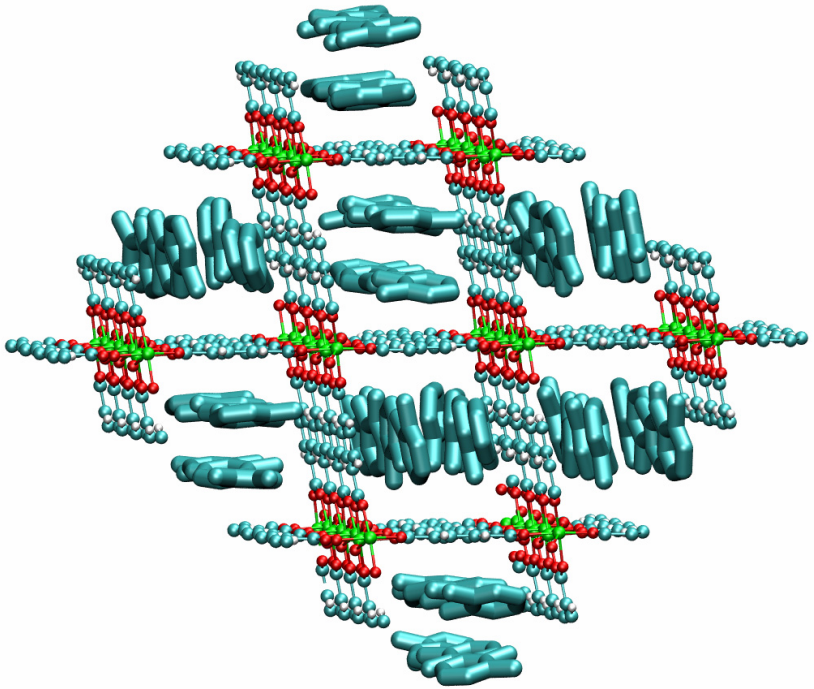

o-xylene

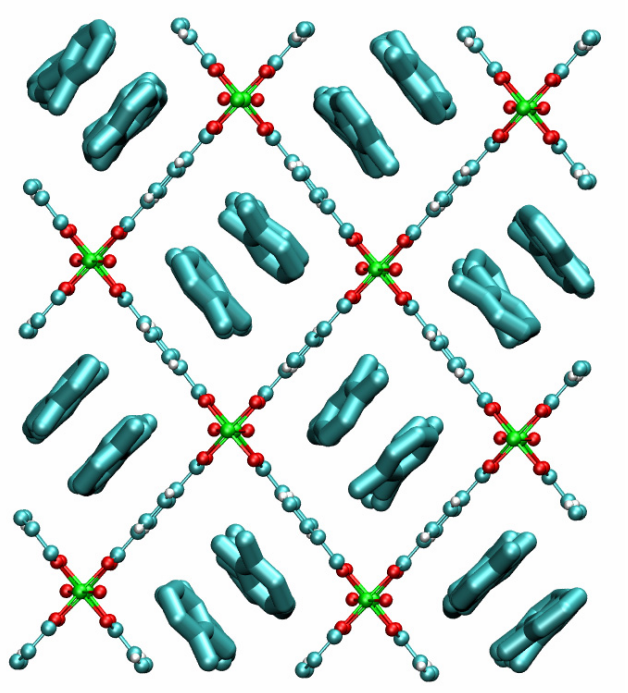

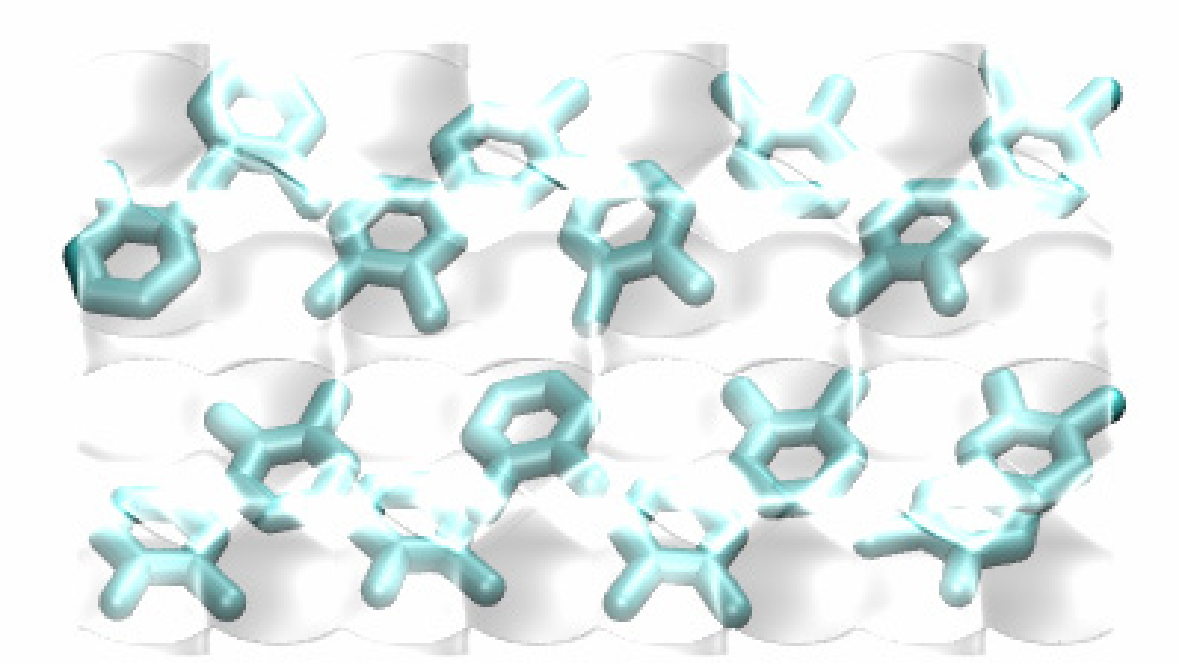

Figure 31

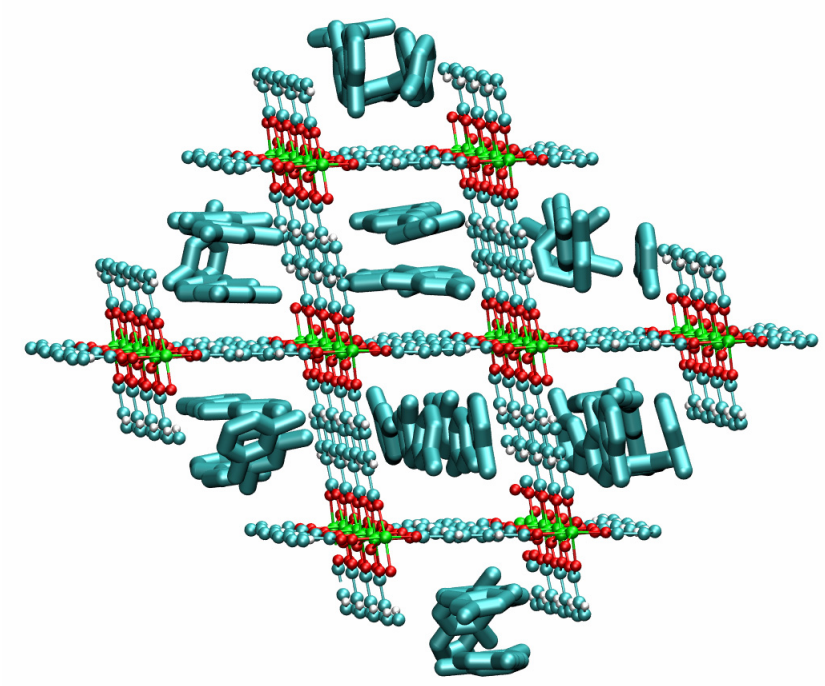

m-xylene

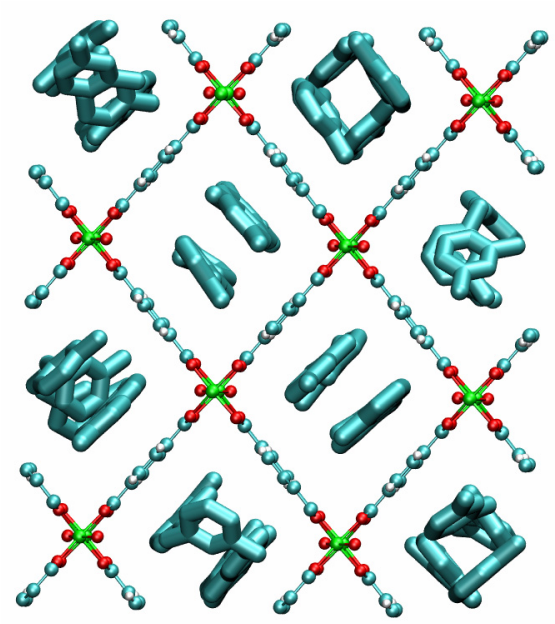

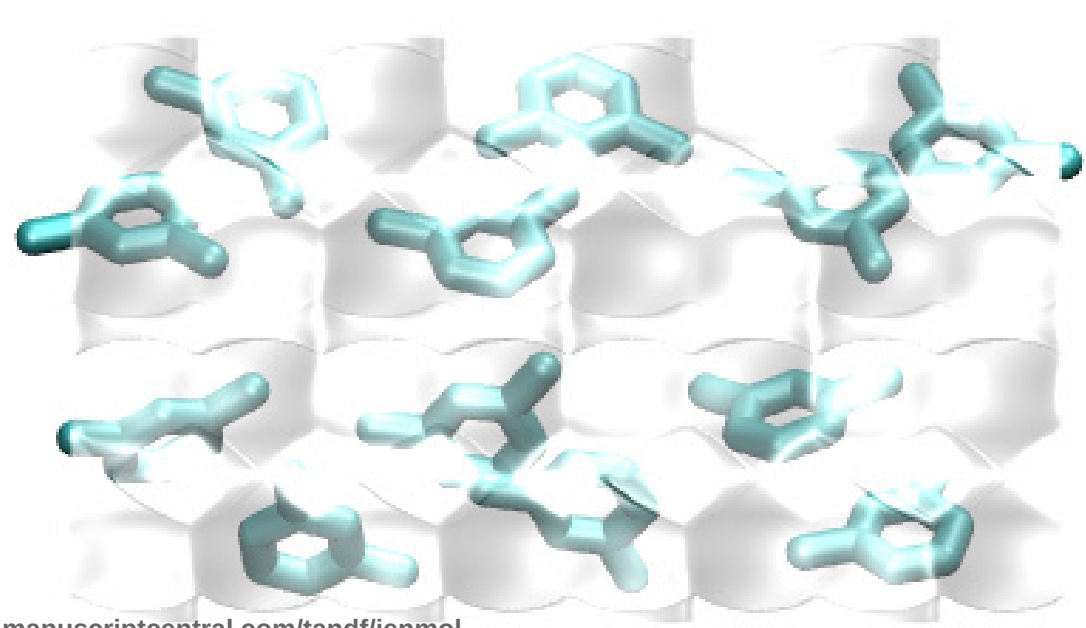

Figure 32

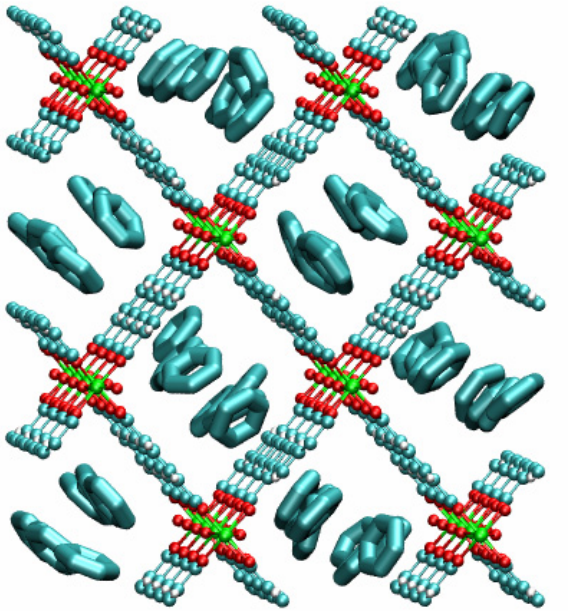

benzene

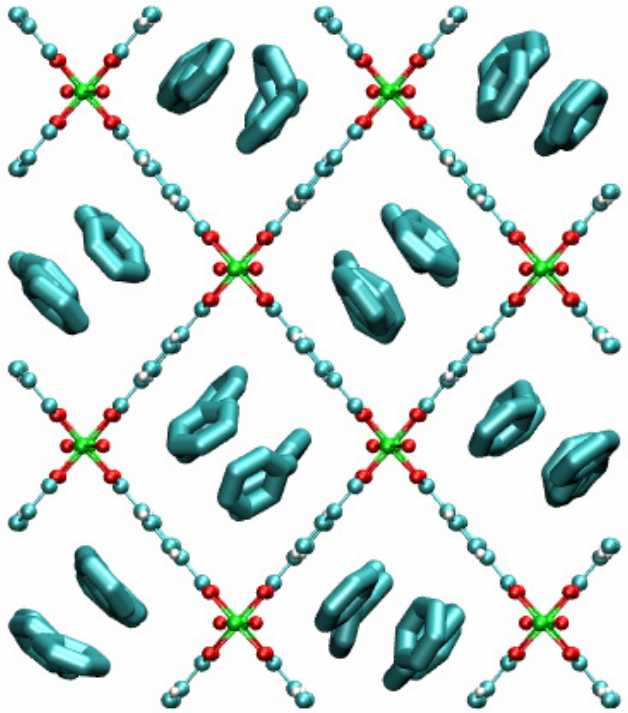

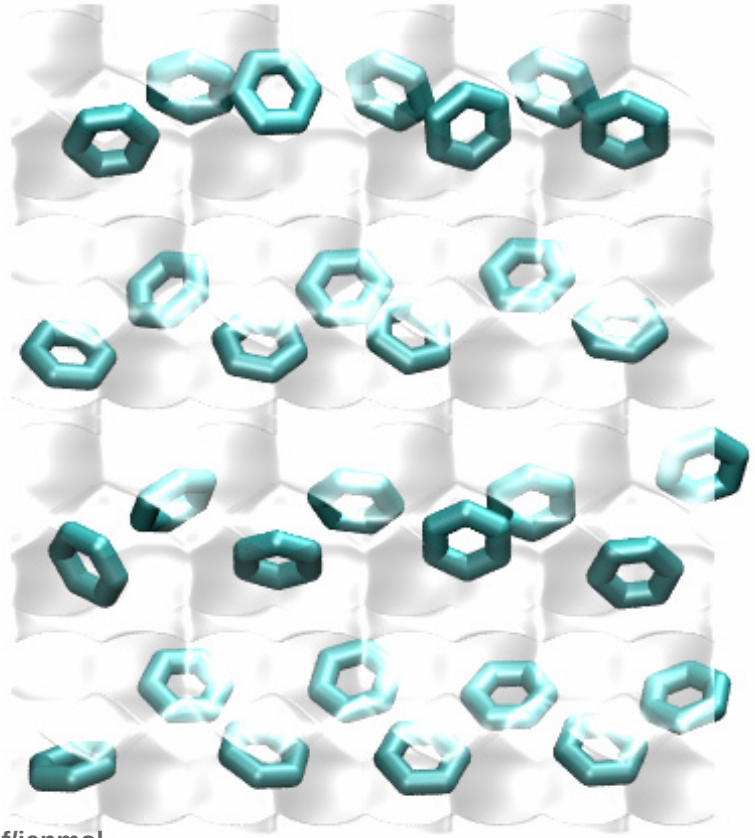

Figure 33

Pure component isotherms

CBMC

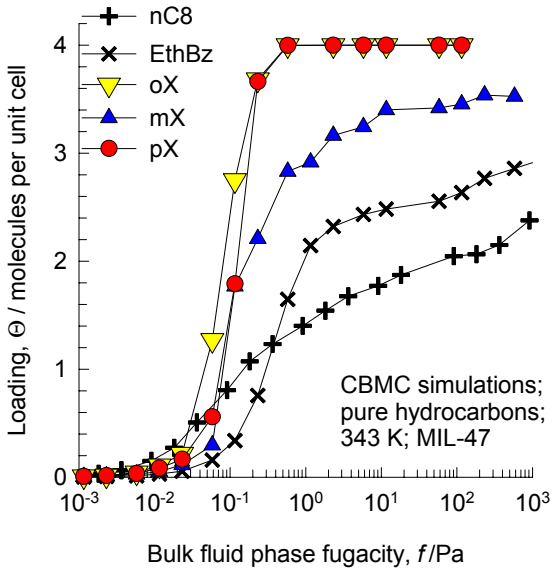

Experiment

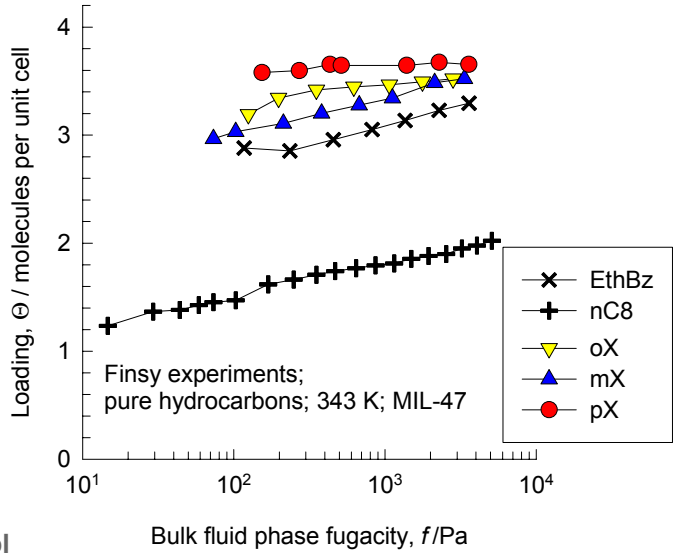

Figure 34

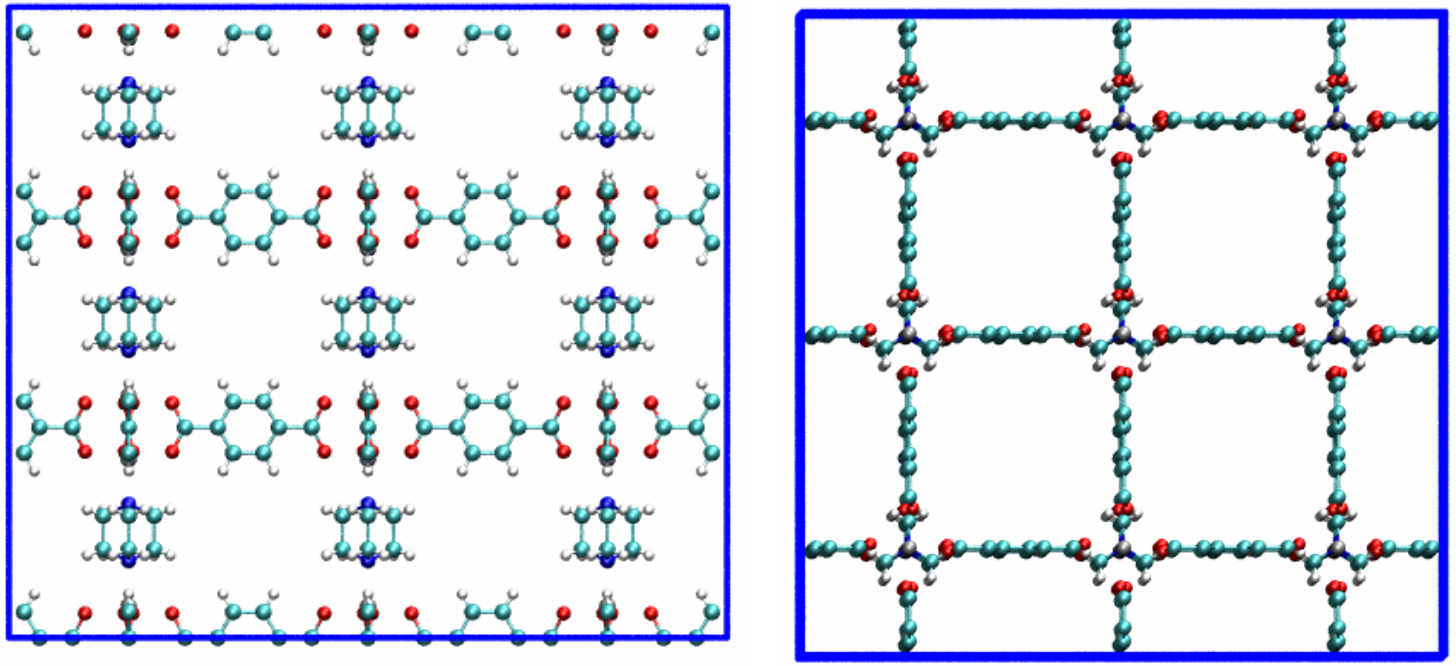

Zn(bdc)dabco structure

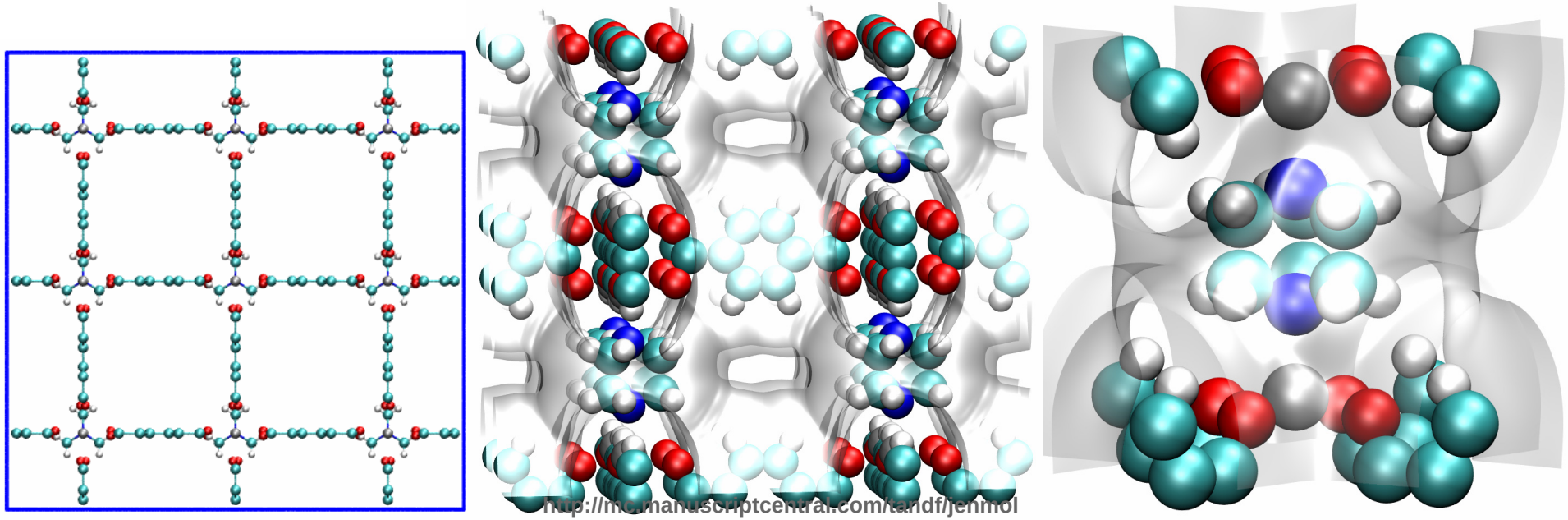

Figure 35

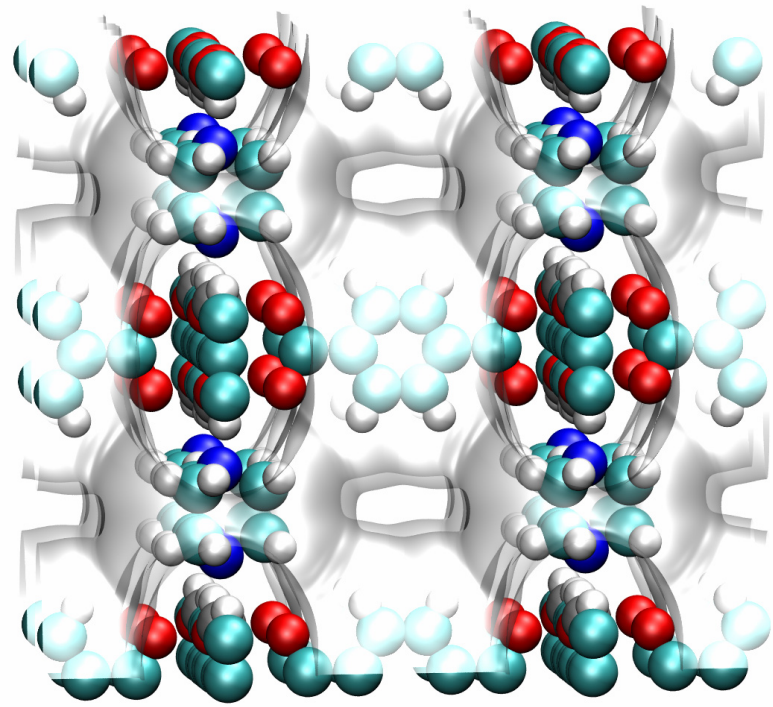

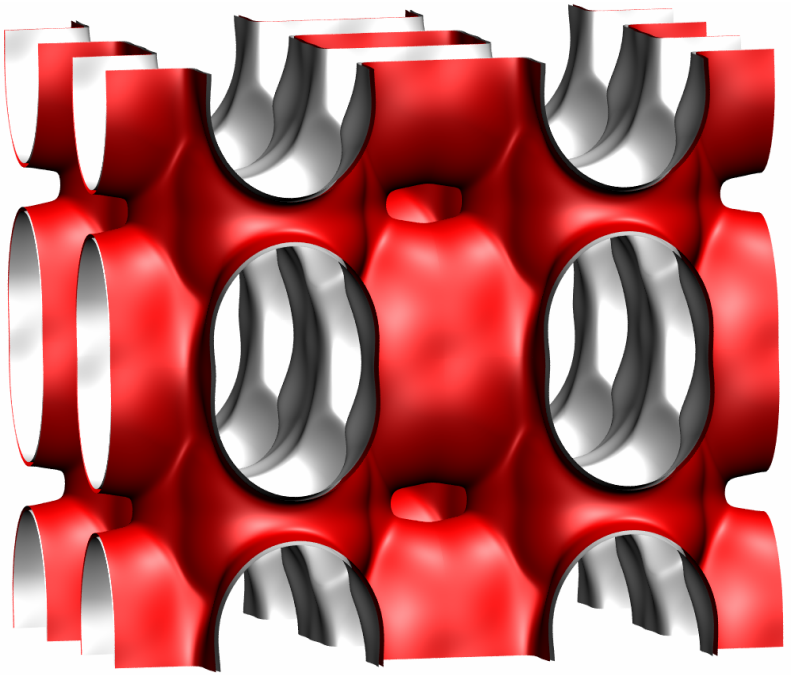

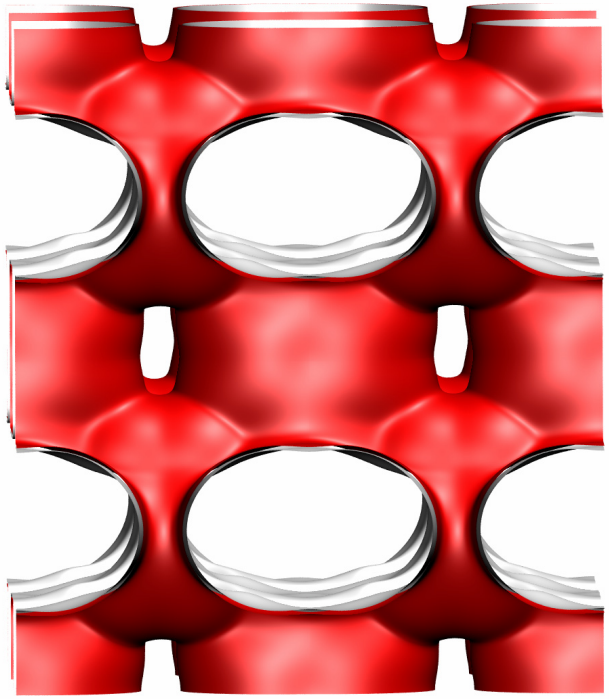

Zn(bdc)dabco landscapes

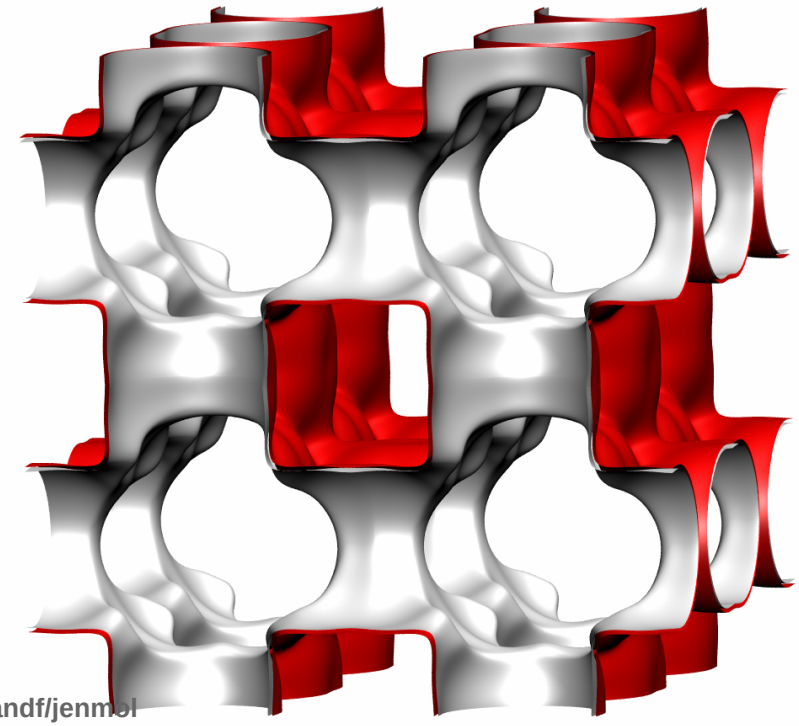

Figure 36

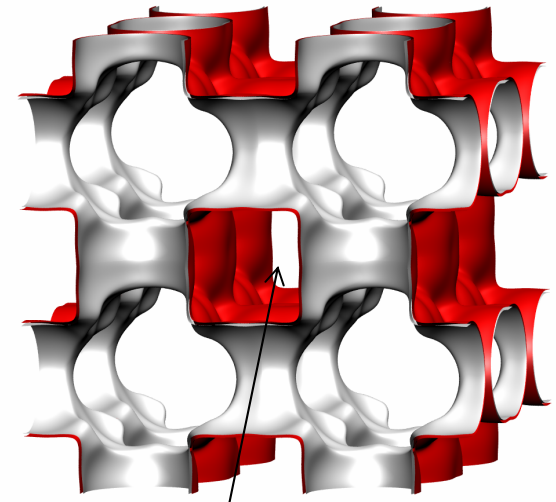

Zn(bdc)dabco landscapes

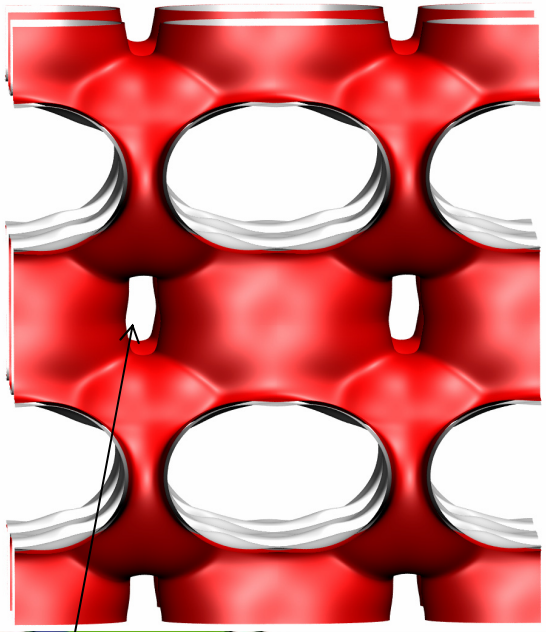

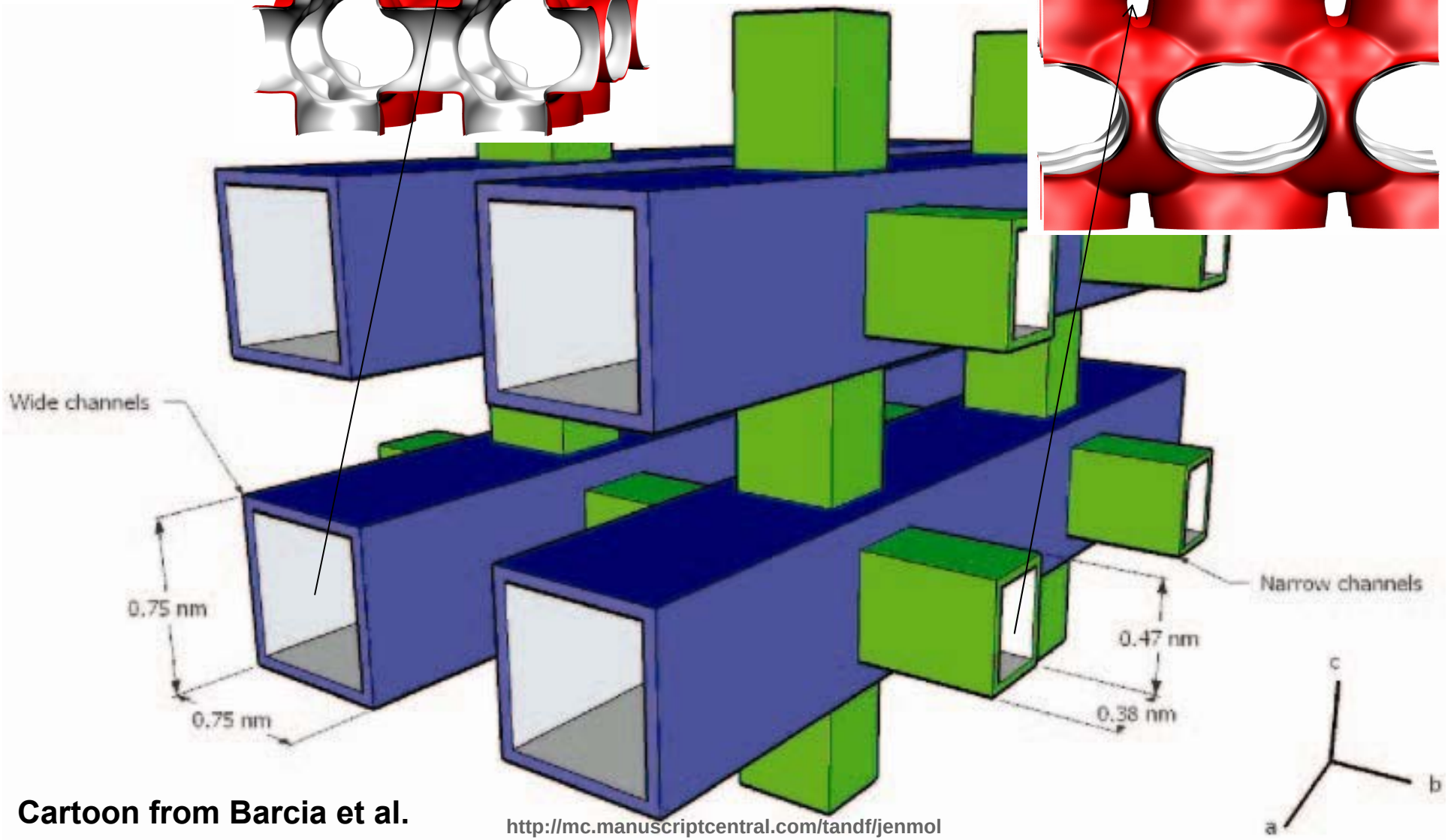

Cartoon from Barcia et al.

Figure 37

C1

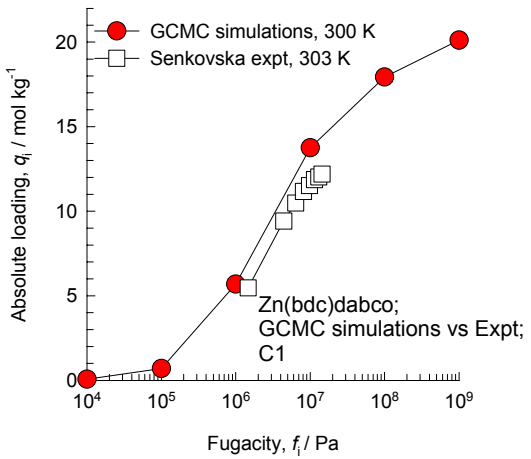

Comparison of simulated isotherm with experimental data of Senkovska and Kaskel, MicroMesoporMat, 112, 108-115 (2008)

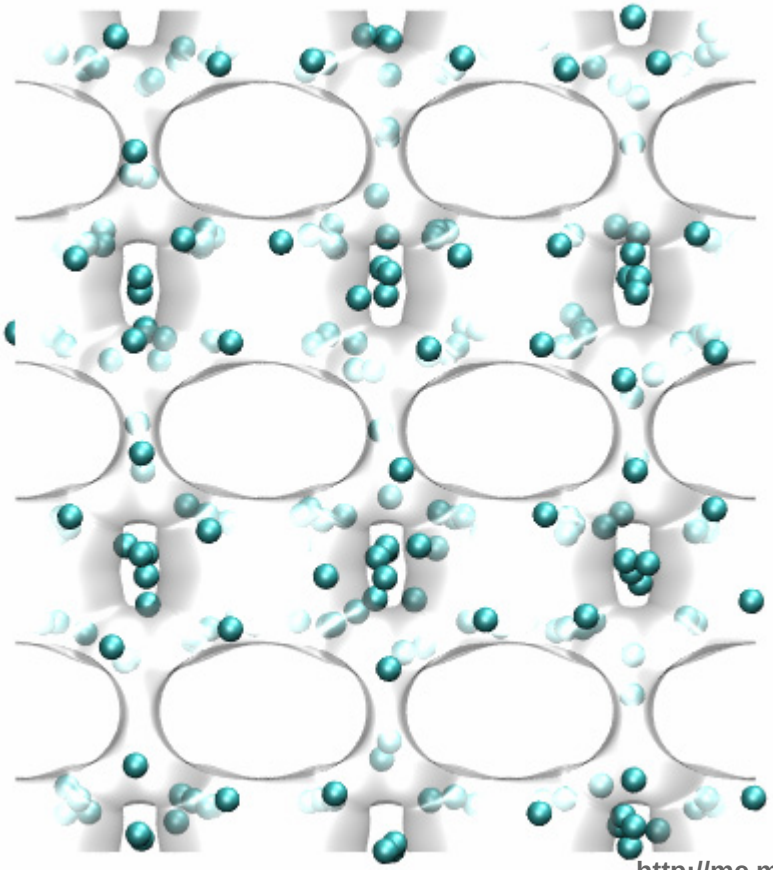

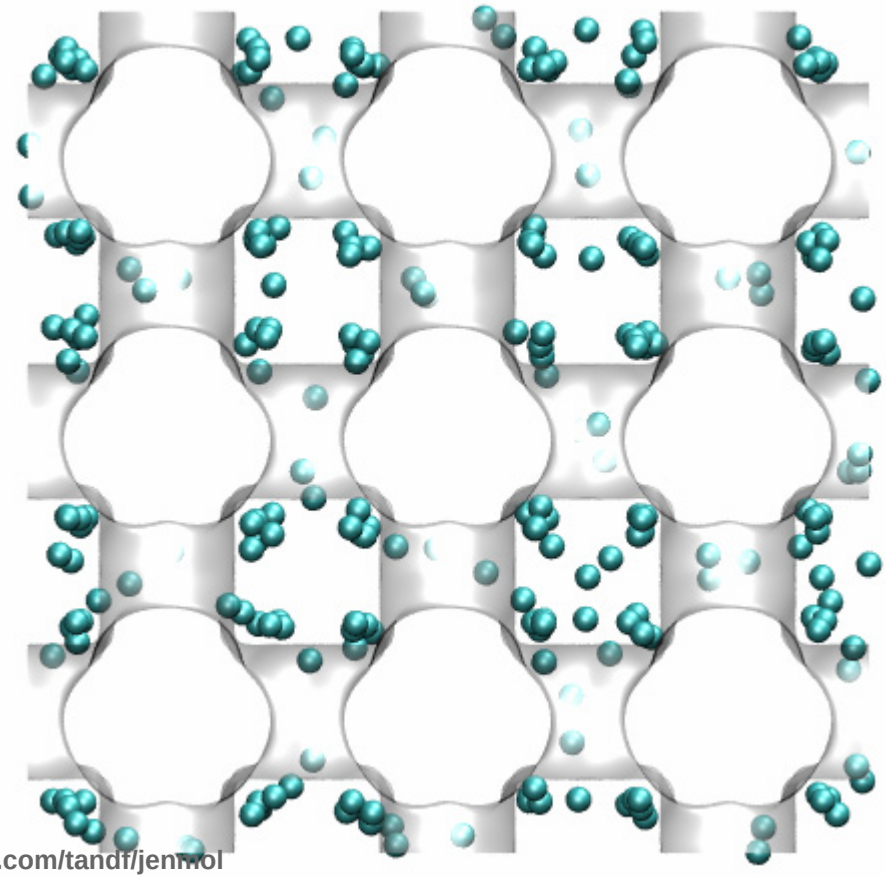

Figure 38

C2

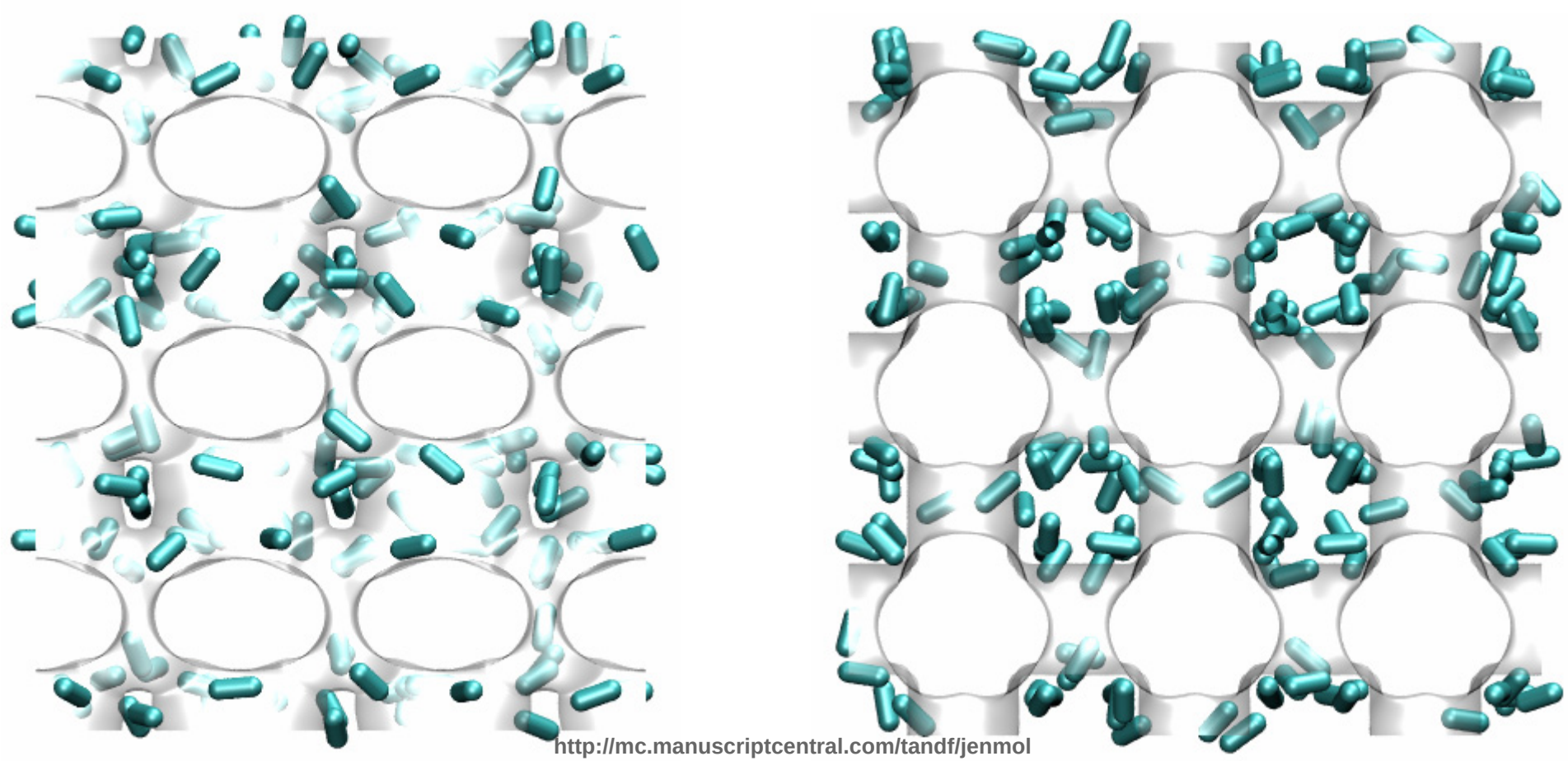

Figure 39

C3

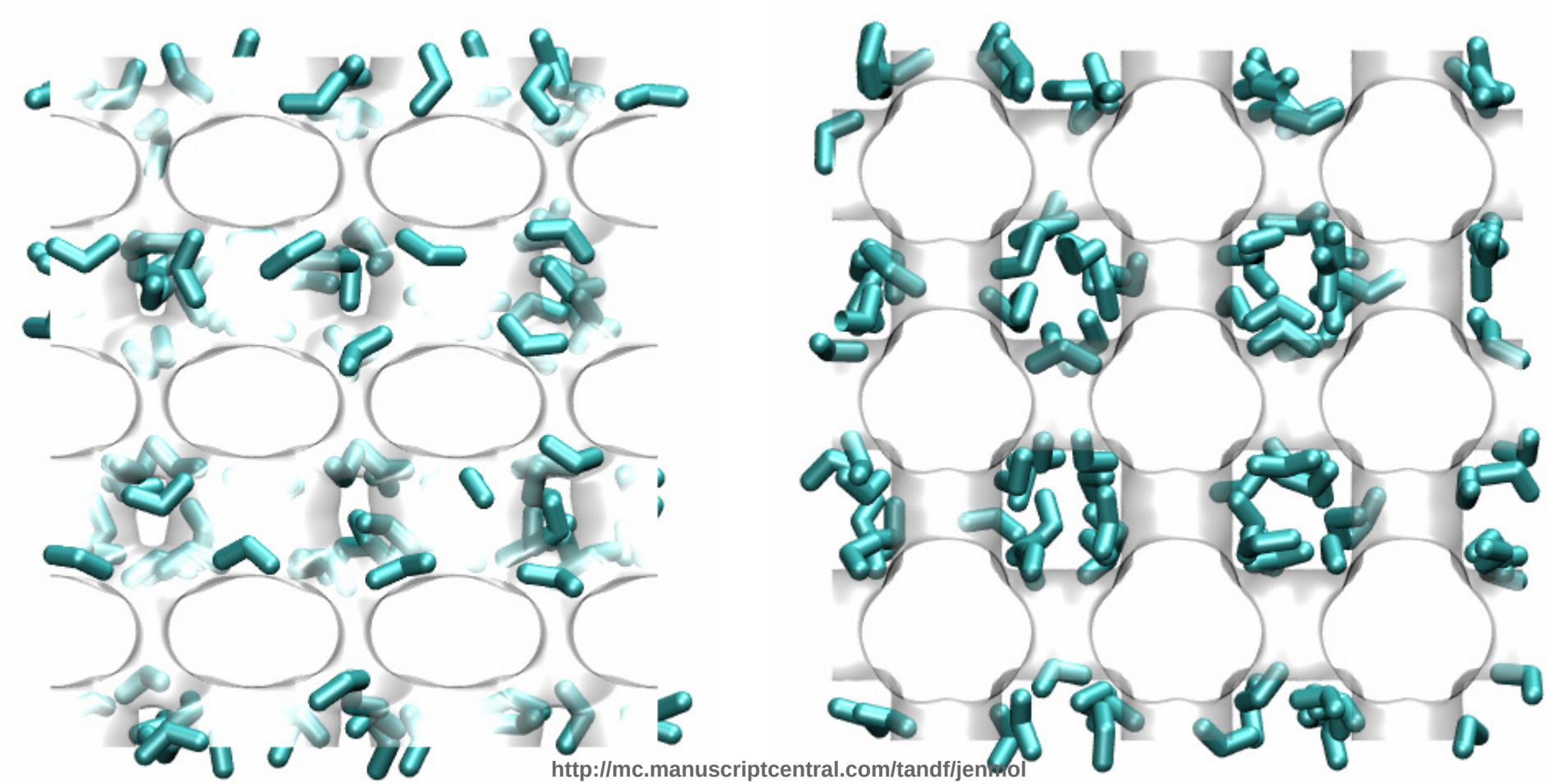

Figure 40

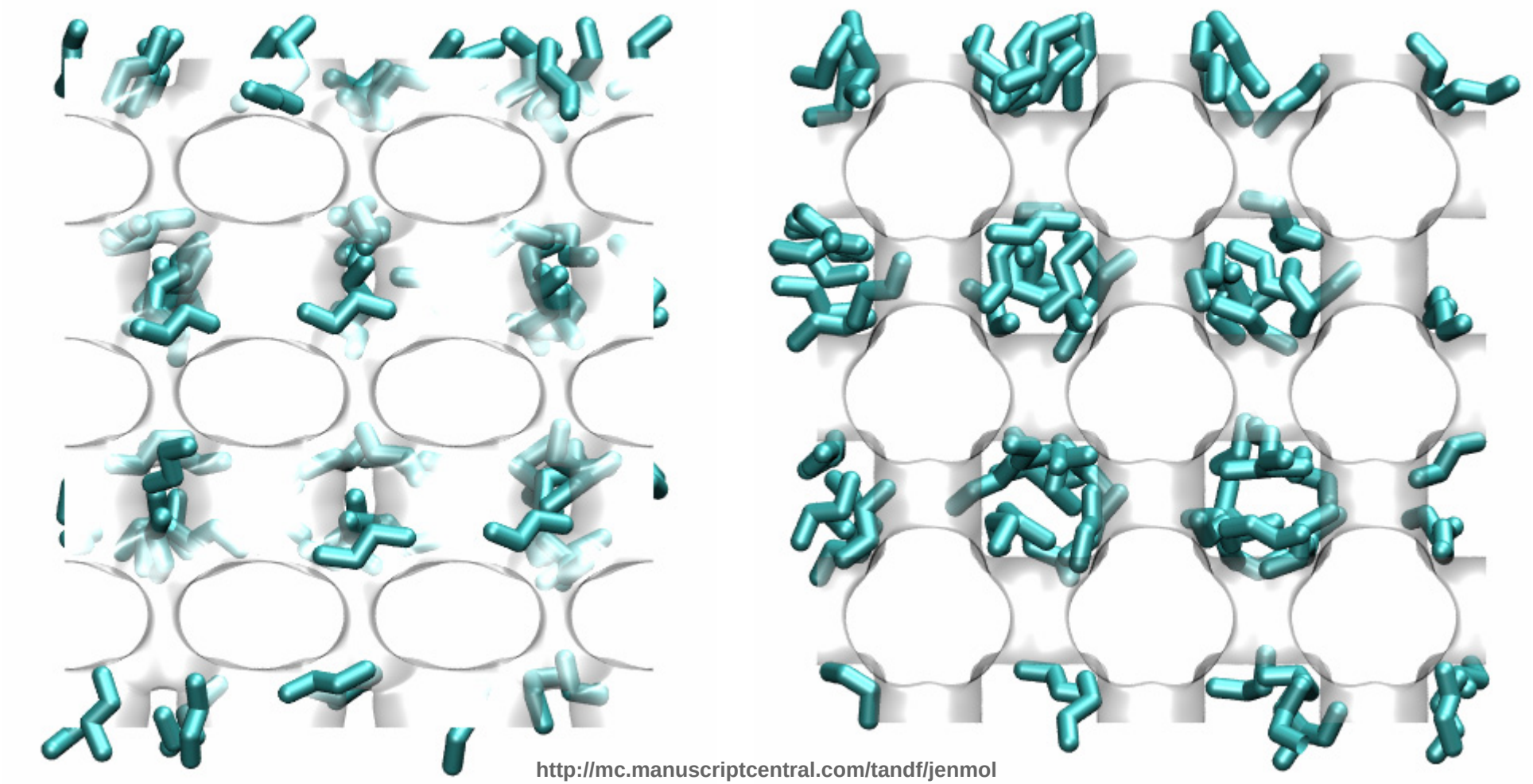

Figure 41

3MP

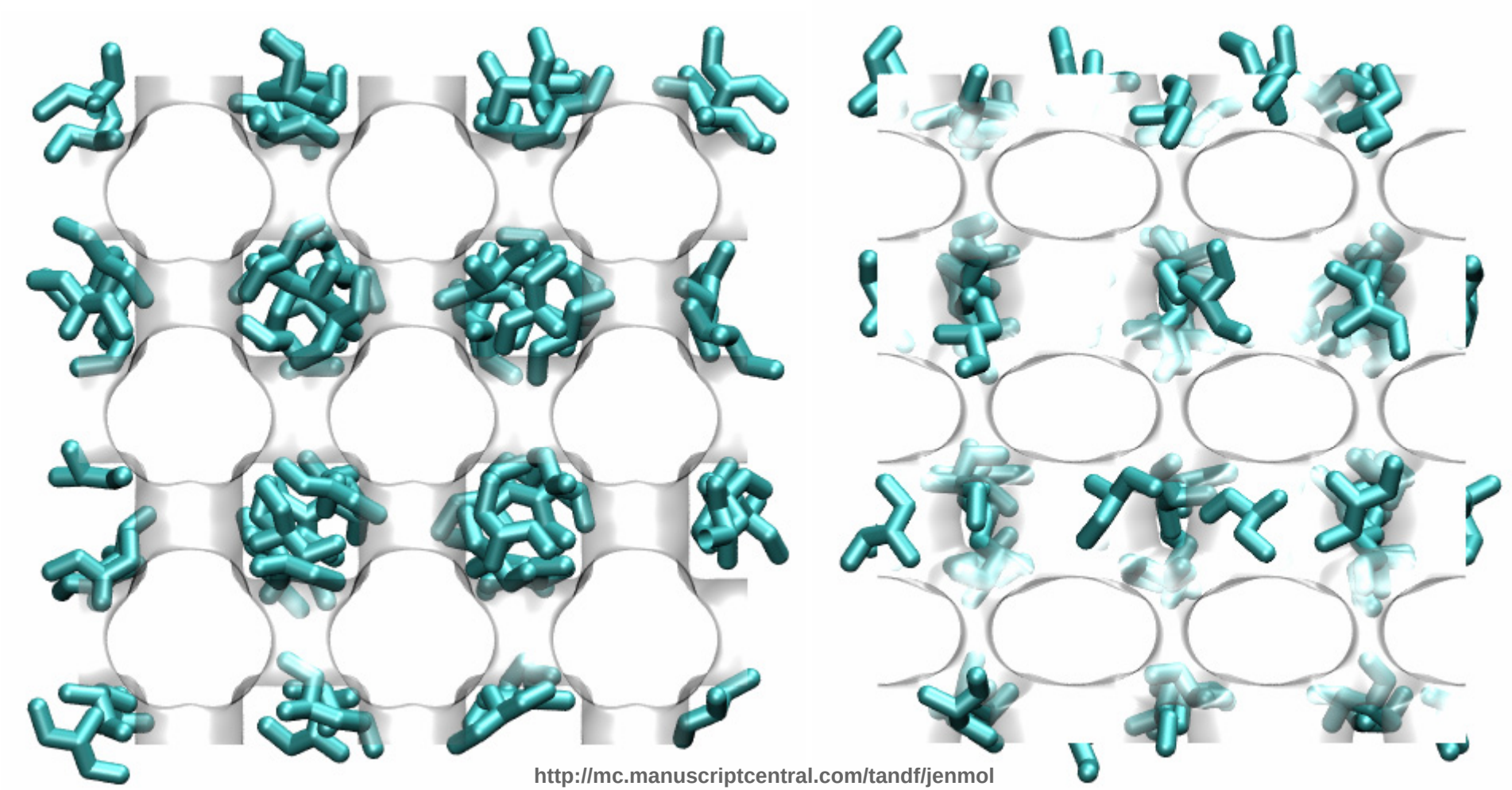

Figure 42

22DMB

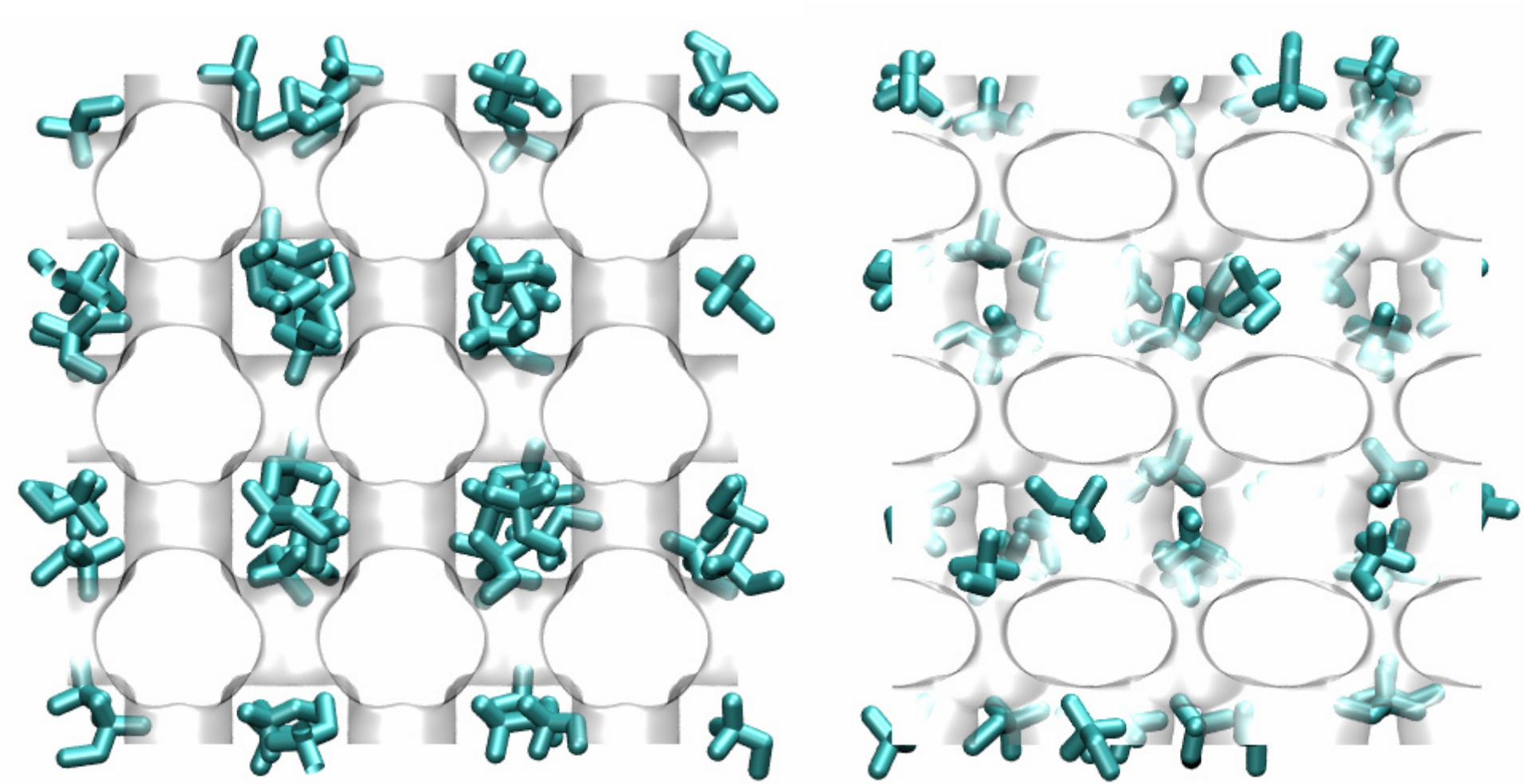

Figure 43

nC6-3MP-22DMB

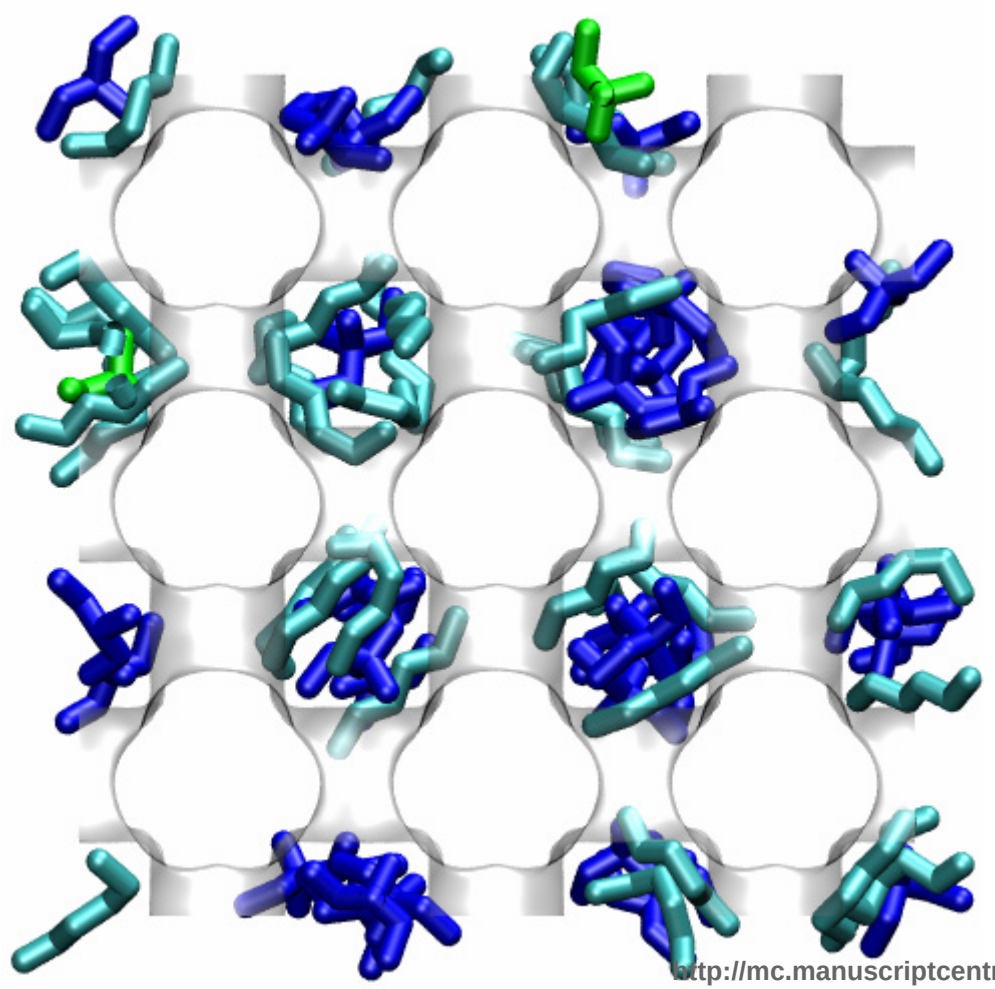

Figure 44

nC6-3MP-22DMB

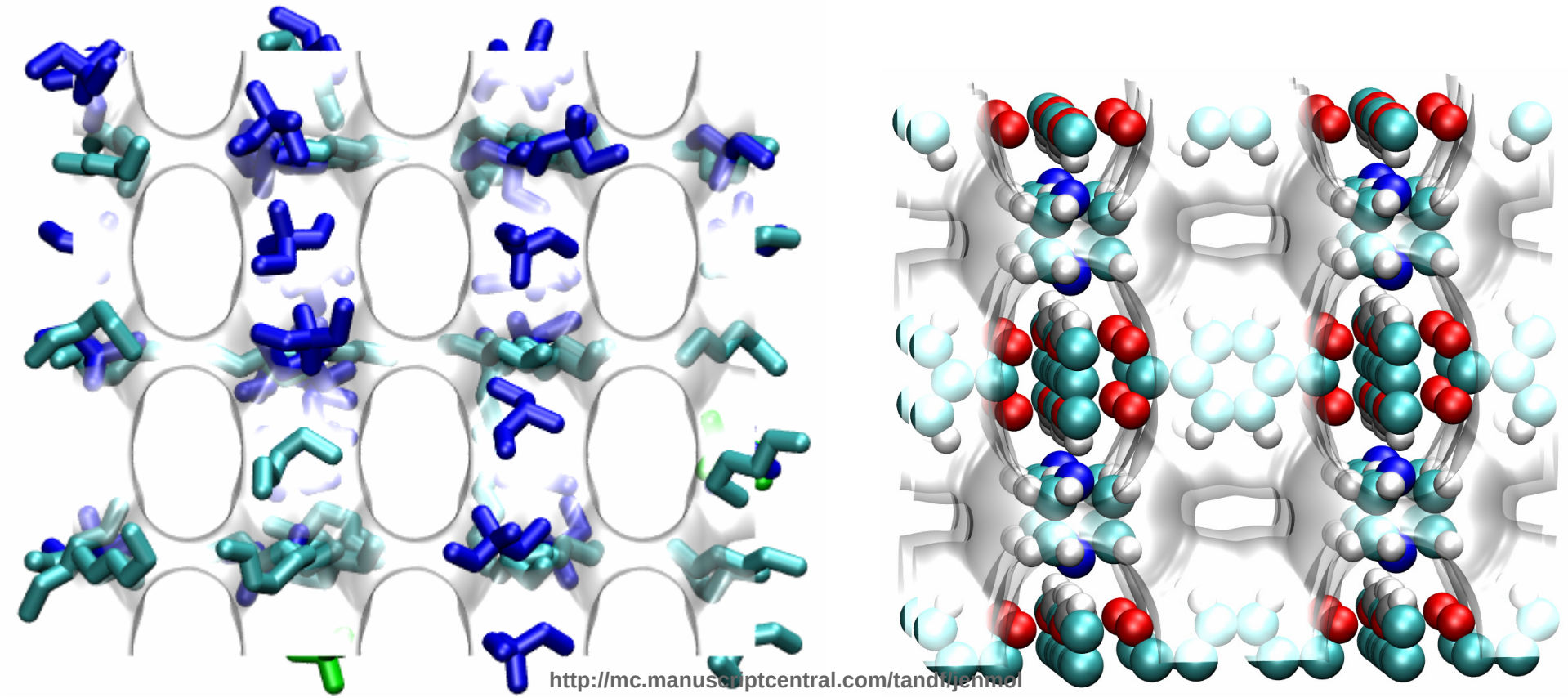

Figure 45

nC6-3MP-22DMB

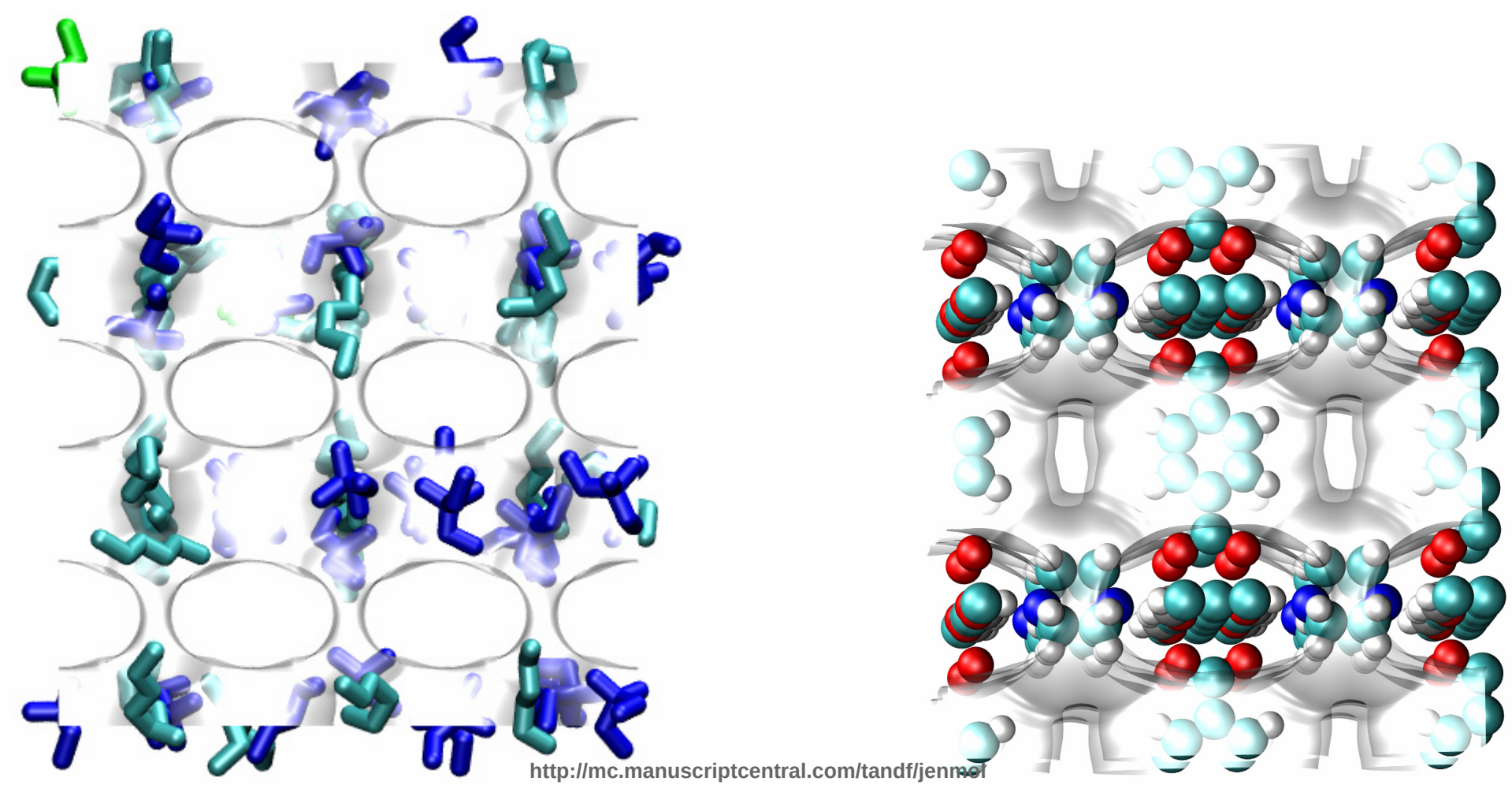

Figure 46

Pure component and ternary mixture isotherms

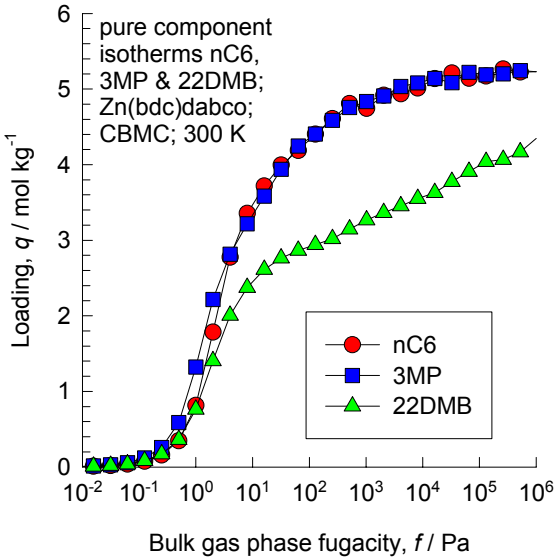

CBMC simulations

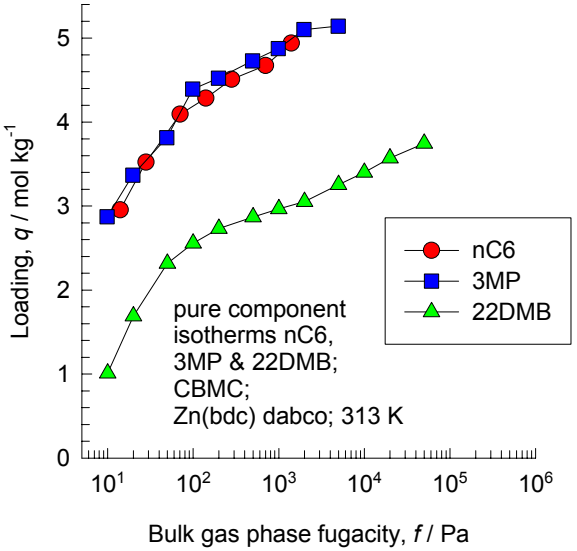

300 K **313 K**

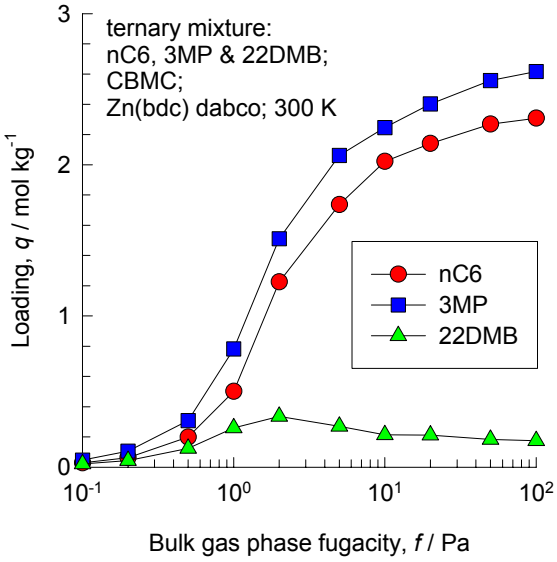

Barcia experiments